MESOSCALE VARIABILITY IN THE GULF OF MEXICO,

ITS IMPACT AND PREDICTABILITY

A Thesis
Presented to
The Academic Faculty

by

Yuley Cardona Orozco

In Partial Fulfillment
of the Requirements for the Degree
Doctor of Philosophy in the
School of Earth and Atmospheric Sciences

Georgia Institute of Technology
August 2013

MESOSCALE VARIABILITY IN THE GULF OF MEXICO,

ITS IMPACT AND PREDICTABILITY

Approved by:

Dr. Annalisa Bracco, Advisor
School of Earth and Atmospheric Sciences
Georgia Institute of Technology

Dr. Judith Curry
School of Earth and Atmospheric Sciences
Georgia Institute of Technology

Dr. Emanuele Di Lorenzo
School of Earth and Atmospheric Sciences
Georgia Institute of Technology

Dr. Yi Deng
School of Earth and Atmospheric Sciences
Georgia Institute of Technology

Dr. Ajit Subramaniam
Marine Microbiology Initiative
Moore Foundation
Lamont Doherty Earth Observatory
Columbia University (on leave)

Date Approved: June 19, 2013

To my parents Luis Hernando and Blanca Libia, my sister Alexandra, my brother Yamid, and my morcy José Manuel. Their undying love and support has made them responsible for all of this.

TABLE OF CONTENTS

ACKNOWLEDGEMENTS

I would like to express my gratitude to my advisor Dr. Annalisa Bracco. I could not have asked for a better guidance during this journey. I deeply admire her passion and commitment for her job. She is a brilliant professor that willing to help you at any moment. It is just amazing. Her intelligence and strong personality made a perfect and unique combination. Thanks a lot for give me the opportunity to learn from you.

Thank you Vincent Combes, you were my academic big brother during the last five years. I truly appreciate your continuous support during my learning process. I cannot count how many nights, Sundays or holidays you spent with me and my complicated relationship with the model. And most importantly thanks a lot for your friendship.

I would like to thank crew and research groups on board of the R/V Oceanus 468, R/V Endeavour 496, 509, and 510. Special thanks goes to my collaborators Ajit Subramariam, Joseph Montoya, and Tracy Villareal, and my sea friends. En el mar la vida es mas sabrosa.

My gratitude also goes to the close and generous friendships I had the opportunity to build along this time. Everything starts with my Colombian paisa team (Manuel, Paula, Carlos, Lina, Paola, and Sara) and end up with a huge international, multicultural and crazy big family. Thanks for the everyday laugh Chente, Jessica, Douglas, Natasha, Shandra, Ricardo, Fernando, Mer, Andres, Sebastian, Rondro, Yisen, Monica, Alejandro, and Angela. I also appreciate those friends that besides the distance were always there for me. To my best friend Beatriz Hernandez and my awesome Colombian group of friends

Carolina, Maria Isabel, Mary Luz, Lina M, Laura, Diana R, Luisa, Joany, Mario, Olver, Jorge M, Carlos, Camilo, Lucho, and Vladimir. Finally, thanks to my first friends all my cousins.

I would like to express my particular gratitude and love to Jose Manuel, the best teammate in this adventure and hopefully in the rest of my life. These words will never be enough to thanks all his patient and encouraging comments. Thanks to pushing me all the way until the final line. I know it was not an easy job. I love you.

Finally, I would like to thank my parents. I am here today writing these lines because of them. They dedicated their whole life to us providing unconditional love.You have been the best parents for your four kids. Thanks, thanks, and thanks. To my sister and my brother, my first and life friends. Love you all.

LIST OF TABLES

LIST OF FIGURES

SUMMARY

The circulation of the Gulf of Mexico is controlled by presence of large mesoscale structures (10-500 km). We investigate its variability and predictability from interannual to intraseasonal time scales, and the dynamical interactions between physical circulation and biological productivity. We do so by analyzing an ensemble of numerical integrations using the Regional Ocean Modeling System and hydrographic and biogeochemistry observations collected during summer field campaigns in 2010, 2011, and 2012.

First, we explore the potential relationships and linkages between Mississippi-Atchafalaya River runoff, nutrient loads, and ocean dynamics from our field data. A negative correlation between nutrient concentration and salinity was confirmed at the surface and in the upper 60m of the water column for nitrite, nitrate, phosphate and silicate. No major changes in the nutrient concentrations were found between our data and previous measurements from twenty years ago. The biological activity in the stations sampled (northern Gulf) is nitrogen limited in 79% of them and phosphorus limited in 8%. Besides the direct input of nutrients from river discharges, the distribution of nutrients in intermediate and high salinity waters in the euphotic layer is influenced by dynamical processes at the ocean mesoscales such as eddies, coastal upwelling events and Loop Current (LC) intrusions.

Then, using an ensemble of four model integrations we investigate how mesoscale motions dominate the variability of the Gulf of Mexico circulation both at the surface and

in deep waters on intraseasonal time scales. We focus on its predictability by exploring the impact of small variations in the initial conditions and the role of the boundary conditions in the circulation evolution. In all runs, the model provides a good representation of the mean circulation features. However, the shedding of the Loop Current Eddies (LCE) differs in each run considered, and our analysis shows that the detachment of the LCE is a stochastic process. We show that the interannual variability at the model boundaries affects the representation of the LC strength and of the Yucatan Channel transport. On the other hand, the circulation in the LATEX Shelf, TAVE Shelf, and Bay of Campeche is insensitive to the details of the model boundaries, is not affected by the LC, but depends only on the wind variability, and it is therefore predictable if the atmospheric conditions are known. On the contrary, the circulation in the central basin is affected by the LC extension and by the Rings, and dominated by mesoscale features. In most of the basin, mesoscale features are coherent in the top ~ 1000 m of the water column, and below it, but not correlated between the surface and the deep layer. Coherency throughout the whole water column is attributed to particular topographic features such as the south-west corner of the Sigsbee Deep. The chaotic behavior associated with the propagation of the LCE and the elevated mesoscale activity restricts the predictability of the system at intra-seasonal scales to the coastal areas. In consequence, assimilation of continuous in-situ measurements is necessary to insure good hindcasts and forecasts at surface and below 1000 m depth.

Finally, since mesoscale activity is key to understand the horizontal and vertical dynamics in the Gulf, we further analyze the model representation of mesoscale circulation under low (monthly) and high (6 hourly) frequency atmospheric forcing. The

temporal scale variation from monthly to 6-hourly in the wind forcing impacts the timing of horizontal dynamics, but not the strength. However, high frequency winds impact the model representation of vertical transport that increases as the temporal resolution of the forcing increases. Vertical velocities in the simulation forced by 6-hourly winds are ten times greater than the one obtained using monthly averaged winds. The energy injected by the winds into the ocean is transported in the water column by mesoscale eddies and near-inertial oscillations. If the forcing used by the model does not resolve the inertial frequency (1.4 days in the Gulf), then vertical transport processes are underestimated. Those processes are particularly important for the model representation of biological activity in the ocean upper layers, since they contribute to the input of nutrients into the euphotic zone.

CHAPTER 1

INTRODUCTION

The Gulf of Mexico is a semi-enclosed tropical basin. It has two openings in the southeastern corner: the Yucatan Channel and the Florida Straits. The Yucatan Channel connects the Gulf with the Caribbean Sea, and the northward Yucatan current flows through it, transporting approximately 23-27 Sv of warm and saline waters into the Gulf (Candela et al., 2002). The Yucatan Current also referred as the Loop Current (LC) loops clockwise and leaves the Gulf through the Florida Strait. After leaving the Gulf, it becomes a major component of the Gulf Stream and Subtropical Gyre in the Atlantic Ocean. The LC is the most energetic and dynamic feature in the Gulf, followed by the anticyclonic eddies that detach from it every 9 months on average (Vukovich, 2012). The anticyclonic circulation in the northwestern part of the Gulf (Lee and Mellow 2003), the cyclonic current in the Bay of Campeche (Vasquez de la Cerda, et al., 2005), and the topographic Rossby waves over the Sigsbee escarpment (Hamilton, 2009) create a collection of the dynamic processes that drive the Gulf circulation. Additionally, around the Texas and Louisiana shelf the circulation is strongly influenced by the Mississippi-Atchafalaya discharge, which is the source of 80% of the freshwater and over 90% of the nitrogen input to the northern Gulf of Mexico (Turner et al., 2007). The Mississippi-Atchafalaya discharge may sets up favorable conditions for nitrogen fixation and algae blooms in the region.

The Gulf of Mexico circulation and coastal biological activity have been extensively measured and modeled, particularly over the last few years after the Deepwater Horizon accident (Camilli et al., 2010). Continuous observational records, however, are limited to the surface via satellite measurements and to the coastal and shelf areas, and only sporadic in waters deeper than ~ 800 m (see http://data.gcoos.org/). Predicting the Gulf of Mexico circulation is still challenging, as evidenced in the aftermath of the Deepwater Horizon spill in 2010, when different data assimilative models, run in both hindcast and forecast modes, diverged in both their predictions of surface oil trajectories and more generally, in the behaviors of their currents (Liu et al., 2011).

This thesis investigates the variability of the mesoscale circulation in Gulf of Mexico system from interannual to daily time scales and its dynamical interaction with biological productivity. In particular, we focus on mesoscale structures (10-100 km) and the role that they play in the Gulf. We do so by analyzing an ensemble of numerical integrations using the Regional Ocean Modeling System (ROMS) and hydrographic and biogeochemistry observations collected during summer field campaigns conducted in 2010, 2011, and 2012.

First, we explore the relationships and linkages between river runoff, nutrient load, and ocean dynamics. We use physical and biological field data collected over the 2010, 2011, and 2012 summer seasons as part as the field campaigns associated with the project *nitrogen Fixation, Nutrient Supply and Biological Production in the Gulf of Mexico* and satellite-derived chlorophyll-a from the moderate resolution imaging spectroradiometer (MODIS) on-board the NASA Earth Observing System (EOS) Aqua satellite. Satellite

images of the color of the ocean's surface show a correspondence between physical and biological activity within mesoscale structures. Patches and swirls of chlorophyll pigments (the basic component in biological production) are related with the structures of eddies (Bakum 2006) and with the upwelling region around the Yucatan Peninsula. In the northern Gulf chlorophyll-a concentrations are strongly affected by the river outflows of the Mississippi-Atchafalaya River and the way that this fresh and nutrient rich waters are transported into the Gulf. The transport is the result of the juxtaposition of the Loop Current, Loop Current eddies, topographic eddies, and intensity of the river outflow. By the same token, the oil that was released in the Gulf in 2010 following the Deepwater horizon oil spill was advected at depth within a number of distinct plumes and at the surface along the chaotic manifolds associated with mesoscale structures. Since the spatial distribution of the biological activity and other tracers have a tight connection with mesoscale dynamic features, in Chapter 3 we evaluate the predictability of the circulation in the Gulf of Mexico. From the results, we answer two questions: (1) Is the deep (> 1000 m) circulation of the Gulf of Mexico predictable, and if so, on which time scale? (2) Are surface mesoscale processes related to the ones that take place in deep waters so that the reliability of the representation of the surface dynamics in a model can be used as an indicator of the representation of deep circulation as well?

Along with the system predictability evaluation, we investigate the model representation of mesoscale circulation under low (monthly) and high (6-hourly) frequency forcing (momentum and head fluxes). Our findings are presented in Chapter 4. In this chapter we address the following questions: (1) How does the use of wind and heat flux products at different frequencies modify the representation of ocean variability? and

(2) Are horizontal and vertical velocity patterns modified by changes in the temporal resolution of atmospheric forcing? Finally, a summary and conclusions are presented in Chapter 5.

CHAPTER 2

NUTRIENT CONCENTRATION AND BIOLOGICAL ACTIVITY ALONG THE SALINITY GRADIENT AT THE SEA SURFACE AND THROUGH THE WATER COLUMN

The relationship between river discharge (quantity and quality), and mesoscale dynamic processes in the coastal and open waters in the northern region of the Gulf of Mexico modulates biological activity in the region. The Mississippi-Atchafalaya River is the most important input of freshwater into the Gulf. Its discharge represents 80% of the annual freshwater input, 90% of total nitrogen load, and 87% of the total phosphorous (Dunn, 1996). According to the USGS more than 70% of the nutrient load is due to agricultural activity in the river basin. Nutrient input along the coastal areas enriches the system and sets up ideal conditions to promote biological activity in the region. The biological activity can have a positive effect in the region as it can trigger fish production or negative as it can create eutrophic and hypoxic coastal waters (Rabalais et al., 1996). An example of a potential relationship between salinity and nutrient/chlorophyll-a patterns at the sea surface is shown in Figure 1. However, we should keep in mind that the connection between nutrients and Chlorophyll is complex. It displays modeled sea surface salinity modeled field and satellite derived chlorophyll-a (Chl-a) concentration in July 2005. From the sea surface salinity and geostrophic currents in panel (a), we can identify the Mississippi-Atchafalaya River freshwater plume, Loop Current extension and mesoscale activity at the western part of the Gulf. The transport of fresh and nutrient rich

waters into the Gulf by the Loop Current is noticeable around 88°W - 27°N in both salinity and Chl-a fields by the relative low salinity waters and high chlorophyll-a concentration in the area.

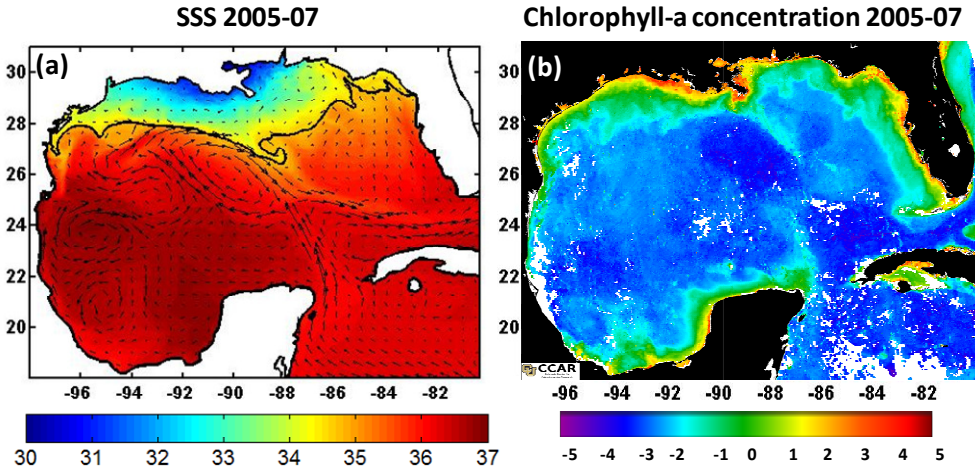

Figure 1. (a) Sea Surface Salinity and geostrophic currents fields (33 psu contour delimited) from ITD-1 model integration described in Chapter 3. The model is forced by observed freshwater inputs only along the northern Gulf coast and not along the Florida Peninsula (b) MODIS ocean chlorophyll concentration.

In this chapter we start our investigation of the different components of the system using hydrographic and nutrient concentration measurements collected during the 2010, 2011, and 2012 summer seasons. In addition to field data we use chlorophyll-a derived from satellite measurements for the same period. We focus in the northern Gulf where our field campaigns sampled the sea surface and the water column. According with the USGS, Six of the thirty-two largest rivers in the United States (Grande, Colorado, Brazos, Atchafalaya, Mississippi, and Mobile) discharge their waters into the northern region of the Gulf. The interannual and multiannual variability of the river discharge lead to different biological activity scenarios in the region. Our measurement campaigns took

place after the annual maximum discharge peak which is typically during April and May, and we sampled the associated river plume extension and nutrient load in 2010, 2011, and 2012. Chlorophyll-a concentration can be interpreted as a tracer of the nutrients distribution and thus of the biological activity. Figure 2 (a) and (c) display the chlorophyll concentration derived from the moderate resolution imaging spectroradiometer (MODIS) on-board the NASA Earth Observing System (EOS) Aqua satellite on July 20, 2011 and May 29, 2012. Areas with high Chl-a concentration in the Gulf cover the Yucatan Peninsula, Florida and Mississippi shelves. The extension of the high Chl-a concentration area around the Mississippi mouth is associated with the magnitude of the river discharge (the highest peak discharge since 1927 was registered in May, 2011. It explains the differences in 2011 and 2012 high chlorophyll area in Figure 2) and the mesoscale features present. As mentioned at the beginning of this chapter, dynamical process such as energetic eddies, internal waves, and the Loop Current all play important roles in the system. Prior studies have provided evidence that patterns of shelf circulation, cyclonic and anticyclonic eddies, and internal waves influence the transport and distribution of nutrients in the Gulf (Chen et al., 2000, Toner, et al., 2003).

The distribution of nutrients in the Gulf is the result of a dynamic system where nutrients are continuously added and removed. The relationship between irradiance, chlorophyll, nutrients, and salinity in the vicinity of the Mississippi mouth around 90°W, 28.5°N was evaluated by Hitchcock et al., (1997), Lohrenz et al., (1990,1997,1999), and Wysocki et al., (2006) using measurements collected from 1988 to 1993 and in 2000. They recorded maximum values of primary production at intermediate salinities and a non-conservative decrease in nutrients along the salinity gradient. They concluded that

primary production was constrained by low irradiance in the most turbid region of the plume and by nutrient limitation outside the plume in waters with associated salinity larger than 30 psu. The influence of fresh water on surface Chl-a and nutrient concentrations was confirmed in the northeastern Gulf of Mexico by Qian et al., 2003 and in the LATEX shelf by Chen et al., 2000. The distribution of our sampling stations allows us to explore the established connection between river input, nutrient load, and chlorophyll concentration in the west, east and vicinity of the Mississippi mouth as a unit (northern Gulf). Because most of the previous measurements were collected around twenty years ago and regulations about land and fertilizer usage have changed in the Mississippi basin over this period, we are interested to see if those regulations impacted the nutrient concentrations in the northern Gulf. In addition, we want to evaluate if the Deepwater horizon oil spill altered nutrient concentrations in the region. Our 2010 field campaign took place one month after the rig was capped on July 15 2010.

The nutrient concentrations and chlorophyll analysis along the salinity gradient at the surface is presented in Section 2.2 along with nutrient limitation analysis for nitrogen, phosphorous, and silicate. The steadiness of the surface relationships described in Section 2.2 is evaluated in the water column in Section 2.3.

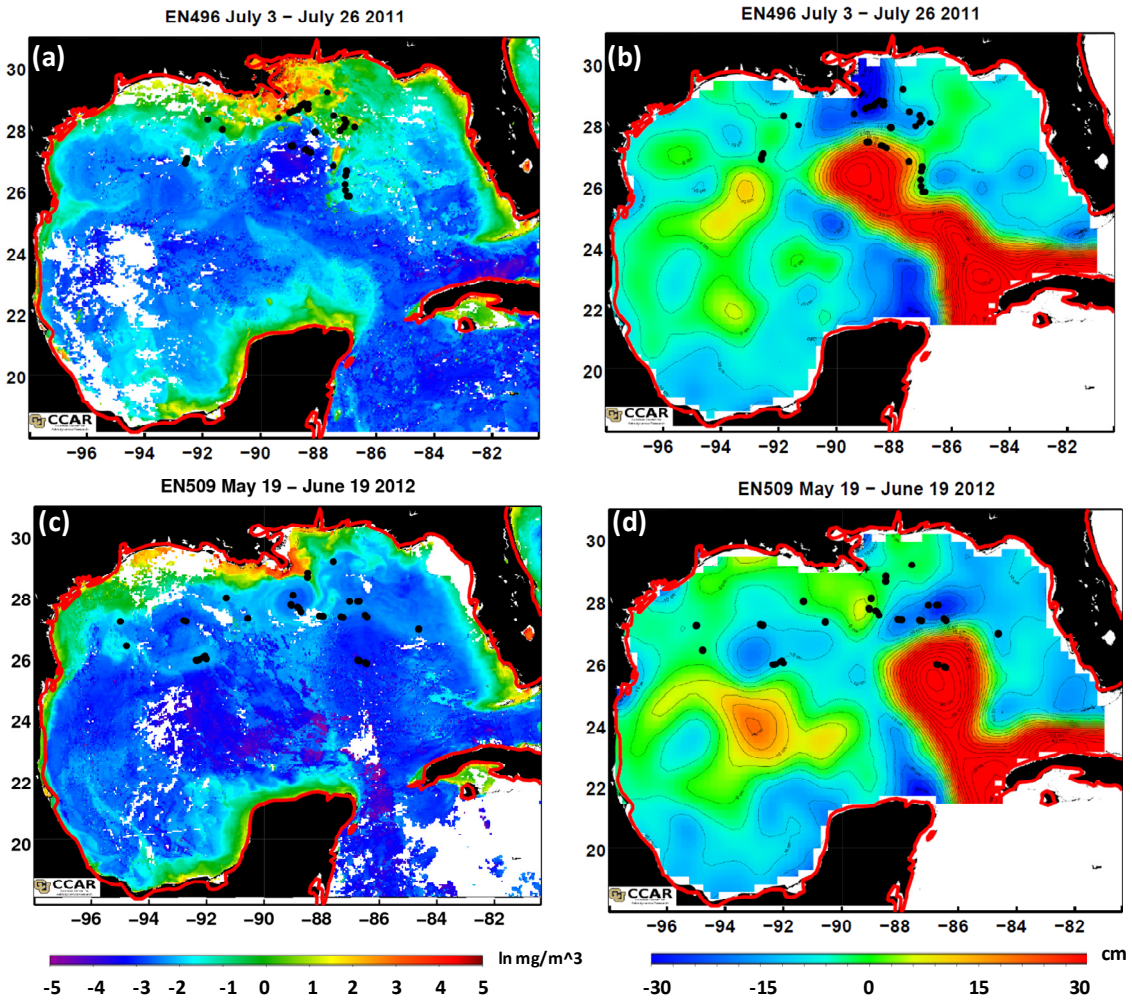

Figure 2. (a) (c) MODIS ocean chlorophyll concentration and (b)(d) Sea surface height anomaly merged solution of Feosat ERM, ERS-1, Topex/Poseidon, ER-2, GFO, ENvidat, Jason-1, Jason-2/OSTM and Cryosat-2. 2011 and 2012 Cruise stations marked as black dots.

2.1 Data

This study analyzed physical and biological data collected during the 2010, 2011, and 2012 summer seasons in the northern Gulf of Mexico as part of the field campaigns associated with the project *nitrogen Fixation, Nutrient Supply and Biological Production in the Gulf of Mexico. NSF0928495*. Samples were collected over the LATEX shelf,

Sigsbee scarp, Mississippi shelf, Desoto Canyon, Mississippi Fan, and west Florida scarp. Surface and water column stations are shown in Figure 3. The domain was sampled at 784 locations at the surface, 121 of them included a water column analysis. The distribution of the stations allowed us to sample along large salinity gradient ranging from 10 to 37 psu. The measurement campaigns took place under very different conditions of the Mississippi river discharge, including the late phase of the 2011 runoff that represents the highest peak discharge since 1927 (http://la.water.usgs.gov/MississippiRiverFlood2011.html). The time series of the Mississippi discharge recorded near to the 306 river mile at Tarbert Landing (2.5 mi upstream from Lower Old River) is displayed in Figure 4. The cruise sampling periods are highlighted in grey shadings and they correspond to: August 22 – September 15 of 2010 (R/V Oceanus, OC468), July 3 – July 26 of 2011 (R/V Endeavor, EN496 and R/V Cape Hatteras, CH07-11), and May 19 – June 19 of 2012 (R/V Endeavor, EN509).

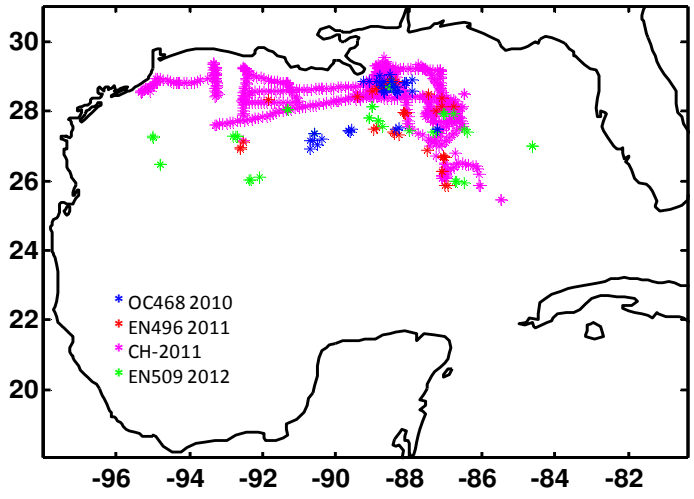

Figure 3. Sampling locations during the 2010, 2011, and 2012 summer cruises.

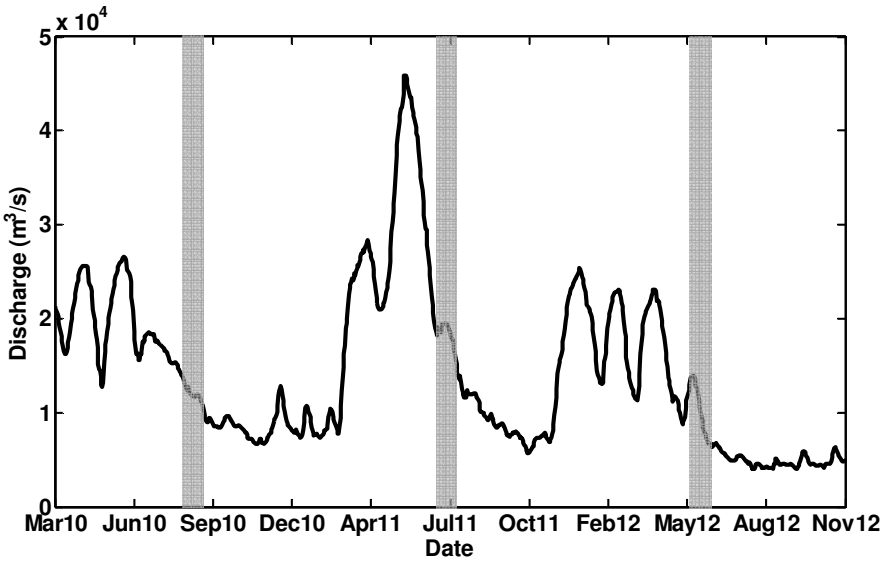

Figure 4. Mississippi River Discharge (m^3/s) at Tarbert Landing station. Cruise times highlighted in grey. (Data from the United States Army Corps of Engineers. Engineering division, hydrology and hydraulics branch).

Seawater was collected at all stations and nutrient analysis was performed for the following macro nutrients: Nitrate, Nitrite, Phosphate, silicate, and Ammonium which are required for phytoplankton growth. A SBE 32 carousel water sampler containing 24 twelve-liter Niskin bottles was used to collect the seawater at depths ranging from surface to ~3200 m. Nutrients were analyzed on board using a SEAL QuAAtro SFA Analyzer immediately after they were collected. When samples could not be analyzed directly after sampling, they were stored at 4°C for no longer than 30 hours (Knapke, 2012). Detection limits for nitrate/nitrite, phosphate, and silicate were 0.05, 0.05, and 0.5 mol L^{-1}, respectively. Along with the seawater sampling, hydrographic data were acquired using a Sea-Bird Electronics, Inc. CTD equipped with conductivity, temperature, and pressure sensors. We also used satellite-derived chlorophyll-a data from MODIS to guide our sampling strategy. We analyzed three day composite maps during the sampling.

2.2 Nutrients, chlorophyll_a and salinity conditions at the sea surface

The distribution of nutrients in the northern Gulf of Mexico is strongly controlled by the discharge of the Mississippi-Atchafalaya River. Seasonal variation of the river discharge and wind patterns determine the nutrient concentrations in the northern part of the Gulf which are usually highest in late spring, following the peak of the river discharge, and lowest during the fall. As described in the previous section our measurements cover three consecutive summer periods (2010-2012) and approximately the same geographical area extending from the Mississippi mouth towards the southwest, the LATEX shelf, and the Sigsbee escarpment.

The evolution of nutrient concentrations along the salinity gradient associated with the river discharges has been analyzed in the close vicinity of the Mississippi mouth by Hitchcok et al., 2006, Lohrenz et al., 1990, 1999, 2007, and Wysocki, et al., 2006, in the LATEX shelf by Chen et al., 2000, and in the northeastern Gulf of Mexico by Qian et al., 2003, but never extending as far into the open waters as in our case. Those previous works reveal the existence of a relationship between salinity and nutrients that is often nonlinear and not monotonic due to different rates of biological activity at different instances and locations. The measurements reported in previous works are compiled together in Figure 5. A total of 281, 157, and 120 Nitrite and Nitrate ($NO_3^- + NO_2^-$), Phosphate (PO_4^{3-}), and silicate (SiO_2) measurements are plotted, respectively. They were collected in April 1988, July-August 1990, and November 1997 through August 2000. In general, an inverse relationship between salinity and nutrients is clearly present in waters with salinity within 0 to 20 psu for all major nutrients.

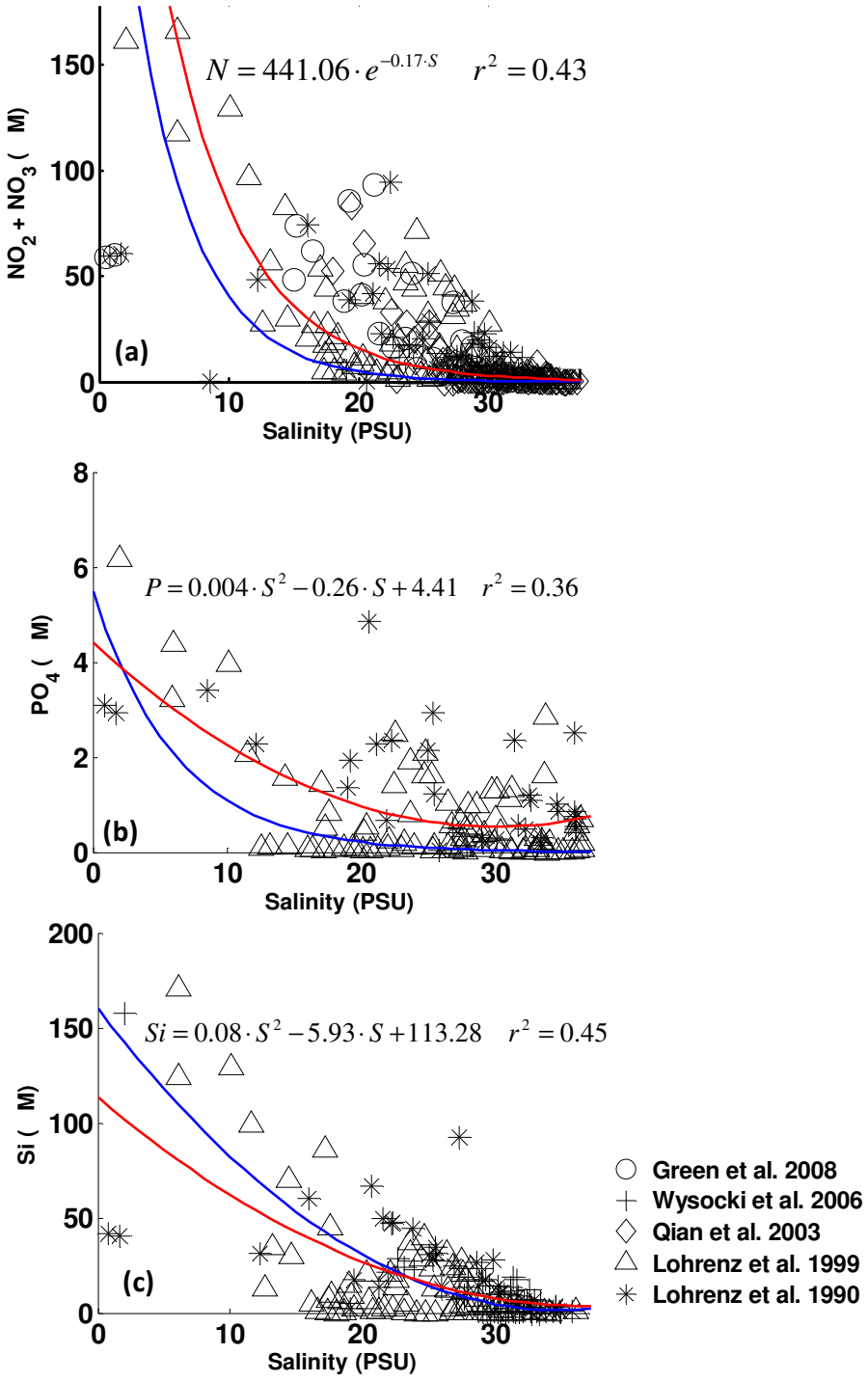

Figure 5. Surface nutrient and salinity distribution for (a) Nitrite and Nitrate, (b) Phosphate, and (c) silicate from previous studies in the region. (—) Best-fit curves for previous work data (equations displayed). (—) Best-fit curves for this study data (2010-2012).

The corresponding examination of surface salinity and concentration of major nutrients from our cruises is presented in Figure 6, Figure 7, and Figure 8, again for Nitrite and Nitrate, Phosphate, and silicate, respectively. We considered a total of 784 data points so our sampling size is about three times (or more) larger than that of the data compiled in Figure 5. Although our stations cover approximately the same area in all campaigns, the extension and magnitude of the river plume in 2011 allowed for sampling a wider surface salinity gradient (10 to 37 psu) than in 2010 or 2012 (30 to 37 psu). In general, concentrations of $NO_3^- + NO_2^-$ fluctuate from 0 to 70 µM with a mean value of 3.24 µM. Nitrite and Nitrate concentrations in waters with associated salinity greater than 30 psu are small, suggesting nitrogen depletion in all years, with mean values equal to 0.1 µM, 0.26 µM, and 0.36 µM in 2010, 2011, and 2012 respectively. Such behavior was also registered in previous cruises over the LATEX shelf in 1993-1994 (Chen et al., 2000), in the Northern Gulf during 1997-2000 (Qian et al 2003), and in the Mississippi mouth area for the period of 1988 to 1992 (Lohrenz et al., 1999).

Overall, high values of $NO_3^- + NO_2^-$ are found in correspondence with low salinities, though the spread is large. Also, the majority of our data points (79%) are confined in a range delimited by $NO_3^- + NO_2^-$ concentrations between 0 - 1 µM and by salinity values between 20 to 37 psu. The depletion of $NO_3^- + NO_2^-$ in intermediate salinity waters is indicative of biological consumption. The curve that best fits the relationship between $NO_3^- + NO_2^-$ and salinity in our data is an exponential function. The goodness of the fit, however, is limited (the coefficient of determination, r^2, is only r^2=0.26) and only a small portion of the data variance can be explained by the exponential function. The majority of

the points not represented by the exponential fit lie within values of $NO_3^- + NO_2^-$, which are greater than 10 µM and are found in the proximity of the river mouth in all years. However, they are close to the best-fit calculated for the previous data in the region which was mainly collected close to the Mississippi mouth. It is confirmed by the coefficient of determination calculated using the estimated nutrient concentrations by the best-fit curves from historical data and our measurements, r^2=0.75; both curves later converge for high salinities.

The relation between phosphate concentrations and salinity is similar to that of $NO_3^- + NO_2^-$ and salinity but with a smaller rate of change. Phosphate concentration varies from 0 to 2.0 µM with a mean value of 0.26 µM. Concentrations close to zero are found in waters with salinity greater than 20 psu. The curve that best fits is again an exponential function with r^2=0.52. Phosphate concentrations from previous data vary from 0 to 6 µM. As a result, the best fit curve from them estimates concentrations in the upper limit of our data range. Finally, silicate concentrations are in the 0 to 80 µM range. They decrease monotonically in the domain bounded by 10 to 23 psu. The best fit curve from previous data is around 1 µM larger than our fit for salinities between 10 to 37 psu. As mentioned, previous data was mainly collected close to the Mississippi mouth where the load of nutrients due to the river discharge is higher. Silicate concentrations associated with intermediate and high salinity waters (>25 psu) are close to zero. The curve that best fits the distribution of SiO_2 versus salinity data is a second order polynomial curve with r^2=0.72. Our and previous best-fit curves for silicate are close. Silica concentrations are conserved along the northern Gulf and are less sensible to the proximity to the Mississippi river mouth. In general, old and new data lie in the same

ranges and follow approximately the same fit-curves if only close to the mouth stations (low salinity) are taken in account.

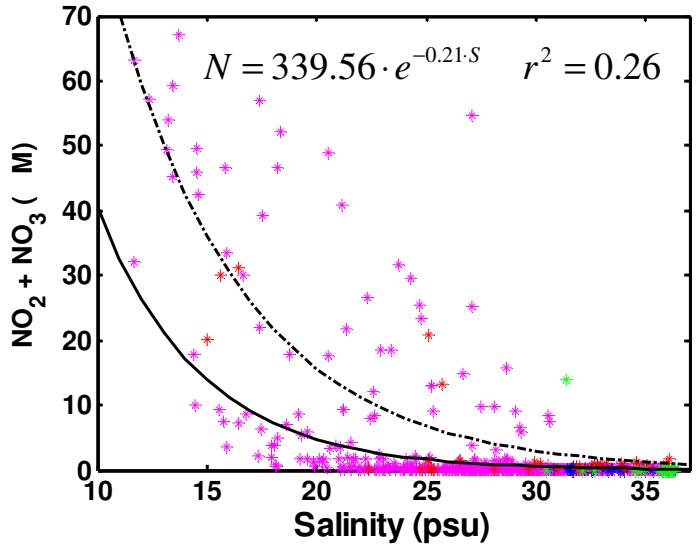

Figure 6. Surface nitrite and nitrate and salinity data distribution in 2010, 2011, and 2012 field campaigns. (—) Best-fit curves for this study data (displayed) and (---) Best-fit curves for previous work data.

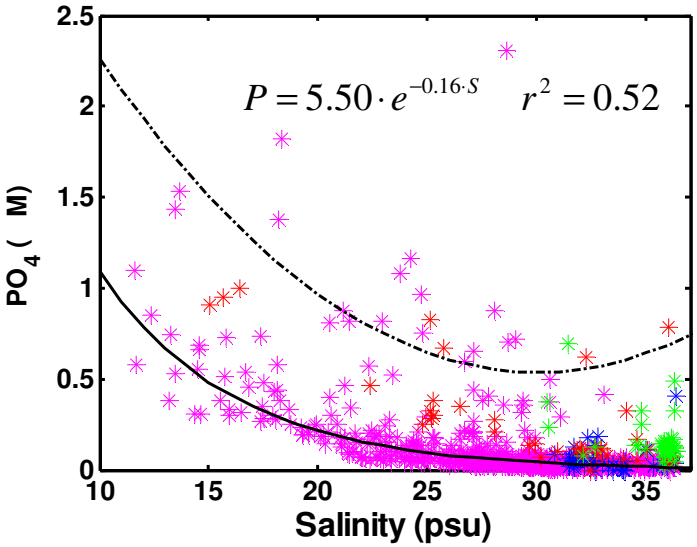

Figure 7. Surface phospate and salinity data distribution in 2010, 2011, and 2012 field campaigns. (—) Best-fit curves for this study data (displayed) and (---) Best-fit curves for previous work data.

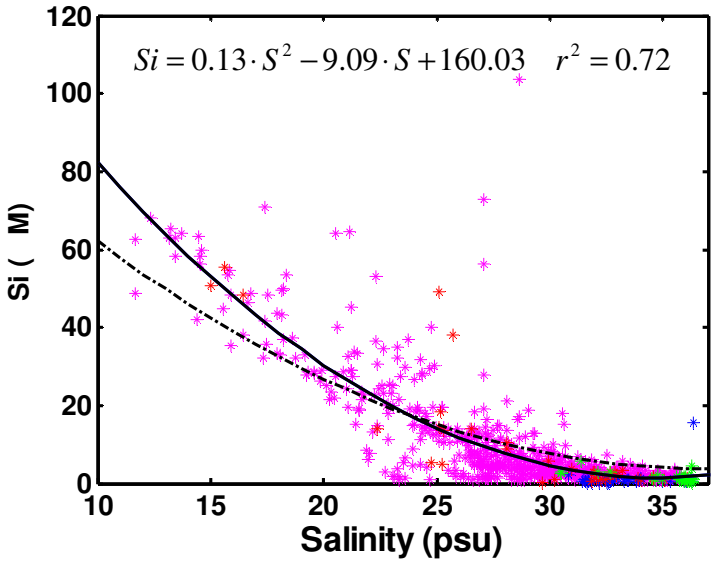

Figure 8. Surface silicate and salinity data distribution in 2010, 2011, and 2012 field campaigns. (—) Best-fit curves for this study data (displayed) and (---) Best-fit curves for previous work data.

Together with the distribution of single nutrients, it is useful to analyze their relative balance to assess if an ocean region can be considered as an optimal or limited system for primary producers. A common measure to evaluate the nutrient balance is the Redfield ratio (Redfield, 1934). It establishes the optimal stoichiometric ratio between nitrogen and phosphorus as N:P=16:1 for ocean biomass. The N:P ratio in the Mississippi River increased from nine in the early 1960's to fifteen in the mid 1980's (Justic et al., 1995). Figure 9 (a) shows the histogram of the N:P ratio for all samples collected. Around 80% of the stations are characterized by ratios below Redfield and 7.4% have ratios above 30. According to Goldman et al., 1979, finding a N:P ratio greater than 30 indicates phosphorous limitation. nitrogen limitation is usually present if $N \leq 1$ µM and N:P<10 (Dorth and Whitledge, 1992, Goldman et al., 1979, Wysocki et al., 2006). Overall, 79% of our stations are potentially nitrogen limited. The relation between the N:P ratio and

salinity is presented in Figure 9 (b) and the spatial distribution is shown in Figure 10. High values of N:P, indicative of phosphorous limitation, are concentrated around the Mississippi and Atchafalaya mouths, in agreement with previous measurements by Loherenz et al., 1999. During 2011, due to the large river discharge, they extended to about 87°W, 27°N where we sampled river plume waters with very low salinity values. In the LATEX shelf, on the other hand, the N:P ratios are low for most of the stations. Finally, an oceanic system may be silicate limited if Si<2 μM, Si:N<1, and Si:P<3 (Wysocki et al., 2003) but these conditions were verified only in one of the stations close to Mississippi mouth .

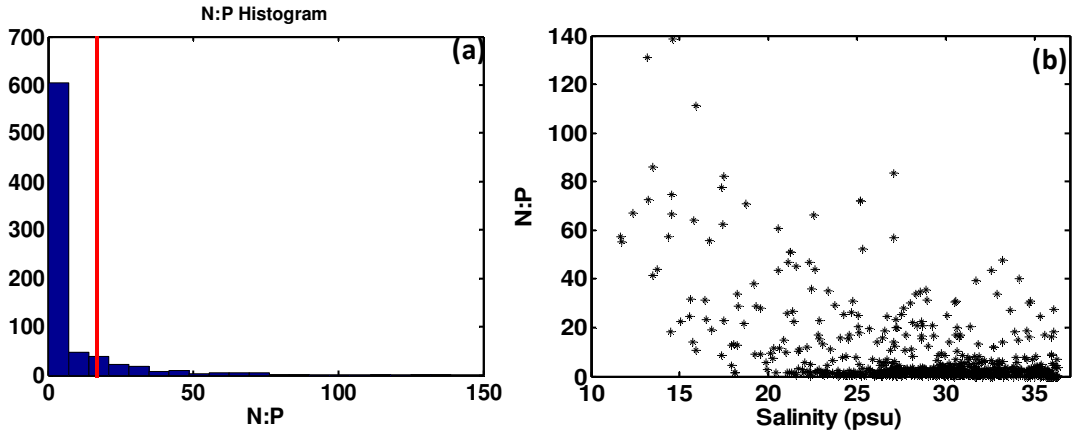

Figure 9. (a) Histogram of the N:P ratio. Red line denote the Readfield ratio N:P 16:1 and (b) N:P ratio versus salinity

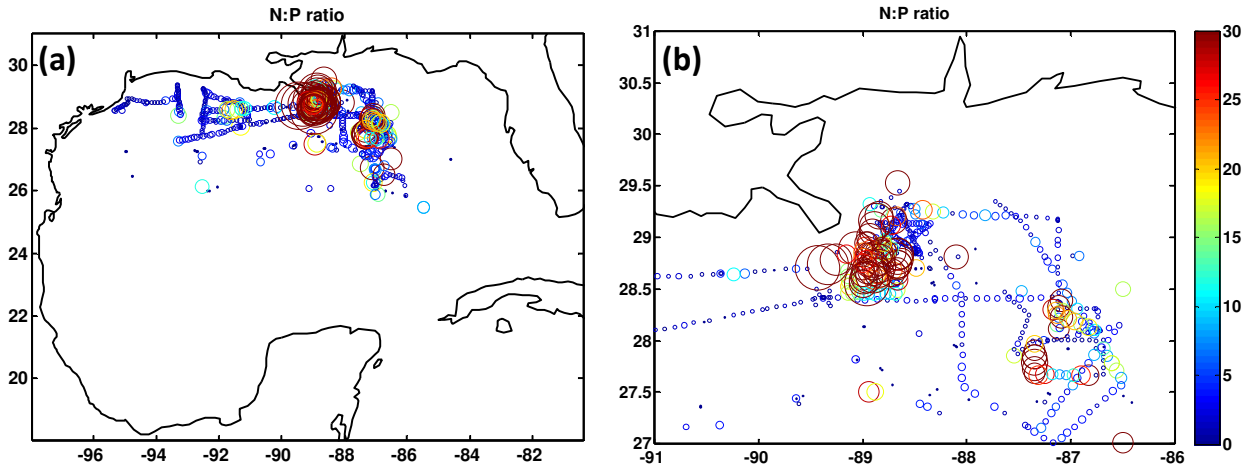

Figure 10. N:P ratio (a) All surface stations sampled in 2010-2012 (b) Zoom in the Mississippi mouth area. The scale was fix with a max of 30.

To conclude this session, we investigated the relation between nutrients and Chlorophyll-a distributions derived from three day composite fields from MODIS. Chl-a concentration provides a proxy for phytoplankton abundance and an indicator of primary productivity. Chl-a varies between 4 to 15 mg/m^3 for the stations with salinities in the 10 to 20 psu range, between 0 to 25 mg/m^3 for waters with salinities in the 20 to 30 psu range, and between 0 to 8 mg/m^3 for waters where salinity is larger than 30 psu (Figure 11 (a)). The Chl-a abundance along the salinity gradient is comparable to the one for nutrients up to 30 psu as shown in Figure 11(b) where nitrite and nitrate concentrations overlap. In low salinity waters (<15 psu) Chl-a is lower than in intermediate salinity waters. This is in agreement with both the N:P ratio results (Figure 9(b)), and with findings in the northern Gulf by Qian et al., (2003), citing to the potential phosphate limitation. In waters with salinity larger than 30 psu, where low nutrient concentrations were measured, on the other hand, it appears to be a significant phytoplankton activity (max 8 mg/m^3). In those waters nutrient concentrations are present in an optimal stoichiometric ratio for biological activity to take place (Figure 10(b)).

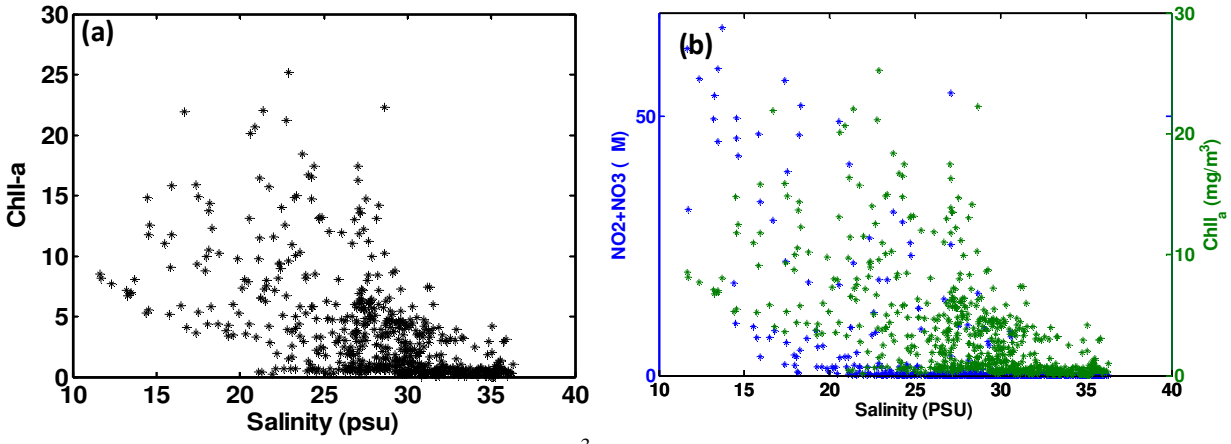

Figure 11. (a) Chlorophyll a (mg/m^3) and Salinity (psu). (b) Chl-a, nitrite, and nitrate versus salinity.

2.3 Nutrients in the water column

The distribution of nutrients in the water column was sampled through 121 profiles during the three field campaigns. In the previous section, we described the relationship between surface nutrients and chlorophyll distributions along the salinity gradient. Here, we explore how nutrient concentrations change in the water column. We pay special attention to the upper layer where light conditions and nutrient concentrations are appropriate for biological activity. The salinity profiles for all stations are shown in Figure 12(a). The x-axis has been restricted to salinities larger than 30 psu at the surface for a better visualization. All profiles display a similar behavior, with fresh water on the top, followed by saltier water below the mixed layer and constant salinity in deep waters (35 psu below 700 m). The nutrient concentration profiles can be seen as a mirror image of the salinity profile. Nitrite and Nitrate measurements in the water column are shown in Figure 12(b) (surface only measurements have been removed). We can then relate nutrient concentrations and salinity in the water column. Panel (c) in Figure 12 shows the

N:P ratio profiles. The N:P ratio is spread over a wide range in the upper ocean where most of biological activities take place and converges to the optimal N:P ratio 16:1 below the top 150 m. Departures from Redfield are all associated with nitrogen deficiencies. Panels (d), (e), and (f) display the upper 200 m. Now, we can distinguish that the fresh water layer is constrained in the upper 40 m and the nutrients spread in the same range in the upper 60 m. The nutrient concentrations continually increases below 60 m until ~700 m where it changes to reach the deep water concentrations of 20 μM, 2 μM, and 30 μM for $NO_3^- + NO_2^-$, PO_4^{3-}, and SiO_2, respectively.

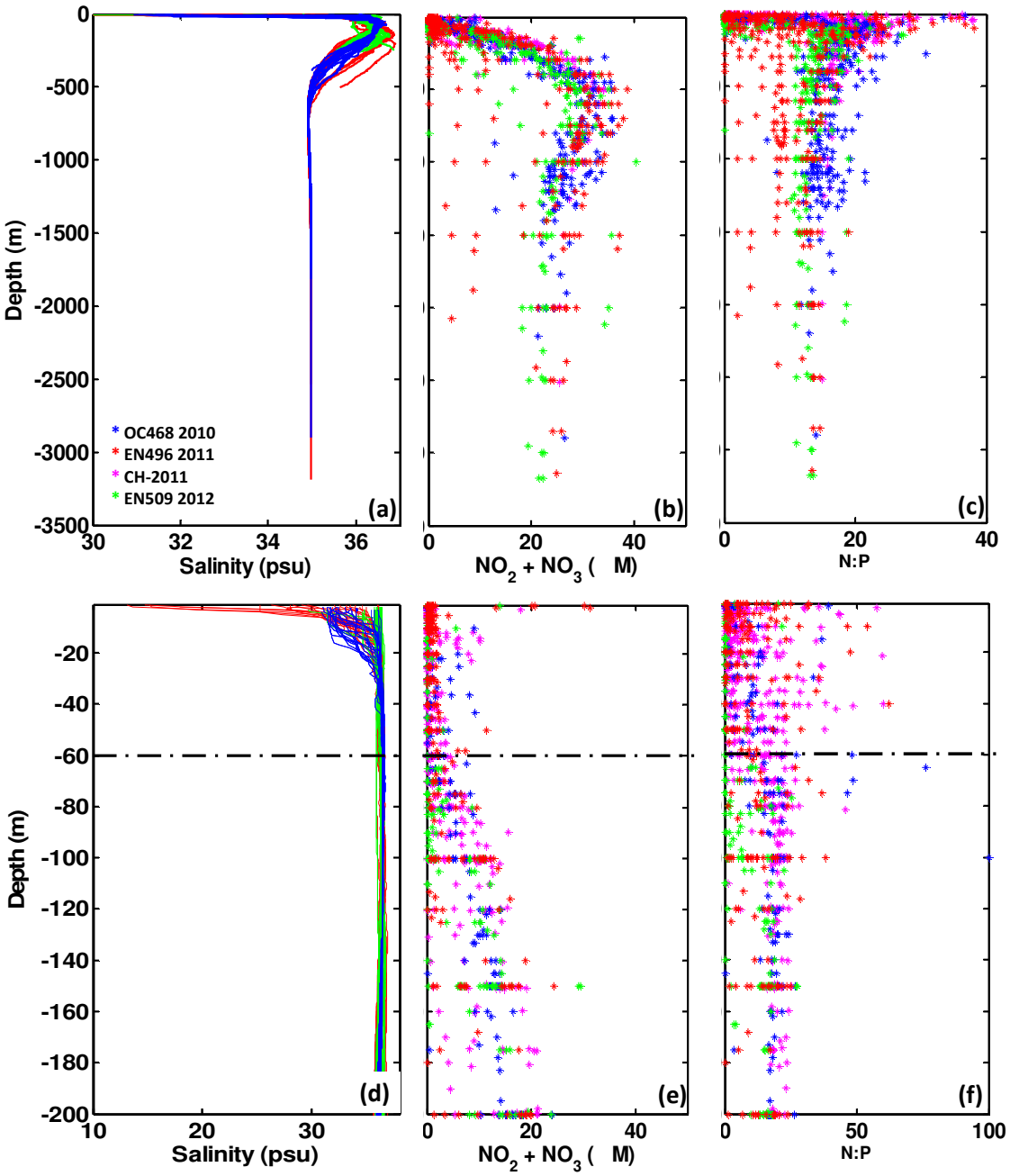

Figure 12. (a) (d) Salinity, (b) (d) Niritre and nitrate concntrations, and (c) (f) N:P ratio profiles across the whole water column (top) and in the top 200 m (bottom)

As a final point, we sought to verity if the established relationship between nutrient concentration and the salinity gradient is consistent through the water column. First, we recalculated it including only the stations where the water column was sampled (121). The recalculated best-fit curves for the surface are shown in Figure 14 (dashed line). Next, we integrated the nutrient concentration in the upper 20 m, 40 m, 60 m, 80 m, and 150 m. The surface relationship was valid in the upper 60 m. The r^2 for the surface best-fits and the integrated nutrients are 0.53, 0.31, and 0.85 for nitrite-nitrate, phosphate, and silicate, respectively. The distribution of the integrated silicate, Nitrite and Nitrate look like the one found for the surface measurements. The surface and integrated best-fit curves are close and follow the same behavior in the salinity gradient. On the other hand, integrated phosphate concentrations for high salinity waters reaches values registered in intermediate salinity waters at the surface. Therefore, while nitrite, nitrate and silicate tend to reduce their mean concentration in the upper 60 m, phosphate concentrations remain the same.

We used 60 m as proxy for the depth of the euphotic layer where most biological activity takes place, and 150 m as proxy for the supply depth (maximum depth where physical processes may contribute nutrients to the euphotic layer). The euphotic layer in the Gulf of Mexico was calculated by Lee et al (2007) from measurements in the Loop Current, West Florida Shelf, and Mississippi River plume waters in April and June 1993. They registered euphotic layer depth ranging from ~4.3 to 82.0 m with associated Chl-a concentration from ~ 0.07-49.7 mg/m^3. Figure 13 displays nitrite and nitrate concentrations at the surface, in the upper 60 m and in the upper 150 m. The largest values are found at the surface and around the Mississippi mouth. It confirmed that the

river input is the main source of $NO_3^- + NO_2^-$. nitrogen integrated over the upper 60 m shows the same patterns present at the surface. The largest values are clustered around the Mississippi mouth while low values populate the west part of the domain. The nitrogen concentrations integrated in the upper 150 m are similar for all stations (Figure 13(c)). Phosphate and silicate exhibit distributions similar to those of nitrite and nitrate (not shown). Phosphate concentrations tend to be constant through the water column. The phosphate range at the surface, integrated at 60 m and integrated at 150 m are (0 - 0.99 M), (0.01 - 0.70 M), and (0.01 - 0.76 M), respectively.

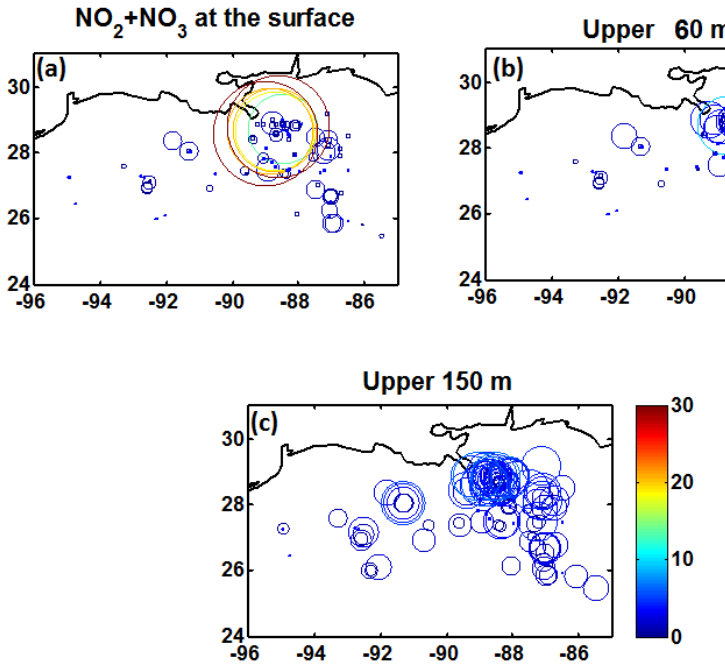

Figure 13. Nitrite and Nitrate concentration in the a) surface, (b) integrated upper 60 m, and (c) integrated upper 150 m.

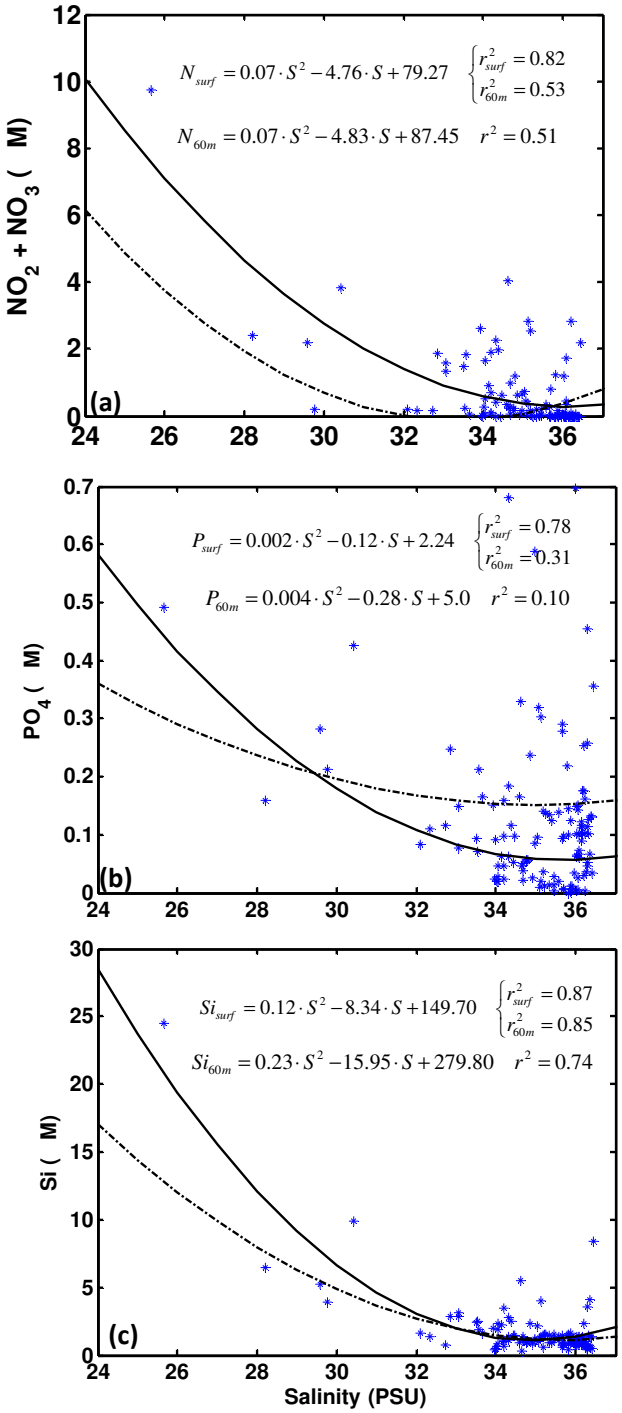

Figure 14. (a) Nitrite and nitrate, (b) phospate, and (c) silicate concentrations and salinity data distribution integrated in the upper 40 m. (**—**) Best-fit curves for the integrated upper 60m. (**---**) Best-fit curves for the surface data.

2.4 Conclusions

A total of 784 locations were sampled at the sea surface during the summer months of 2010, 2011, and 2012 in the northern Gulf. They cover a salinity gradient from 10 psu to 37 psu, an average (2010, 2012) and extraordinary high (2011) Mississippi river discharge, and different stages of the Loop Current extension. The negative correlation between nutrient surface concentration (nitrate, nitrite, phosphate, and silicate) and salinity is strongly influenced by discharge from the Mississippi River. The highest values registered for all nutrients are close to its mouth. However, the salinity and nutrients relationship is not strictly followed along the salinity gradient due to processes that add and remove nutrients in the system as biological activity, mixing, and remineralization.

No major changes in the nutrient concentration were found between the data collected in our field campaigns during in the period between 2010 and 2012 and the measurements from 1988 to 1994 reported by Loherenz, et al., 1990, 1999, Qian et al., 2003, Wysocki et al., 2006, and Green et al., 2008. Nitrate, nitrite, phosphate, and silicate concentrations lied within the same range today as twenty years ago; they also kept a similar relationship with salinity besides changes in the land and fertilizer uses in the basin (Alexander et al., 2008, Turner et al., 2007) and the occurrence of the largest accidental marine oil spill in the history in April 2010.

The biological productivity in the domain is not uniquely defined by the amount of nutrients. It also depends on the relative proportions between them. We follow the criteria used by Dorch and Whitledge, 1992 and Chen et al., 2000. Both N and P could limit

phytoplankton growth in the northern Gulf. A location was considered nitrogen limited if N<1 μM and N:P<10 and phosphate limited if P<2 μM and N:P>30, as a result 79% of our stations are nitrogen limited and 7.9% phosphorous limited. silicate does not limited in the system (only one station out of 784 satisfied the criteria Si<2 μM, S:N<1, and S:P<3; it is located close to the Mississippi mouth). However, the type of nutrient that limits the productivity may vary over time (Loherenz, et al., 1999). The region has been classified as N limited by Johnson et al., (2006), Turner et al., (2007), P limited by Scavia and Donnelly (2007), Sylvan et al., (2006), Johnson et al., (2006) and Smith and Hitchcock (1994) in the past.

Chlorophyll-a concentration derived from MODIS was used as a tracer of the biological activity in the region. The Chl-a concentration was extracted in all surface stations. Chl-a along the salinity gradient behaves in a similar way as all macronutrients analyzed, except that high values concentrate at intermediate salinities instead of low salinities. Similar behavior was registered by Hitchcock et al., (1997). They have concluded that this happens because intermediate waters have longer resident times than low salinity waters close to the surface plume.

Nutrients in the water column distribute in a mirror image of the salinity profile. They converge to 20 μM, 2 μM, and 30 μM for $NO_3^- + NO_2^-$, PO_4^{3-}, and SiO_2 respectively when salinity converges to 35 psu below 1500 m. Also, the N:P ratio reaches 16:1 (Redfield ratio) at around the same depth. Close to the surface, the nutrient concentrations spread from zero to their maximum values. The biological activity, uptake, and other process contribute to the wide spread concentrations in the upper ocean.

However, the relationship between nutrients concentration along the salinity gradient at the surface is conserved in the water column until 60 m depth.

CHAPTER 3

PREDICTABILITY AND MESOSCALE CIRCULATION THROUGHOUT THE WATER COLUMN IN THE GULF OF MEXICO

Predictability in the ocean is limited whenever high levels of kinetic energy are concentrated at spatial scales of few tens of kilometers, usually in the form of eddies or fronts, as their behavior is often chaotic. Furthermore, predictability studies in general are limited by several factors, as noticed by Lorenz (1984). First, climate (ocean and/or atmospheric) models use equations that approximate physical laws. Those equations are usually reduced to the minimum possible number of variables by omission of terms that are very small compared to other terms. Secondly, the ocean (or atmosphere) state is expressed by a finite number of grid points.

While keeping those limitations in mind, this Chapter evaluates the predictability of the circulation in the Gulf of Mexico, answering two questions: (1) Is the deep (> 1000 m) circulation of the Gulf of Mexico predictable, and if so, on which time scale? (2) Are surface mesoscale processes in related to the ones that take place in deep waters so that the reliability of the representation of the surface dynamics in a model can be used as an indicator of the representation of deep circulation as well?. These questions are answered by exploring a) the impact of small variations in the initial conditions, and b) the role of the boundary conditions, in the evolution of the Gulf of Mexico circulation. We do so by using an ensemble of four model integrations for the period 2000-2008 with the Regional Ocean Modeling System (ROMS). ROMS is forced in all runs by identical, monthly varying, heat and momentum fluxes.

The content of this chapter has been submitted to Deep Sea Research II and is currently under revision.

3.1 Model setup and domain

The dynamics in the Gulf of Mexico are modeled using the Regional Ocean Model System (ROMS). ROMS is a free-surface, terrain-following, hydrostatic ocean model (Marchesiello et al., 2003). We implement the IRD version of the code, ROMS-Agrif 2.1 (Debreu et al., 2012). All integrations are on a 5 km horizontal resolution grid that covers the Gulf within the region delimited by (97.9751° W, 80.3849° W) and (18.0236° N, 31.0788° N) (see Figure 15). The vertical resolution is 35 terrain-following layers, with no less than 17 in the upper 500 m in the deepest areas. The minimum depth is set up as 5 m. The model bathymetry is derived from Etopo2v2, which has been smoothed using a Shapiro smoother with r_{MAX} of 0.35. r_{MAX} is defined as a ratio of the maximum difference between adjacent grid cell depths and the mean depth at that point (Penven et al., 2008), which is the maximum slope of topography allowed in order to have negligible pressure gradient errors.

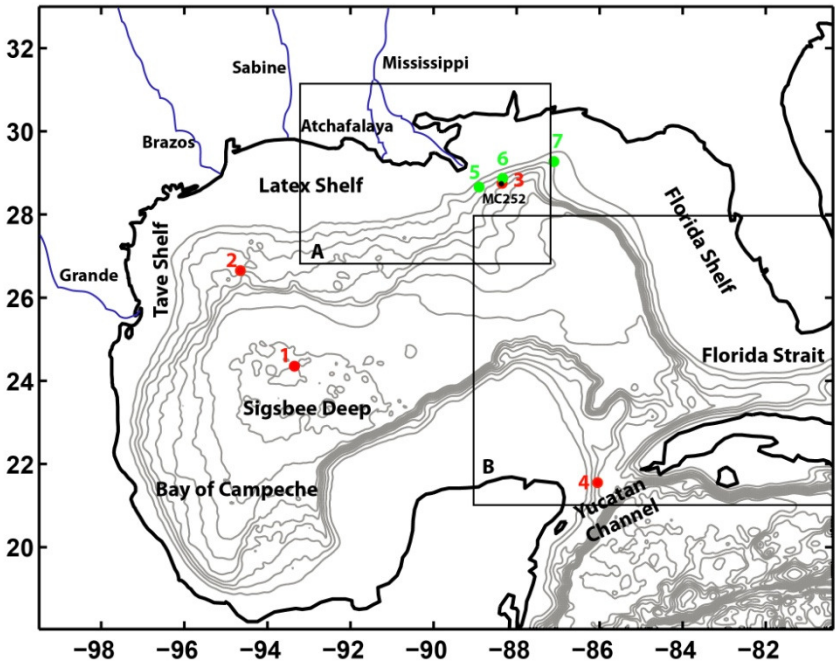

Figure 15. Model domain. Subregion A indicates the nested grid at 1.6 km horizontal resolution for two of the runs analyzed, and subregion B the Loop Current area considered in the analysis in Section 3.4.1 analysis. Temperature and salinity profile locations are marked with green and red dots.

In this chapter we analyze four integrations. They are all initialized from a run forced by momentum and heat fluxes monthly averaged over the period 1958-2008. The fluxes are from the National Center for Environmental Prediction/National Center for Atmospheric Research (NCEP/NCAR) reanalysis (Kistler et al., 2001). The model has open boundaries to the east and the south, and in this spin-up integration, the boundary fields are nudged to monthly fields derived from Soda 2.1.6 (Carton and Giese, 2008), again averaged over the period 1958-2008. The seasonal cycle of all forcing and boundary fields is therefore repeated identically during all years, and the interannual variability in boundary and atmospheric forcing is removed. A stationary state is reached

after two years, and the integration is continued for another ten. Three simulations that retain interannual variability (i.e., interannually time dependent (ITD) forcing), covering the period 2000-2008 are then performed. They are initialized using the last January of the simulation described above with the addition of a small, random perturbation to the velocity field. The ITD runs are forced with monthly varying NCEP/QUICKSCAT blended winds from Colorado Research Associates (version 5.0) (Millif et al., 2004; Chin et al., 1998) and NCEP reanalysis surface heat fluxes. To avoid long-term drifts in the SSTs associated with errors in the NCEP surface fluxes (Josey, 2001), the model corrects the surface heat fluxes in all runs once a month using the National Oceanographic and Atmospheric Administration (NOAA) extended SST (Smith and Reynolds, 2004) at a resolution of 2°×2°. Formally, the heat fluxes forcing the model surface, or QROMS, are calculated according to $Q_{ROMS} = Q_{NCEP} + Q_{ROMS}/dSST_{ROMS}$ x $[SST_{ROMS} - SST_{NOAA}]$, where $dQ_{ROMS}/dSST_{ROMS}$ quantifies the constrained net heat flux sensitivity to SST in the model. Again, the boundary conditions come from Soda 2.1.6, but the interannual variability is now retained, and no further time averaging is performed on the available monthly data. In two of the ITD runs, we exploit the two-way nesting capability of ROMS-Agrif (Debreu et al., 2012), and we introduce a nested area with a horizontal resolution of 1.6 km, covering the region comprised between (97.9751° W, 80.3849° W) and (18.0236° N, 31.0788° N) (see Figure 15, subdomain A). The nested area includes the mounts of the Mississippi and Atchafalaya Rivers and a large portion of the shelf in the northern Gulf. The location of the Deepwater Horizon (MC252), also contained in the nested domain, is show in Figure 15.

The fourth simulation is a variation of the ITD integrations. Instead of interannually varying boundary conditions, we adopt the climatology boundary conditions (BClim) used in the spin-up run, but we retain the interannual variability in the atmospheric fluxes. BClim helps us isolate the role of year-to-year variability in the transport of Atlantic water into the Gulf in the predictability of its circulation. In all of the runs, the fresh-water river input, which plays a fundamental role in setting the density gradients in the Gulf, is directly simulated prescribing the river runoff input of the major rivers: Mississippi, Atchafalaya, Sabine, Brazos, and Grande Rivers. The monthly river runoff series come from the U.S. Geological Service and the U.S Army Corps of Engineers and are all available with at least monthly frequencies over the period 2000-2008. For the remaining rivers, we use climatological monthly varying fluxes.

3.2 Gulf of Mexico mean circulation and model validation

The large scale circulation of the Gulf of Mexico can be approximated to a two layer system (Hamilton, 1990, 2009; Sturges, 1993; Welsh and Inoue, 2000). The upper layer extends from the surface until 1000 - 1200 m depth, and its circulation is dominated by the presence of the Loop Current (LC) that brings salty and warm waters from the Caribbean Sea into the Gulf. The LC path starts in the Yucatan channel and ends in the Straits of Florida, influencing the dynamics along the Florida shelf in its transit (He and Weisberg, 2003; Weisberg et al., 2000). Sometimes, the LC is confined in the southern part of the Gulf, while at others times, it extends northward reaching the Louisiana-Texas shelf (LATEX) before looping and returning to Florida. The LC transit in the Gulf is accompanied by the formation of small cyclonic and anticyclonic eddies through instabilities and interaction with the bathymetry (Hamilton, 2009), and, occasionally, by

the detachment of large anticyclonic eddies, known as Loop Current eddies or Rings. LC eddies travel through the Sigsbee Deep and extend in the vertical to least 800 m (Hamilton 1990; Lee and Mellor, 2003; Nowlin et al., 2000). The Rings may interact with the anticyclonic surface flow in the northwest of the basin while dispersing anticyclonic vorticity (Di Marco et al., 2005; Lee and Mellor, 2003), and usually loose coherency once they reach the continental shelf on the western boundary. The circulation in the southeastern part of the Gulf, in the so-called Bay of Campeche (BOC), is cyclonic and driven by the mean wind stress over this area (Vazquez de la Cerda et al., 2005). Geopotential and sea surface high (SSH) anomalies highlight the permanent cyclonic, gyre-like, circulation within 18°N-22°N and 92°W-97°W, which is amplified and confined by the bathymetry. Its variability results from changes in the size, position and intensity of the gyre and it is linked to the interaction with northern Gulf eddies originated mostly from the LC (Nowlin et al., 2000; Perez-Bruins et al., 2012; Vazquez de la Cerda et al., 2005).

The wind stress is the main driver of the circulation in the Tamaulipas-Veracruz shelf (TAVE), LATEX shelf and the west Florida shelf (DiMarco et al., 2005; Weisber and He, 2003; Zavala-Hidalgo et al., 2003). Wind and circulation vary seasonally in the LATEX shelf (Di Marco et al., 2000; Ohlmann and Niiler, 2005), while no clear seasonal variability has been found in the Florida shelf (Ohlmann and Niiler, 2005). The variability of the anticyclonic circulation in the central – western portion of the basin is driven by a combination of wind stress and LC eddies (Dehaan and Sturges, 2005; Lee and Mellor, 2003; Nowlin et al., 2000; Sturges, 1993).

Below the top 800 – 1200 m, the analysis of historical current-meter mooring data and floats reveals a cyclonic circulation underneath of the LC, in the west central part of the Gulf, and in the BOC. Field measurements demonstrate that the deep circulation in those regions is influenced by topographic Rossby waves (TRWs), intrusions of cold deep water from the Caribbean and vortex stretching (DeHaan and Sturges, 2005; Hamilton, 1990, 2009; Kolodziejczyk et al., 2012; Perez-Brunius et al., 2012; Salas-Perez and Granados-Barra, 2008;Vazquez de la Cerda et al., 2005). TRWs play an important role in the deep circulation of the northwest Gulf, where they manifest as intensification of deep currents over steep bathymetry (Rhines, 1970), and in the Sigsbee escarpment, where the bottom energetic currents are aligned and trapped, and TRWs refract and are reflected by the bathymetry (Hamilton and Lugo-Fernandez, 2001; Hamilton, 2007,2009; Dukhovskoy et al., 2009).

In the eastern Gulf, the circulation at depth is cyclonic and fed by LC water, as shown by DeHaan and Sturges (2005) using historical data and by Lee and Mellor (2003) with model simulations. In the Bay of Campeche the deep circulation is cyclonic, as in the upper layer, and driven by the wind stress curl and the local bathymetry. Vidal et al., (1992) using hydrographic data in this region established that the collision of LC eddies with the south west shelf transfers mass and angular momentum to the south, causing the formation of a cyclonic eddy in the BOC. This was not confirmed by the current meters mooring data analyzed by Perez-Brunius et al., (2012) for the period 2007-2010, that suggest that the variability in the Bay of Campeche is locally driven.

3.2.1 Model Validation

To evaluate the model climatology we consider the geostrophic velocities derived from altimeter products, the velocities measured in the Yucatan Channel (YC) and the temperature and salinity profiles collected during a 2000 Northeast Gulf of Mexico cruise and others assembled in the World Ocean Atlas 2009 (WOA09). First, we compare the surface model geostrophic velocities during the integration period (2000-2008) and the ones derived from the altimeter by Ssalto/Duacs and distributed by Aviso, with support from Cnes (http://www.aviso.oceanobs.com/duacs/). The comparison was made by grouping the data over two periods defined according to the mean wind patterns in the Gulf region. The Gulf of Mexico atmospheric circulation is indeed characterized by two distinct seasons: Southeasterly winds blow between April and August, and Northeasterlies are predominant from September to March. Using sea level atmospheric pressure time series, Zavala-Hidalgo et al., (2003) attributed the seasonality of the wind patterns in the Gulf to the temporal and spatial variation of two high-pressure systems. From September to March the leading wind pattern results from the high-pressure systems that move from the continental United States into the Gulf, while from April to August the mean winds arise from the intensification and westward displacement of the Bermuda high. Figure 16 (a), (b) display the multiannual seasonal mean wind stress for the period 2000-2008 from QuickScat. The remaining panels in Figure 16 show the seasonal mean geostrophic velocities (separated in u_g and v_g components) from the satellite measurements and the four model integrations (no differences are found in the mean circulation between ITD and BClim). The feature that stands out in the domain is the Loop Current. The velocities associated with it are the strongest in the domain and

clearly distinct from anything else. The dynamics in the West part of the Gulf are dominated by eddies shed by the LC. Due to the randomness of this behavior, the velocities associated with them are hidden in the mean fields. Comparing left and right panels in Figure 16(c)-(j), it is clear that the model well represents the surface velocity components in both patterns and magnitude in the whole domain. High values of vg and ug are associated with the LC close to Yucatan Chanel and Florida Strait, respectively.

An important quantity that an ocean model of the Gulf needs to simulate correctly to insure a good representation of the deep circulation in the basin is the transport through the Yucatan Channel. The averaged YC transport in the ITD simulations is 21.43 ± 0.01 Sv to the northwest, and it oscillates between 12 Sv and 30 Sv during the period considered, and 24.26 Sv in BClim. The ITD ensemble spread is used to quantify the uncertainty and such spread is very small (0.01 Sv), indicating that the boundary conditions, identical in the three runs, force the transport. Figure 17(a)-(b) shows the mean transport direction and time series from one of the ITD runs (the time series are indistinguishable within the ITD ensemble). The modeled YC transport (2000-2008) compares well with the observations collected during the Canek program (Sheinbaum et al., 2002) over the period September 1999 to June 2000. The observational estimate is of a net transport of 23.8 ± 1 Sv. Also, the observed mean velocity field along the Yucatan Channel (Figure 2(a) in Sheinbaum et al., 2002) is in excellent agreement with one in the ITD integrations (Figure 17(c) below).

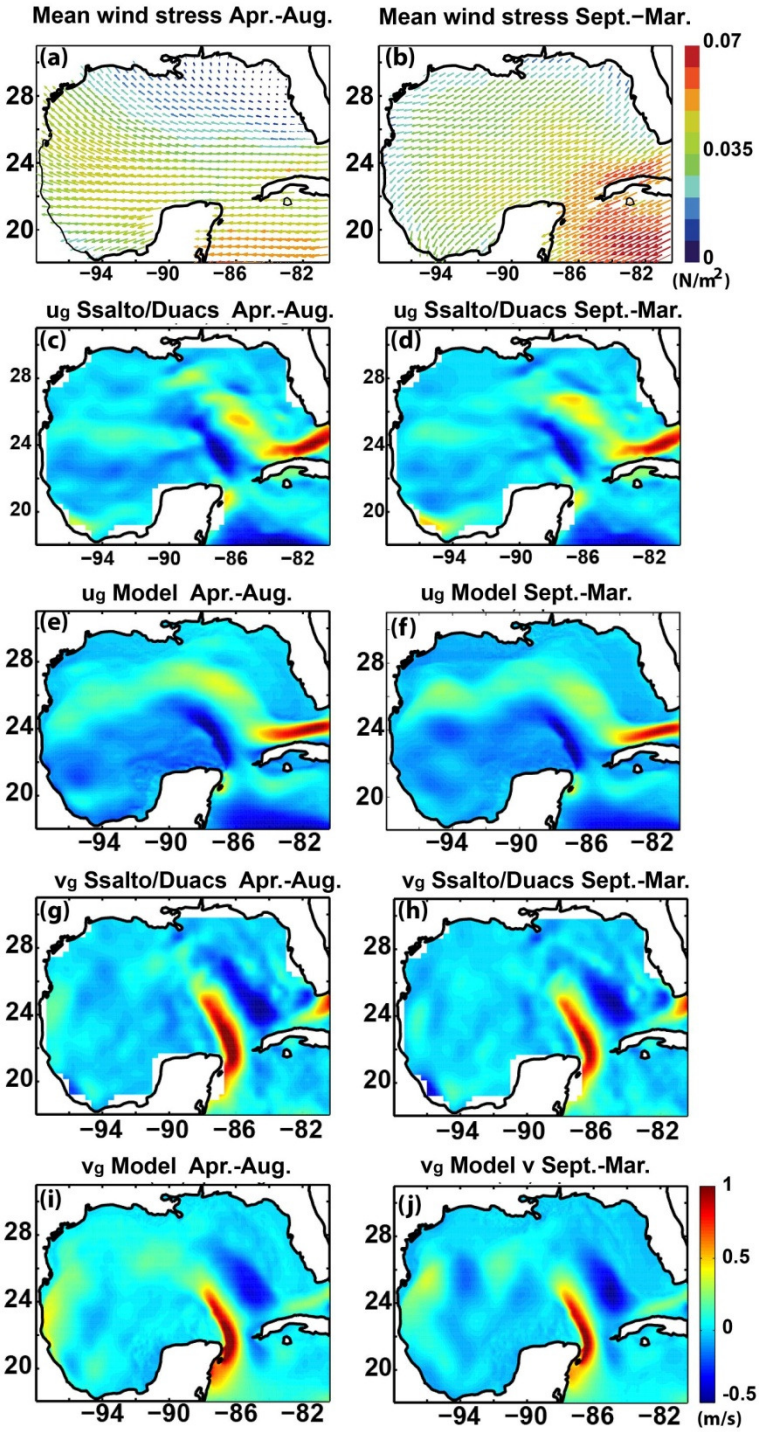

Figure 16. Wind stress (N/m^2) and geostrophic velocity components (m/s), u_g and v_g, averaged for the periods April to August (left panels) and September to March (right panels). (a)-(b) Wind stress (c)-(d) Ssalto/Duacs mean u_g, (e)-(f) model mean u_g, (g)-(h) Ssalto/Duacs mean v_g, (i)-(j) model mean v_g.

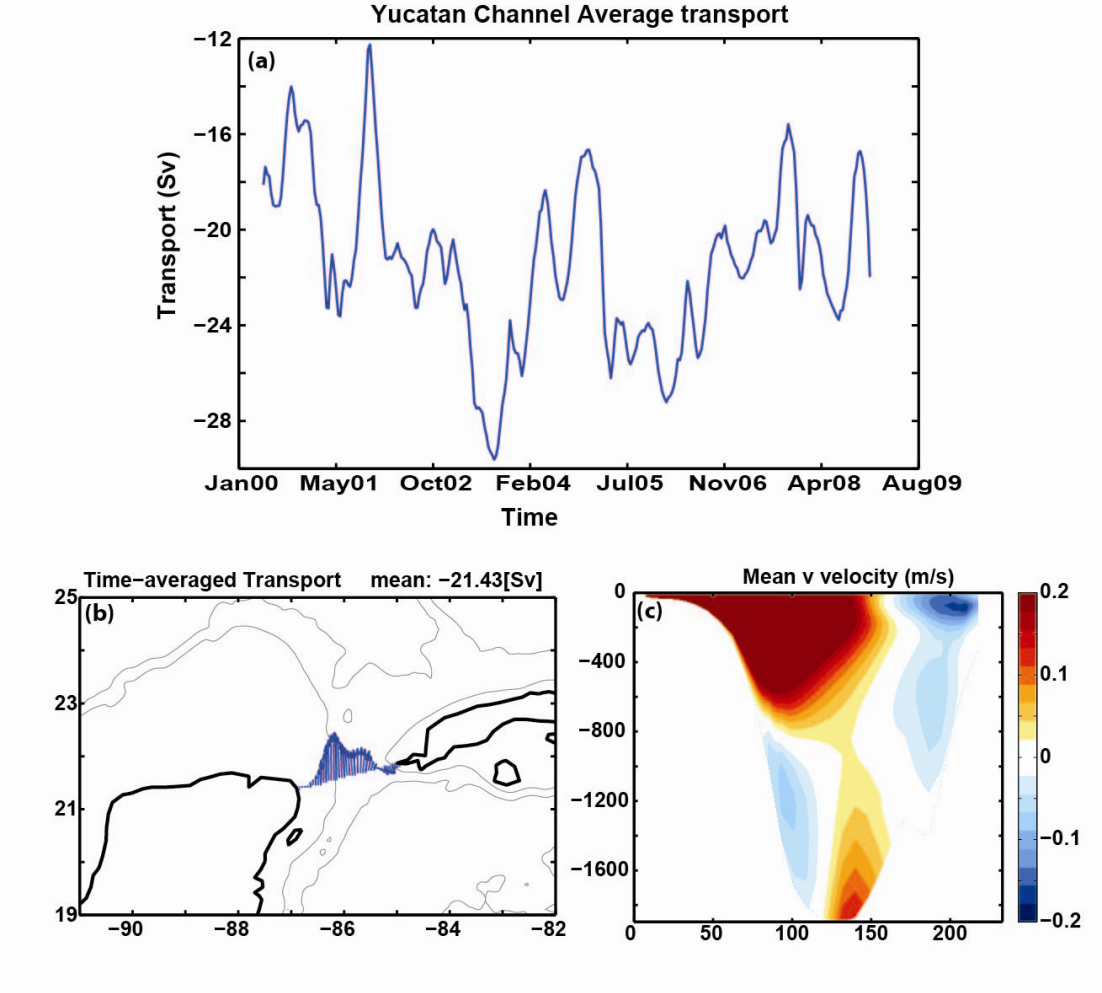

Figure 17. (a) Yucatan Channel (YC) transport time series from ITD1. The negative sign is indicative of transport in the NW direction (b) Mean multiannual tranport direction at YC, and (c) Mean v velocity component at YC.

Our last validation exercise is completed comparing salinity and temperature profiles from the World Ocean Atlas 2009 (WOA09) and from the model over the two main seasons identified previously for the surface circulation in the Gulf. The salinity and temperature profiles are located in correspondence of points 1 to 4 in Figure 15. The salinity profiles (Figure 18 (a)-(d)) from model (red lines) and WOA09 (blue lines) have overall similar shape. The model underestimated the sharpness of the salinity gradients

between the base of the mixed-layer and the main thermocline. However, the disagreement between modeled and observed salinity profiles is limited to 0.25 psu at most. Better agreement is found in the shape of the temperature profiles. In general the model is warmer than WOA09 in the first 1000 m of the water column by up to 1°C. It should be noticed that the modeled means are not expected to be identical to those in WOA09, since the first were calculated averaging nine model years, while the WOA09 database averages all –sparse in time - available records from 1955 until 2006. Panels (e) and (j) display temperature and salinity profiles for locations 5, 6 and 7 in Figure 15. The observed profiles (in blue) are from CTD (Conductivity, Temperature, and Depth) measurements collected by the Northeast Gulf of Mexico (NEGOM) program in Cruise N9 in July 29 and August 1 of 2000, while the modeled ones (in red) correspond to July 30 of 2000 for one of the ITD integrations. The comparison between model and observed profiles clearly improves when using data from the period we simulate, particularly at depth, but we have a limited number of stations available in deep waters.

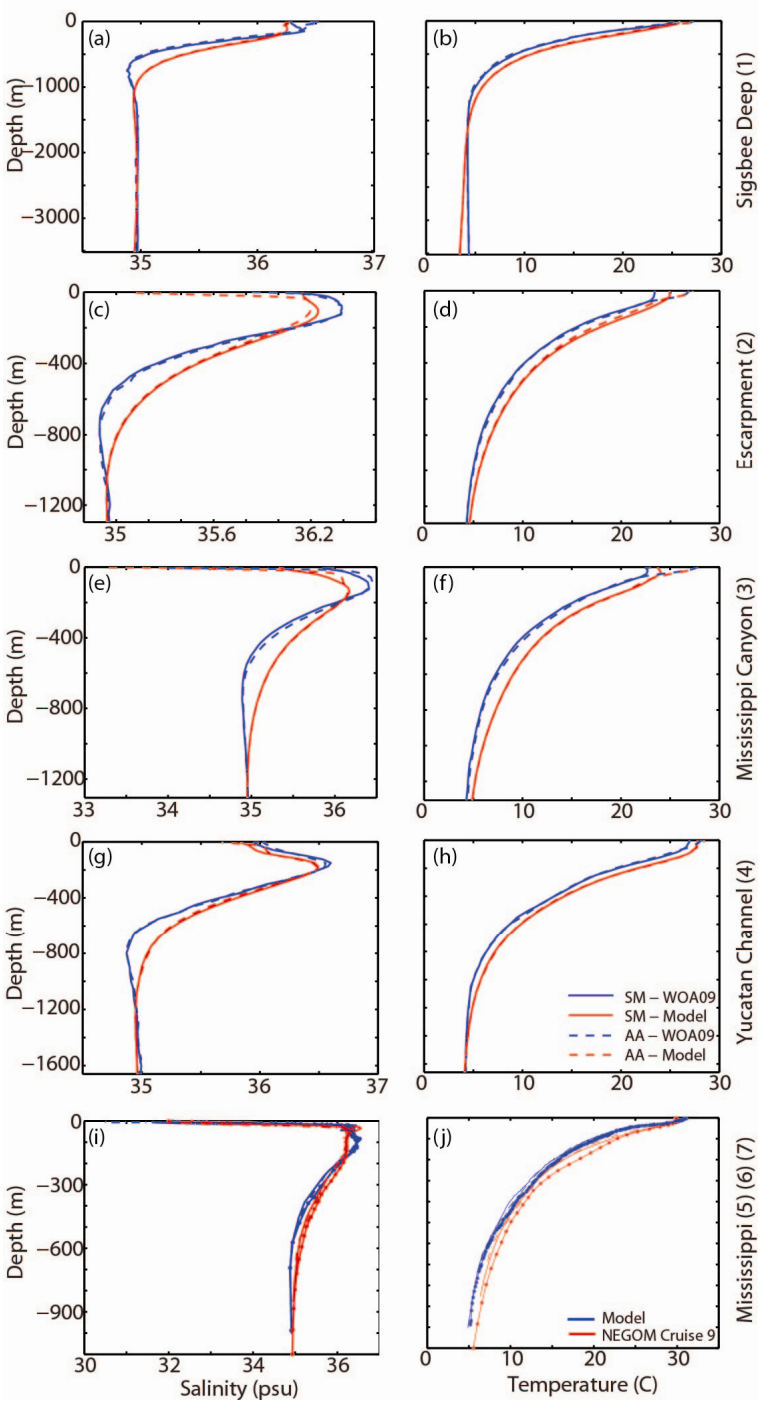

Figure 18. Salinity (left) and temperature (right) profiles at the locations marked in Figure 15. Panels (a) to (h): Model (red lines) and WOA09 seasonal means (blue lines) at locations 1 to 4. Panels (i) and (j): Model (in red) and in situ profiles collected during Cruise 9 of the NEGOM project (blue lines) at locations 5 to 7 on July 29 and August 1, 2000.

3.3 Interannual variability - Model and Observations

As already mentioned, the circulation in the Gulf of Mexico is dominated by the presence of the Loop Current and by the occasional detachment of Loop Eddies. In the following section, we analyze the model representation of the Loop Current variability, its relationship with the Yucatan Channel transport, and the formation and detachment of the Loop Eddies.

3.3.1 Loop Current variability

To quantify the temporal variability of the LC we consider the monthly Eddy Kinetic Energy (EKE) anomalies over the region bounded by [90W - 80W] and [18N - 30N]. This region encompasses the full path of the LC within our domain, from its entrance at the south model boundary until its exit at the east boundary. The EKE is computed as $EKE = \left[\left(u^{'2} + v^{'2}\right)\right]/2$, where $u^{'}$ and $v^{'}$ are the anomalies of the zonal and meridional velocity components, respectively. The anomalies are calculated subtracting first the total mean, u and v, over the simulation period (2000-2008) at each grid point, and then the monthly averages, in order to remove the seasonal cycle. In Figure 19 we compare the monthly EKE anomalies time series derived from satellite altimeter data (Ssalto/Duacs) to the ones from the ITD integrations (a-c), and BClim (d). The average correlation coefficient (cc) between model and observed EKE anomalies time series is cc = 0.43+/- 0.11 for the ITD runs and cc = 0.06 for BClim in the period 2000-2008. Additionally, the ITD EKE time series are highly correlated between them (cc varying from 0.56 to 0.67).

The temporal agreement between the EKE anomalies in the ITD runs and in the satellite data improves SODA performances considerably (the correlation coefficient between surface EKE anomalies in SODA and in Ssalto/Duacs is cc=0.17), likely stemming from the better representation of the mesoscale variability due to the improved horizontal resolution, and is not too far from the correlations obtained using data assimilative models of analogous resolution. For example, the correlation between EKE anomalies in the eastern Gulf in the Hycom-expt. 20.1integration (Chassignet et al., 2007; Counillon F. and L. Bertino, 2009; http://hycom.org/dataserver/goml0pt04/expt-20pt1) and Ssalto/Duacs for the period 2003-2008 and over the same area is 0.63. Incidentally, over the integration period considered, the mean EKE time series is particularly high in 2003, and all ITD runs capture this feature, but not BClim or SODA.

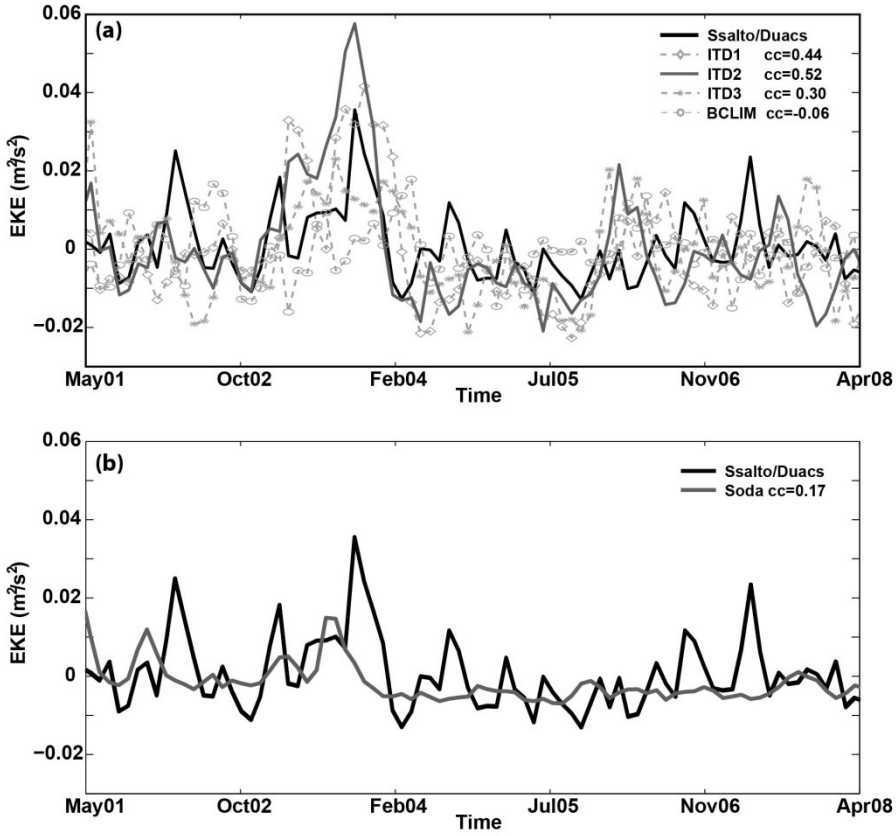

Figure 19. Time series of mean EKE anomalies in the region [90W - 80W] and [18N - 30N] from simulations and Ssalto/Duacs (a) ITD 1-3, BClim, and (b) Soda 2.1.6.

To establish the statistical significance of the correlations above, we computed the Eulerian time scale (T_E) for the basin, defined as the integrals of the autocorrelation functions. T_E was calculated following Chiswell and Rickard (2008), as

$$T_E = \int_0^\infty r_e(\tau)d\tau \tag{1}$$

$$r(\tau) = \lim_{\Gamma\to\infty}\left[\frac{\frac{1}{\Gamma}\int_0^\Gamma u'(t).u'(t+\tau)dt}{\frac{1}{\Gamma}\int_0^\Gamma u'^2(t)dt}\right] \tag{2}$$

where r_e is the autocorrelation function, τ is the lag, and $u'$is the Eulerian velocity anomaly. Given that the model output has been saved every 10 days during the nine years of integration, the correlations were calculated with $\tau = 10$ days. The autocorrelation and Eulerian time scale were computed separately for the zonal and meridional velocity components for six locations along the coast, and six grid points distributed over the deeper central basin (see Figure 20). Independently on the group, the first zero crossing of autocorrelation functions happens after 50 days or less for the sea surface and 30 days at the depth of 1500 m and the comulative integrals provide T_E of 25 and 15 days at most for surface and deep circulation, respectively. Therefore, with a conservative estimate, we consider the EKE anomalies to be uncorrelated on a scale of 50 days or longer for the sea surface and one month or longer for the deep layer (below 1000 m). Using a t-test with 60 degrees of freedom (7 per each year of integration), the correlation between ITD runs and observations is significant at the 95% level if above 0.25.

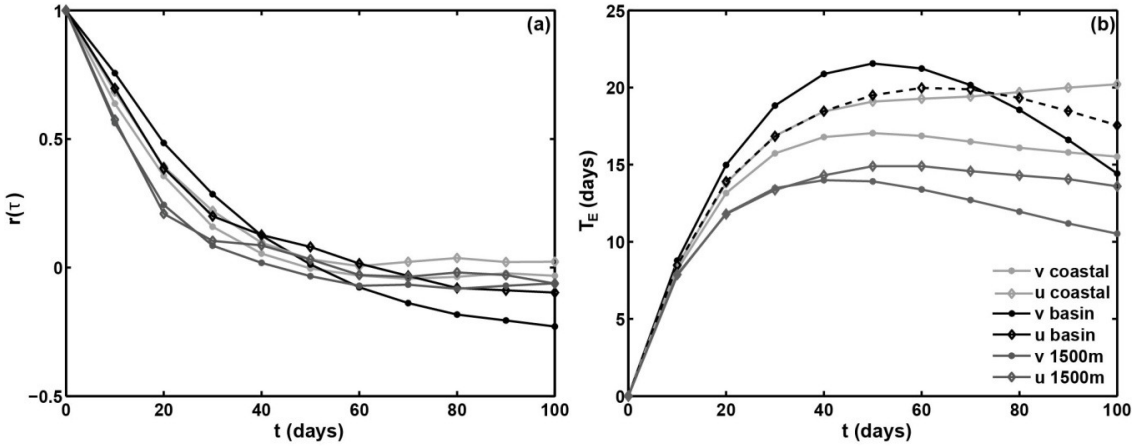

Figure 20. (a) Zonal and meridional Eulerian autocorrelation and (b) cumulative integrals of autocorrelations as a function of lag at the sea surface and at 1500 m depth.

The EKE time series presented provide information on the spatial averaged representation of the surface circulation in the eastern part of the Gulf. Moving our attention to the spatial distribution of the EKE anomalies, we plot the correlation between the modeled EKE anomalies time series and Ssalto/Duacs observations at each grid point (Figure 21). Looking at the patterns of EKE anomaly correlation, we notice that large values are concentrated in specific dynamical features of the Gulf of Mexico (Figure 21 (a)-(c)). Correlations are high in the LC, LATEX shelf, TAVE shelf, and particularly in the Yucatan Channel region. The LATEX and TAVE shelves are well simulated by both ITD simulations and BClim, pointing to the role of the atmospheric forcing as main precursor. Along the shelves the wind forcing is indeed the main dynamic driver of the circulation. Several works (Cho et al., 1998; Cochrane and Kelly, 1986; Nowlin et al., 1998; Waker et al., 2005; Zavala-Hidalgo et al., 2003) have shown that the along-coast wind stress is highly correlated with the local currents. In those regions it can be expected that observed versus modeled correlations will vary over the two main wind seasons. This is displayed in Figure 22, where we compare one of the ITD runs (the other two being very similar) and BClim with the satellite data during September to March and April to August. ROMS performances are better over the LATEX and TAVE Shelves when the wind blows toward the coast, in spring and summer.

Over the Florida shelf, on the other hand, the seasonal maps show that the agreement between the model and the observations improves in fall to early spring but only if time dependent boundaries conditions are implemented. In the YC area, however, correlations are high year-round in the ITD integrations, and always much lower in BClim.

Finally, the west part of the Gulf, away from the shelf region, contains the lowest correlation values in all runs. Its dynamics are affected by eddies originated in the LC and in the Bay of Campeche, whose behavior, and sometimes generation, are chaotic. In this area predictability is limited, and high resolution data assimilative models offer the only way forward to properly simulate the evolution of EKE anomalies.

The differences between ITD and BClim identified so far suggest that the variability imposed by the boundaries is fundamental for the correct representation of the LC dynamics. This has been already noticed by Chang and Oey (2010a), Ezer, et al., 2003, and Oey (1996, 2004) using idealized integrations, and we investigate this possibility next using our runs.

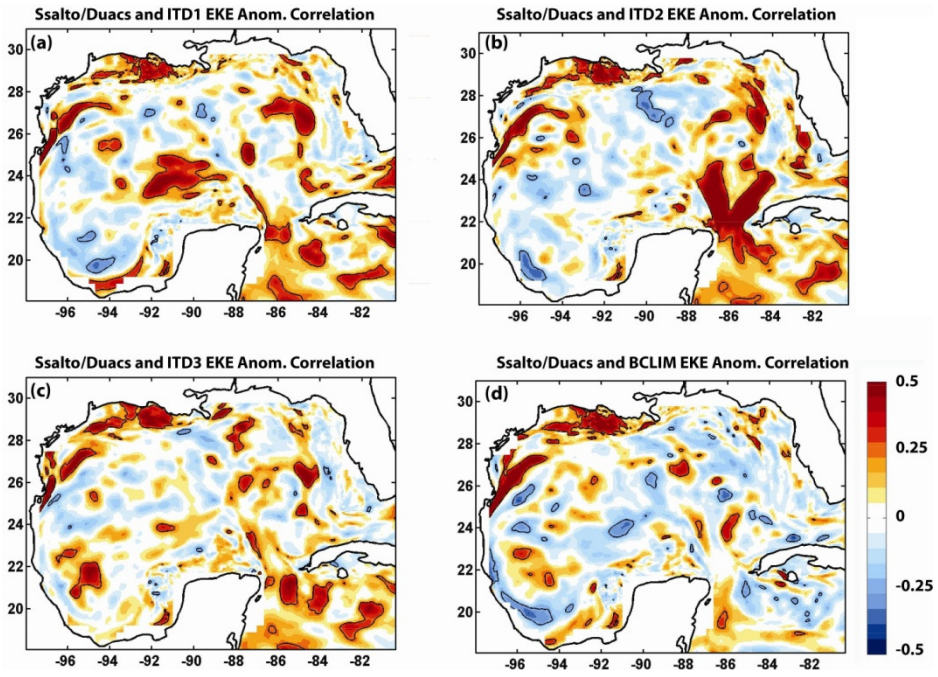

Figure 21. Spatial correlation between the model and Ssalto/Duacs EKE anomalies. (a), (b), (c), ITD simulations, and (d) BClim. Areas where correlations are higher than the 95% significance level are contoured.

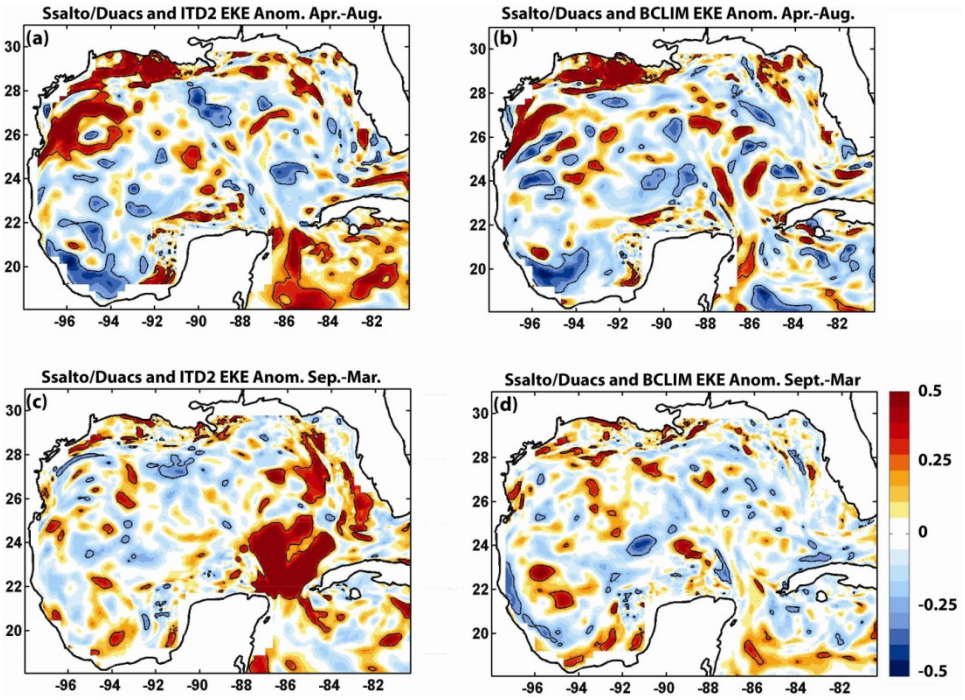

Figure 22. Season spatial correlation of the model and Ssalto/Duacs EKE anomalies. Top April to August. Bottom: September to March. Left to righ t: ITD2 and BClim. Areas where correlations are higher than the 95% significance level are contoured.

3.3.2 Yucatan Transport and its relation with Loop Current extension and West Gulf conditions

The internal variability of the Gulf of Mexico dynamics is strongly influenced by the LC, and the ITD runs are all capable of representing correctly a statistically significant portion of such variability, but not BClim. Thus, the variability of the inflow at the southern boundary of our domain carries important information that commands the LC path in the Gulf.

The interaction between the North Atlantic Ocean, Caribbean Sea and the Gulf of Mexico has been studied by Oey and collaborators with a series of model integrations

(Oey and Lee, 2002; Oey et al., 2003). They performed a variety of experiments with a combination between quasi-realistic forcing and steady conditions. For example in Oey and Lee (2003), the authors performed and analyzed a simulation including annual and monthly climatology boundary conditions, prescribed constant transport at 55W, and time dependant wind forcing. They concluded that the wind stress over the South part of the Atlantic Subtropical Gyre drives the transport through the Greater Antilles Passages, which then interacts with the Caribbean circulation southwest of Hispaniola, where anticyclones grow and drift westward into the YC. The authors conclude that the correct estimation of the YC transport is essential for simulating the Gulf of Mexico dynamics, as all the dynamic information from the Atlantic and Caribbean Sea contributes to it. The links between the YC transport and the LC variability, Loop Eddy shedding, and the overall dynamics in the Gulf of Mexico have been further investigated in a number of studies using numerical simulations (Chang and Oey, 2010a; Ezer et al., 2003; Le Henaff et al., 2012; Oey, 2004). In those papers, the model setup always includes some combination of steady or climatological (monthly varying but not interannually varying) boundary conditions and/or atmospheric forcing. The authors conclude that the LC variability (expansion, retraction and shedding) is correlated with the flow conditions in the YC. They found a correlation in the expansion of the LC and the deep return flow below 800 m at the YC. Also, they conclude that vorticity and transport fluctuations at the YC may explain the irregular eddy shedding. However, they also point out that LC behavior cannot be wholly explained in terms of YC flow conditions due to the complexity of the system.

Our setup in the ITD runs differs from all those previous studies since it includes interannually varying, time dependent surface and boundary forcing, and it is therefore more realistic. We have already shown that at the surface, the ITD integrations represent the EKE anomalies in good agreement with the satellite data (see Figure 21) and the mean circulation around and south of the YC is well reproduced (see Figure 17). If any dynamical link exists between the YC transport and LC variability, then the spatial-mean EKE anomalies time series that represent the LC (Subdomain B in Figure 15) should be temporally connected with the YC transport. The ITD simulations support this idea, in partial agreement with idealized studies by Ezer et , al. (2003), and Oey (1996, 2004), and partially realistic setup in Chang and Oey (2010a) and Le Henaff et al., (2012), as well as observations by Candela et al., (2002). In our runs the mean correlation between monthly EKE and YC transport anomalies is cc = -0.42 ± 0.10 for the ITD ensemble and non significant (cc = 0.0) for BClim (see Figure 23). Comparing the time series, it is also clear that the EKE anomaly peak in 2003 is linked (and proportional) to the higher than normal North-West transport in the YC in the same period. Ezer et al., (2003) performed a similar analysis, studying numerically the variation in the YC and the LC extension in the interval 1993-1996. They implemented a configuration forced by six hourly ECMWF atmospheric forcing, and climatological boundary conditions, imposing a steady transport at 55°W. They compared the total, surface (above 800 m) and deep (below 800 m) inflow transport at the YC and the sea surface elevation, and found a significant correlation between changes in the LC extension and the deep return flow at the YC.

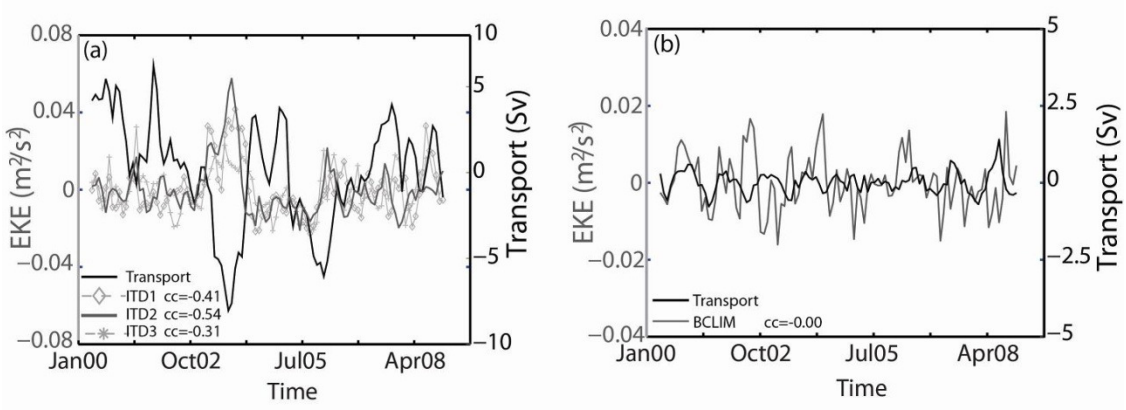

Figure 23. Time series of mean EKE anomalies and Yucatan transport anomalies in (a) ITD1-3 and (b) BClim integrations. The range of the y-axes in panel (b) is half than in panel (a).

3.3.3 Loop Eddies

The LC transit is occasionally accompanied by the formation and detachment of large anticyclonic eddies, called Loop eddies or Loop Rings, sized between 150 and 300 km in diameter. Their surface temperature signature is often lost in seasonal heating of the upper water column, but sea surface anomalies are easily tracked using satellite altimetry (Leben and Born, 1993). Once formed, eddies move westward across the basin at a speed of approximately 2-5 km d-1 (Elliott, 1982; Vukovich and Crissman, 1986), and persist for months to years until they decay through interactions with the continental shelf. The eddy shedding process and driving mechanism are both not fully understood, and stochastic processes are likely to play a significant role (Nowlin et al., 2000; Zavala-Hidalgo et al., 2006). Several hypotheses have been explored on the controlling factors of the LC shedding, focusing primarily on the role of the wind forcing (Chang and Oey, 2010b; Oey et al., 2003), of the Yucatan Channel transport strength (Bunge et al., 2002; Ezer et al., 2003), of the variability in the circulation in the Florida Straits (Sturges et al.,

2009), and of the potential vorticity fluxes into the Gulf (Candela et al., 2002; Oey and Lee, 2003; Oey, 2004). More recently, Lugo-Fernandez (2007) concluded that the LC and its eddy-shedding behave as a nonlinear oscillator with a very short memory, with periodicity and amplitude linked to the North Atlantic Oscillation (NAO), while Chang and Oey (2012) associated the eddy–shedding seasonality (more Loop Eddies shed in summer and winter than fall and spring) to the seasonal variability of the winds in the Caribbean Seas and in the Gulf of Mexico.

The analysis of our simulations suggests that the LC behavior is governed by both stochastic and deterministic components, in agreement, for example, with the work by Oey and Lee (2003) and Nowlin et al., (2000). Oey and Lee (2003), which analyze the LC behavior with both an idealized and a quasi-realistic model set-up, show that the transport and vorticity fluctuations in the YC contribute to the irregular time scale of the eddy detachments, but their results, while indicative of a tendency for the LC to shed preferably under specific conditions, do not suggest that such shedding is predictable.

A detailed Loop Ring separation analysis has been performed by Vukovich (2012) using sea surface temperature, ocean color, sea surface height, and in-situ data from ships in the Gulf of Mexico. Vukovich considered three periods: 1972-2010, 1972-2000, and 2001-2010 due to changes in the eddy shedding periodicity. The average separation period between two consecutive rings is ten months over 1972-2010, nine months over 1972-2000 and eleven months for the period 2001-2010 (Leben, 2005; Sturges and Leben, 2000; Vokovich, 2007). In particular, Vankovich (2012) identifies 13 Loop eddies that shed from the LC between 2000 and 2008. Using the Ssalto/Duacs data, we

find 12 separation events. In the ITD and BClim runs we attest to the shedding of 14, 13 15, and 15 eddies, respectively, and we conclude that the number of eddies detaching from the LC in our simulation is a reasonable result, even if slightly larger than observed. Another characteristic of the LC shedding is that Loop Eddies can form in any month of the year (Vankovich, 2012) as shown in Figure 24, where we compare ROMS integrations and the Ssalto/Duacs data.

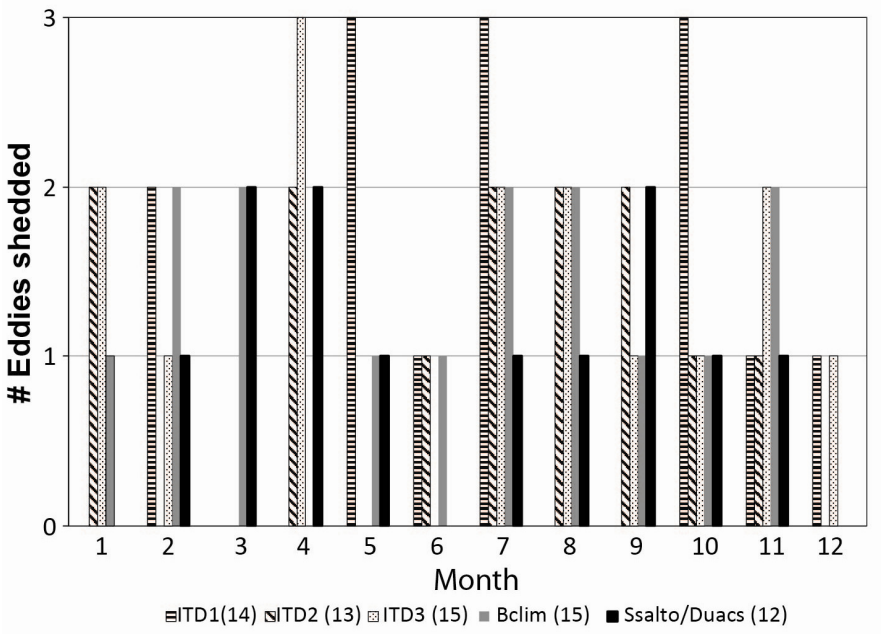

Figure 24. Distribution of the Loop eddies shedded in the period 2000-2008 as funcion of their month of detachment.

Comparing each LC detachment in the model integrations and in the altimetry observations (Ssalto/Duacs), we find that the observed timing (plus or minus two weeks) of few - usually two or three - detachments is correctly reproduced in each run. Table 1 summarizes all Loop Eddy detachments and highlights the ones that match the observations. The greatest number of matches is found in ITD3, in August 2003, September 2004, and November 2007, and in BClim, where the boundary conditions do

not vary interannually, in February 2006, again November 2007, and March 2008. Overall, our results suggest that the local atmospheric forcing in conjunction with the Gulf bathymetry, contribute to the eddy-shedding process, as already proposed by Chang and Oey (2010b) and Le Henaff et al., (2012), but are not sufficient to determine the exact timing of each event.

Table 1. Eddies detached from LC in the period 2000-2008

Ssalto/Duacs	**ITD1**	**ITD2**	**ITD3**	**BClim**
	10-2000	06-2000	10-2000	11-2000
04-2001	05-2001	01-2001	01-2001	09-2001
	10-2001	08-2001	12-2001	
03-2002	05-2002	09-2002	07-2002	01-2002
	10-2002			07-2002
08-2003	05-2003	04-2003	02-2003	05-2003
		10-2003	**08-2003**	07-2003
				10-2003
09-2004	02-2004	11-2004	04-2004	03-2004
	11-2004		**09-2004**	
09-2005	07-2005	07-2005	04-2005	02-2005
		08-2005	11-2005	06-2005
02-2006	**02-2006**			**02-2006**
05-2006	07-2006	04-2006	04-2006	
10-2006		09-2006		08-2006
11-2007	06-2007	01-2007	01-2007	05-2007
	12-2007	07-2007	07-2007	**11-2007**
			11-2007	
03-2008				**03-2008**
04-2008				
07-2008	**07-2008**		08-2008	

3.4 Predictability of the Gulf of Mexico circulation

So far we have compared our integrations to satellite or in-situ observations, highlighting similarities and differences. An ensemble of simulations that differ only slightly in their initial conditions also allows for the evaluation of the potential predictability of a region, even if the model physics or the forcing fields are not perfect and, subjected to model biases. The simulations analyzed here provide a good, even if not

perfect, representation of the general dynamic conditions of the Gulf of Mexico in the period 2000-2008 including multiannual mean velocities, temperature or salinity profiles, EKE variability, and Yucatan transport. The integrations, however, are characterized by significant differences in the timing of Loop eddy shedding. Given that the mesoscale variability associated with the Loop Eddies drives the circulation in the central basin, it is to be expected that predictability would be limited by the stochastic behavior of LC eddies.

The ITD runs share the same momentum and heat flux forcings as well as identical boundary conditions, however, they do not reproduce identical outputs, as noticed in subsection 3.3.3 In this section our goal is to better quantify those differences, comparing the three ITD runs, and to evaluate the role of interannually variable boundary conditions on the mesoscale circulation, comparing the ITDs and BClim outputs. In the following, we use the ITD2 integration as control run, and we analyze the correlation between ITD2 and ITD1/ITD3/BClim for EKE and salinity anomaly fields at the surface and at 1500 m depth. Spatial correlation maps of the time series at each model grid point are presented in Figure 25 and Figure 26. At the surface, all simulations reproduce almost identical results in the LATEX, Florida, TAVE, and Yucatan shelves for both variables analyzed (up to correlations close or equal to one). As pointed out in section 3.2, the circulation of those regions and its variability are mainly wind driven, and the variability at the ocean boundaries does not affect their reproducibility whenever the same atmospheric forcing products are used to force the model. The ITD integrations also show a consistent representation of the surface circulation from the southern boundary to the Yucatan Channel, with correlation coefficients between different ensemble members mostly

greater than 0.6, and slightly higher for salinity than EKE, particularly in the center of the domain. Correlations between ITD2 and BClim are mostly non significant in this area, with the exception of a small region along the northwestern coast of Cuba. High correlations in the EKE maps also identify the quasi-permanent cyclonic circulation in the South West of Campeche Bay, close to the Veracruz coastal area, in all four runs, and contour the LC extension in the ITD2-ITD1 map (Figure 25 (a)), but not in the ITD2-ITD3 one (Figure 25 (c)). This inconsistency between ITD runs again indicates that internal chaotic variability plays an important role in the evolution of the system, and that the behavior of the LC is, for most part, not predictable if only external forcing fields and boundary conditions are known. At 1500 m depth EKE anomalies are not significantly correlated anywhere except south of the Yucatan Channel, where all three ITD runs behave similarly, while BClim displays lower correlation coefficients (Figure 26). Analogous maps are obtained looking at temperature or salinity (not shown). This suggests that the mesoscale variability in the center of the Gulf at depth is independent on the atmospheric forcing and boundary conditions, and the eddy formation, even when associated with bathymetric features, is chaotic, as found in other ocean basins (e.g. Bracco et al., 2008). Summarizing the results of this section so far, we have shown that the modeled circulation is chaotic and unpredictable in the central basin of the Gulf of Mexico, both at the surface and at depth, while is atmospherically forced along most of the shelves.

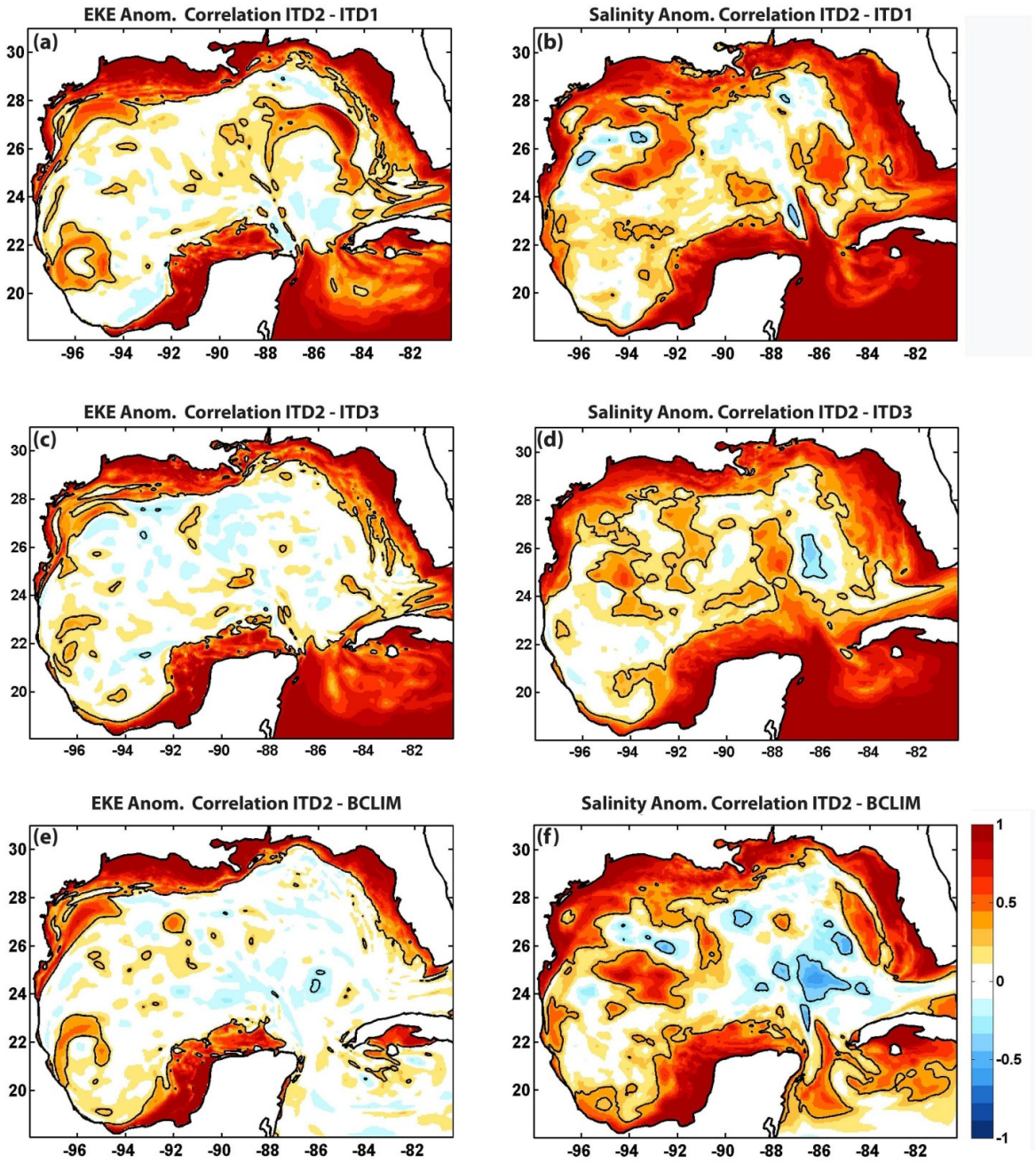

Figure 25. Spatial correlations of EKE anomalies (left) and sea surface salinity anomalies (right) between (a,b) ITD2 simulation and ITD1, (c,d) ITD3, and (e,f) BClim. Areas where correlations are higher than the 95% significance level are contoured.

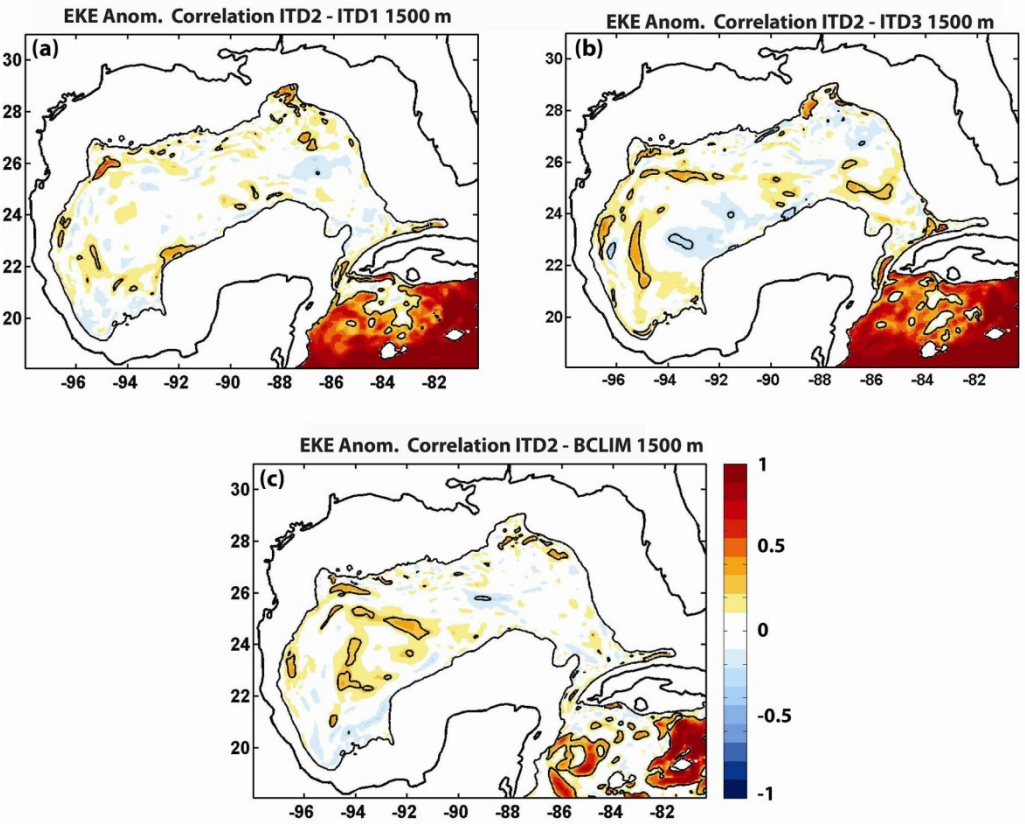

Figure 26. Spatial correlations of EKE anomalies between ITD2 and (a) ITD1, (b) ITD3, and (c) BClim at 1500 m depth. Areas where correlations are higher than the 95% significance level are contoured.

3.4.1 The role of model resolution

Two of the ITD integrations, ITD1 and ITD2, include a nested grid with 1.6 km horizontal resolution in the central north part of the domain (Subdomain A in Figure 15) where submesoscale processes are partially resolved, while ITD3 resolves only the mesoscale circulation at 5 km. The nested area contains the Mississippi and Atchafalaya river mouths, the LATEX shelf, and the location of several natural oil seeps and of the Deepwater Horizon oil spill. In all analyses performed so far, it is evident that nested and not-nested solutions provide a similar representation of the circulation both at the surface and at depth and that resolving the submesoscale details do not substantially improve

predictability in the nested areas. For example, in Figure 27 we show the vorticity field in the nested area from ITD1 and ITD3 in August 19th of 2000. Those two runs showed a similar evolution of the Loop Current during the summer of 2000 but diverged later on. While the representation of the details of the circulation increases in the 1.6 km solution at the LATEX shelf, all major frontal and mesoscale structures are common to the two runs, even if more intense in the nested one. The greater intensity of the vorticity filaments does not affect the predictability in this region at the surface or in the water column. North-south vertical sections of temperature and vertical velocities across the Atchafalaya-Mississippi shelf are displayed in Figure 28. All panels also include a zoom on the shelf region from 28.5°N to 29.8°N. Temperature profiles are very similar (see Figure 28 (a)-(b) and their insets), despite changes in the model representation of the topography. The roughness of the sea floor, which is better resolved in the nested simulations, is associated with the differences in the vertical velocity fields, with larger velocities meaning greater bathymetry gradients. Those differences, however, are not sufficient to drive significant density changes, and 5 km horizontal resolution is thus sufficient in our model set-up for a proper representation of the main dynamical features in the Gulf and also over the continental slope. An important caveat to this conclusion, however, is that we imposed monthly varying momentum and heat fluxes, which do not resolve the inertial frequency for the Gulf of Mexico. The use of high frequency atmospheric forcing is likely to change more dramatically the representation of vertical mixing by exciting quasi- and near-inertial waves as ageostrophic expression of the mesoscale eddy field (Cardona and Bracco, 2012; Danioux and Klein, 2008), and may potentially influence the density structure of the water column. On the other hand, we do

not expect that the frequency of the atmospheric forcing will significantly change the eddy population and, therefore, the predictability potential for the region.

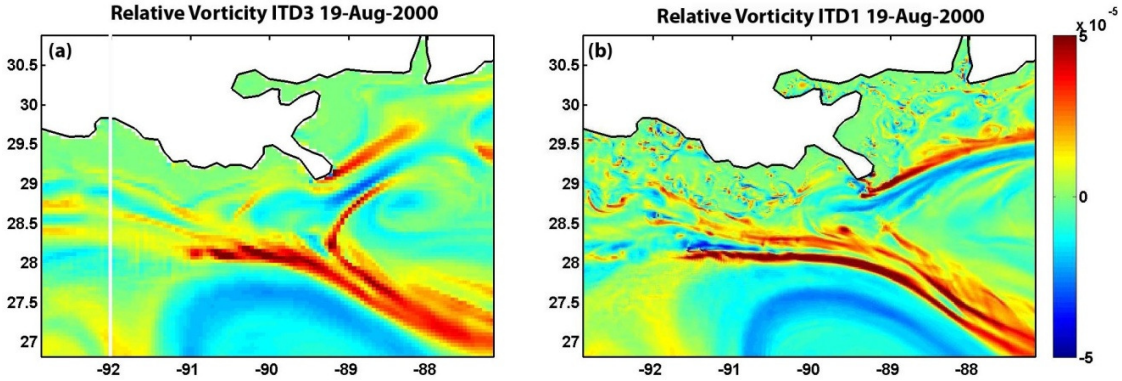

Figure 27. Relative vorticity field in the nested area on August 19, 2000. (a) ITD3 (no nesting) and (b) ITD1 (nested). The solid white line indicates the cross-section shown in Figure 28. Unit s^{-1}.

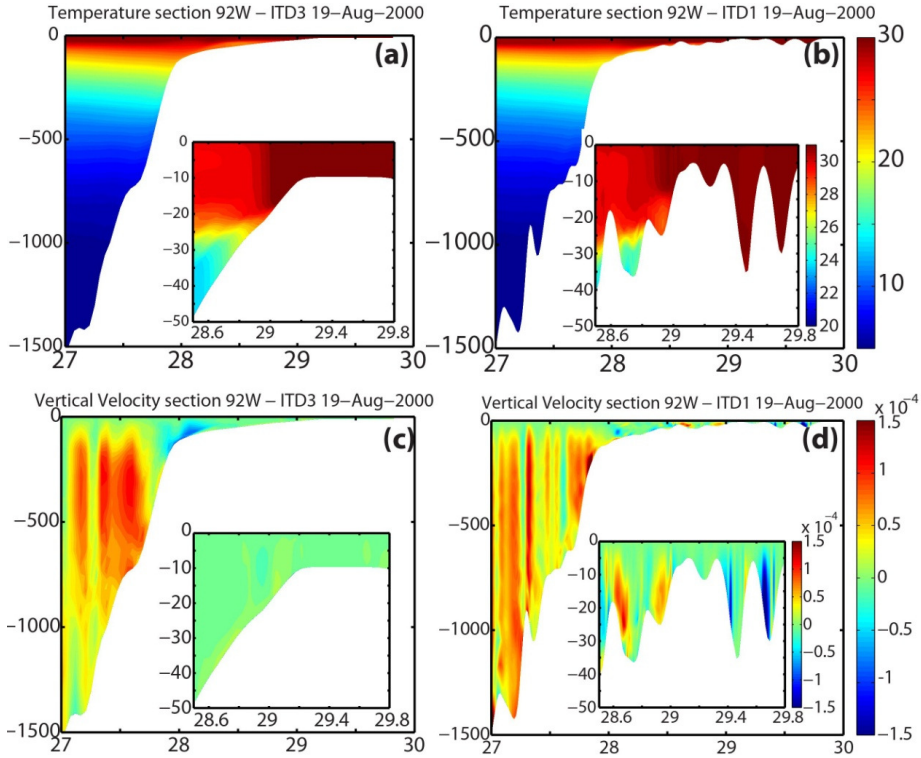

Figure 28. Vertical profiles across the section indicated in white in Figure 27, from top to bottom, of temperature in ^{o}C and vertical velocity in m/s. Left: ITD3. Right: ITD1. Zooms in the shallow region from 28.5°N until 29.8°N are displayed as insets in each panel.

3.5 Deep and surface circulation connections

The aim of this section is to explore the relationship between the surface and deep mesoscale circulation in the Gulf and to establish if and where knowledge of the surface mesoscale dynamics (as provided for example by satellite data) can be used to infer something valuable about the variability at different depths. In other words, can an assimilative ocean model, which provides a detailed and faithful representation of the surface dynamics at the mesoscale (or submesoscale) level by assimilating satellite data, help with predicting the mesoscale variability at depth, in spite of the absence of a detailed set of continuous in-situ measurements? Such question is particular relevant for the Gulf of Mexico, where deep ocean drilling is likely to continue.

As mentioned in Section 3.2, the Gulf behaves, approximately, like a two-layer system, with a top layer extending to approximately 1000 m and, the one below it extending to the bottom. The two layers display different large scale circulation patterns (Hamilton, 2009). The first question we pose in analyzing our runs is relative to the role of mesoscale variability at depth. Its relevance to the circulation can be measured by the ratio of EKE and kinetic energy (KE). EKE is computed as described in section 3.3.1 and kinetic energy is simply $KE = [(u^2 + v^2)]/2$, where u and v are the zonal and meridional horizontal velocity components of the flow field, respectively, after removing the seasonal cycle. We calculated the seasonal mean of EKE and KE ratio at the surface, 500, 1500, and 2000 m depth for all simulations. Results are almost identical between runs, and in the following we display only ITD1 (Figure 29). Regions with small EKE/KE values are indicative of limited mesoscale variability. In those regions, the knowledge of the mean flow and currents is sufficient to describe the circulation. On the

contrary, eddies, filaments, and transient coherent structures dominate high EKE/KE ratio areas. At the surface, small EKE/KE ratio areas are found in correspondence to the Yucatan, Florida, LATEX, and north part of TAVE Shelves, where the circulation is predominantly wind driven. Additionally, low EKE/KE values contour the inflow and outflow paths of the LC. Around the Florida and LATEX shelves lower values of EKE/KE ratio are found in the fall-winter season, in association to Northeasterly winds, than in spring-summer. On the other hand, ratios close to one populate the central basin of the Gulf, where mesoscale structures control the dynamics. A similar analysis was conducted by Nakamura and Kagimoto (2006) in the North Atlantic using the output from an eddy-resolving model that integrated particles trajectories. The authors concluded that eddy mixing is repressed in small EKE/KE ratio areas, and that those regions act as mixing barriers. Particles traveling in small EKE/KE regions move along the mean flow, while, in contrast, they follow chaotic trajectories in large EKE/KE ratio areas where eddy mixing is large. This is in agreement with the analysis of particle trajectories in the Gulf of Mexico by Ohlman and Niiler (2005). The authors analyzed more than 750 surface drifters deployed over the northern Gulf shelf during the period 1993-1998 as part of the SCULP observational program, and concluded that the mesoscale circulation was responsible for moving the drifters away from the shelf, where all were released, and into the Gulf and then out in the Atlantic Ocean. At 500 m and below, EKE/KE ratios are not affected by the seasonality of the wind field and almost identical maps are obtained for both seasons. Low EKE/KE values linked with the inflow/outflow LC paths are still visible at 500 m, but not at 1000 m or below. The central part of the basin is consistently populated with high EKE/KE ratio values through

the whole water column. Values around or lower than 0.5 can be found only at the south west corner of the Sigsbee Deep and Bay of Campeche, where the deep water circulation is locally controlled by the bathymetry.

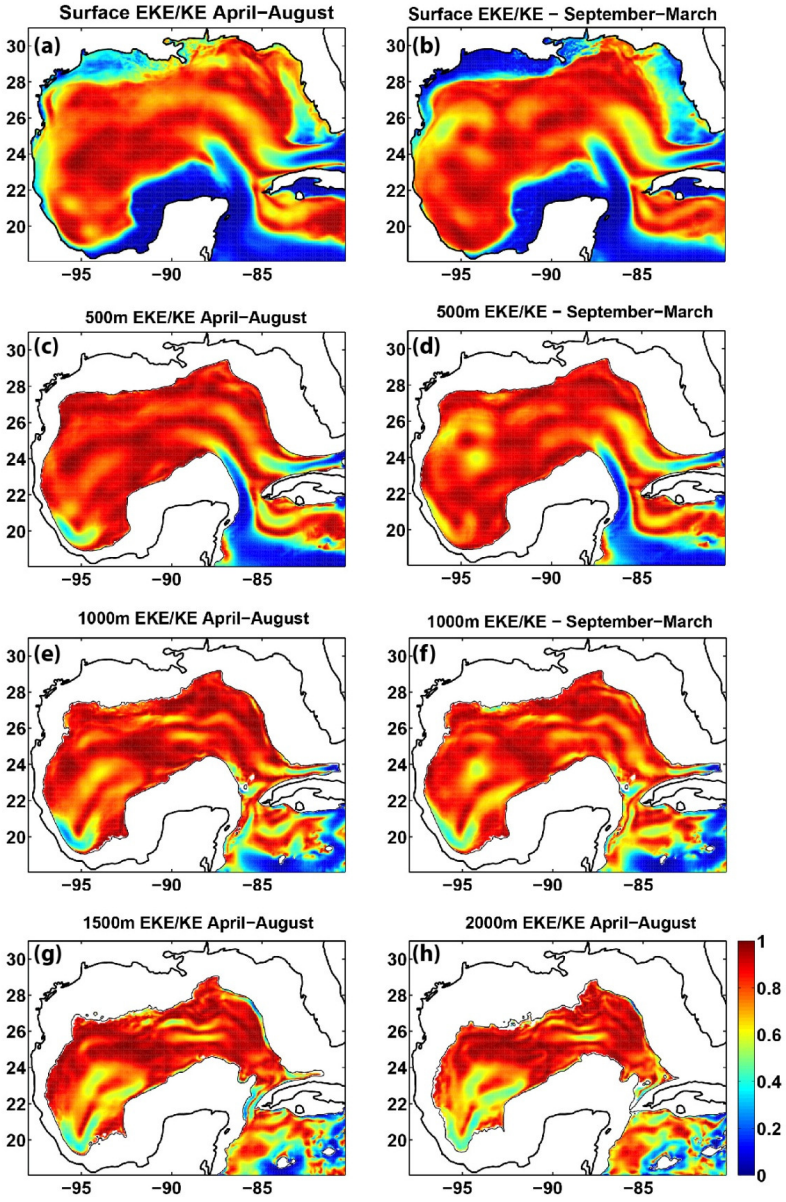

Figure 29. EKE/KE ratio in ITD1 for the period April to August (on left) and September to March (on right) . Top to Bottom: Surface, 500 m, 1500 m, and 2000 m.

Next we consider the correlation between monthly anomalies of the relative vorticity field at the surface and 500 m, 1000 m, 1500 m, and 2000 m for each grid point. The correlation maps are displayed in Figure 30. The mesoscale circulation at 500 m is highly correlated with the surface one (Figure 30 (a)). As described in section 3.2, LC and LC eddies disturbances extend to at least 800 m in the water column. Below 1000 m, correlations between vorticity at depth and at the surface decrease drastically. High values are restricted to mesoscale features formed by interaction of the mean flow with the bathymetry at the southwest corner of the Sigsbee Deep, around the Sigsbee Escarpment (around 26° N - 92°W), in the LATEX Slope, and Mississippi Canyon. Below the Loop Current, immediately north of the Yucatan Channel, we also find correlations between 0.3 and 0.5. At 2000 m, even fewer areas are significantly correlated with the surface, and those are concentrated at the LATEX Slope, the southwest corner of the Sigsbee Deep, few spots in the Bay of Campeche, and in the central portion of LC path. This analysis suggests that the dynamics over most of the Gulf of Mexico are dominated by mesoscale features at all depths, the eddy component drives the kinetic energy evolution, and surface mesoscale structures are not representative of what happens below 1000 m.

In Figure 31 we then show the correlations between the monthly anomaly vorticity time-series at 2000 m and the ones at 1500 m, 1000 m, 500 m and again 5 m (this last map is obviously identical to Figure 30 (a)). The mesoscale variability at depth is a better indicator of the structures found at 500 m than the surface mesoscale is of the structures at 1500 m. This suggests that the interaction of the deep currents with the topography is

more important than the interaction between the atmospheric forcings and the surface circulation in influencing the dynamics across the water column. It is important to notice that if we had used velocities or EKE anomalies instead of relative vorticity, maps would have shown lower correlation values (approximately 0.15 lower everywhere).

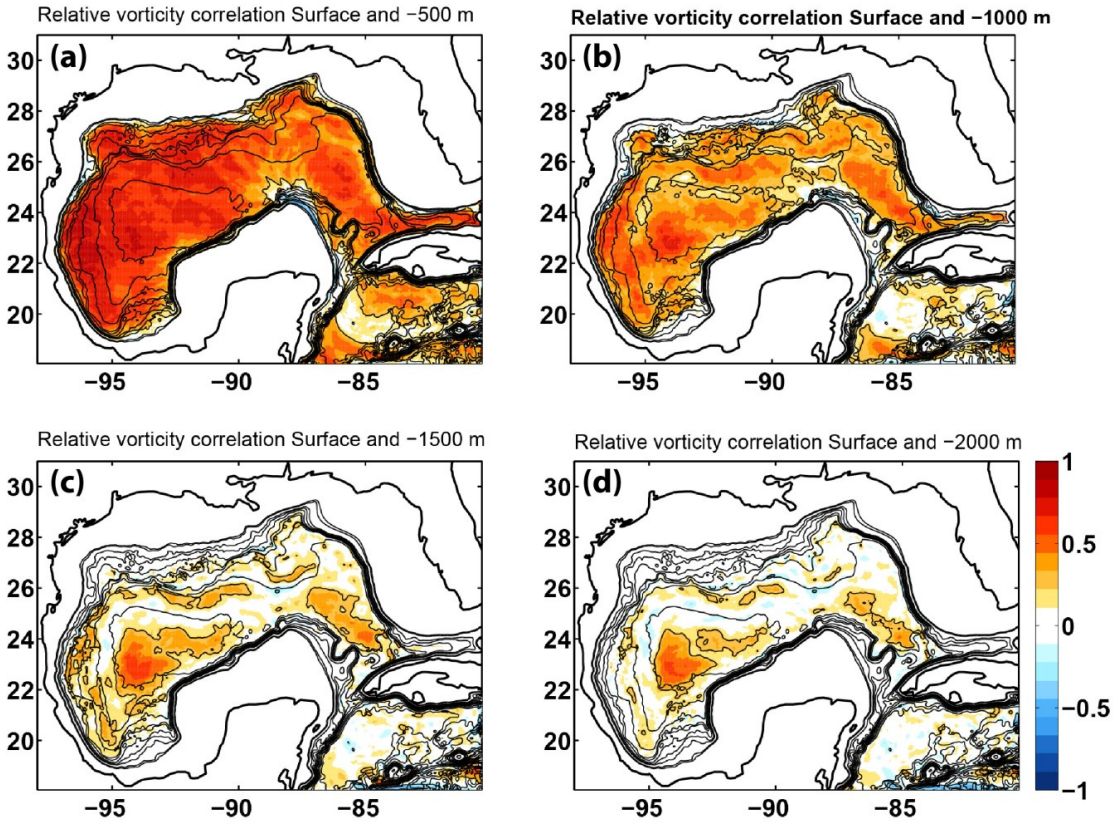

Figure 30. Correlation between monthly anomalies in relative vorticity at 5 m (surface) and (a) 500 m, (b) 1000 m, (c) 1500 m, and (d) 2000 m depth. Areas where correlations are higher than the 95% significance level are contoured.

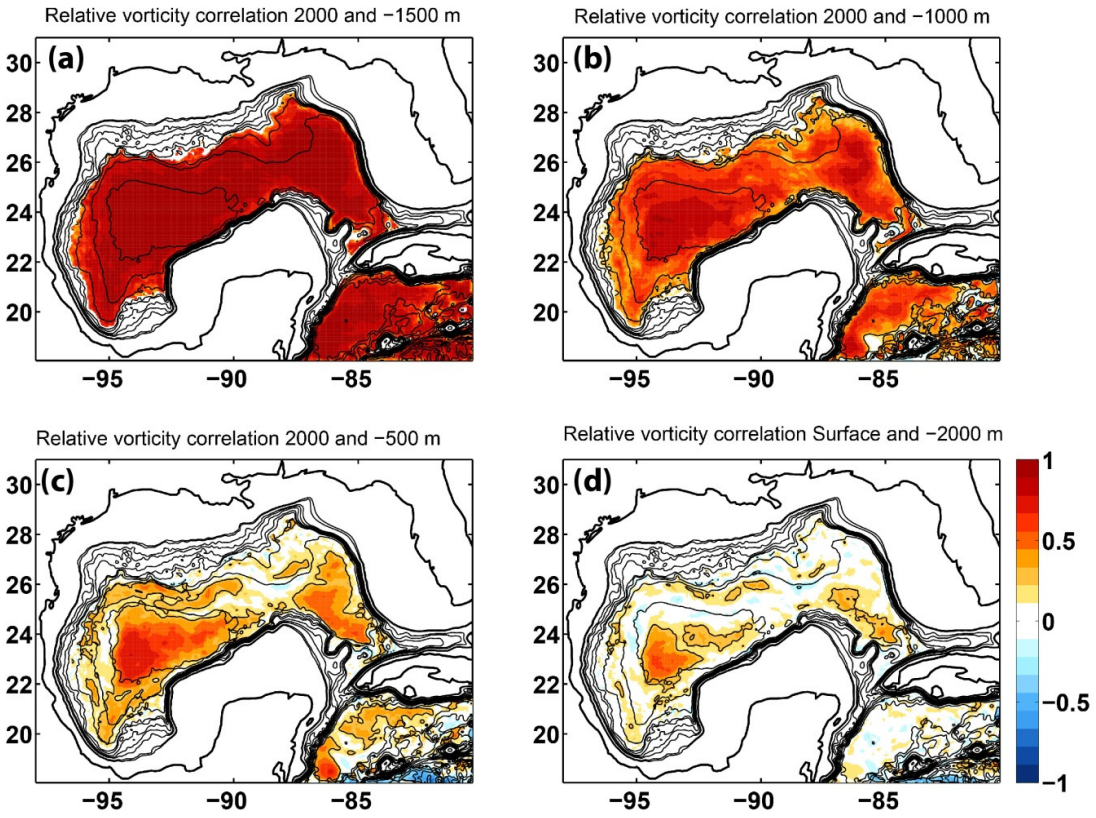

Figure 31. Correlation between of monthly anomalies of relative vorticity at 2000m depth and at (a) 1500 m, (b) 1000 m, (c) 500 m, and (d) 5 m. Areas where correlations are higher than the 95% significance level are contoured.

The vorticity fields at different depths can provide further information about the structures (eddies in particular) that may extend through the two layers. Three examples are provided in Figure 32. They represent typical snapshots of the mesoscale variability in the Gulf. The LC can be tracked to approximately 1000 m depth, but its signature is not always visible below it. This is evident in the snapshots from July 2006. At other times a small anticyclone of low intensity can be tracked to the bottom (i.e. in October 2003), bounded by Yucatan and West Florida Shelves. Alternatively, a deep cyclonic circulation, bounded by topography in the eastern Gulf of Mexico, is spun up by the LC

below its southward eastern limb as described in Lee and Mellor (2003) (i.e. in October 2007). The signature of the LC eddies is lost below 1000 m soon after their detachment at all times. The cyclonic eddy at the southwest corner of the Sigsbee Deep, on the other hand, can be tracked from the bottom to the surface most of the time, with July 2006 being one of the few exceptions. A large number of small vortices, both cyclonic and anticyclonic, of size comparable to the Rossby deformation radius in the Gulf, populate the deep layer.

Focusing on the Deepwater Horizon site and around the location of most deep seeps, the predictability of the bottom circulation given the surface one is very limited. Data assimilative models will, therefore, need to include both satellite and in-situ data to infer the details of the mesoscale circulation in the water column. In-situ data at locations where accidents like the 2010 disaster, have the potential to happen should be collected at high temporal frequency (higher than the Eulerian time scale) and should be assimilated in ocean hindcasts and forecasts to insure a proper representation of the variability throughout the water column.

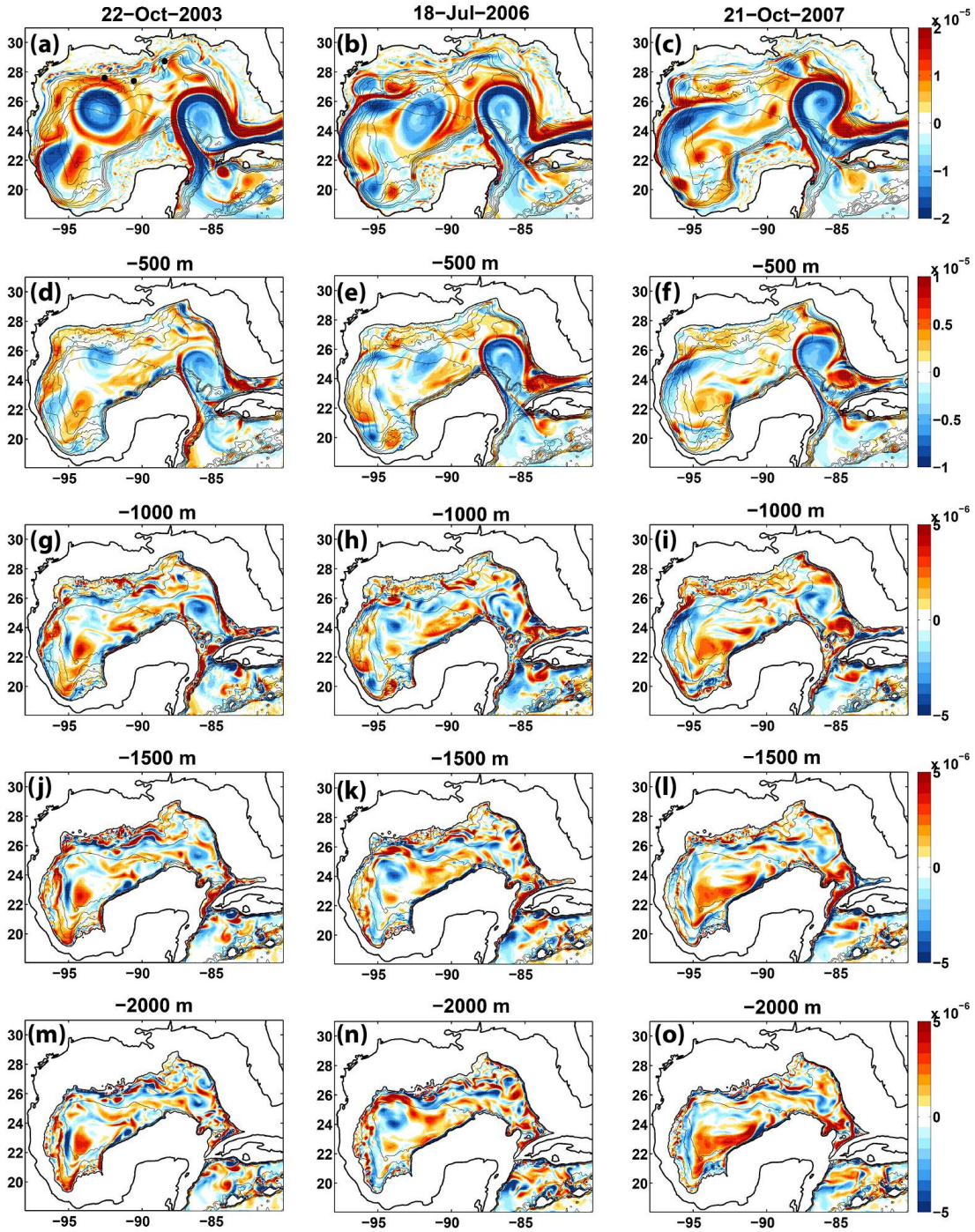

Figure 32. Instantaneous relative vorticity field (unit s^{-1}). Top to bottom: Surface, 500 m, 1000 m,1500 m, and 2000 m depth. Left to right: 22-October-03, 18 July 2006, and 21-October-2007. Black dots in panel (a) left to right: Garden Banks, Green Canyon and MC 252.

3.6 Summary and conclusions

In this Chapter we analyzed an ensemble of simulations performed with ROMS over the Gulf of Mexico covering the period 2000-2008. The main objective was to investigate the predictability of its circulation, both at the surface and in deep waters on intraseasonal time scales, when mesoscale motions dominate the variability. In all runs, the model provides a good representation of the mean circulation features. The magnitude and spatial distribution of the mean geostrophic velocities are almost indistinguishable from the ones derived from altimetry data. The transport at the Yucatan Channel is well represented. The frequency of formation and the horizontal and vertical extension of the Loop Current eddies are realistically modeled. The shedding of the Loop Eddies differ in each run considered, and our analysis shows that the detachment of the Rings from the Loop Current is essentially a chaotic process, even if more likely under certain wind forcing and Loop Current strength conditions.

By comparing a simulation performed with climatological (monthly varying, but repeated identically every year) boundary conditions, with three runs that adopt interannually varying boundary conditions, we show that the interannual variability at the model boundaries affects the representation of the Loop Current strength and of the Yucatan Channel transport. On the other hand, the circulation in the LATEX Shelf, TAVE Shelf, and Bay of Campeche is insensitive to the details of the model boundaries, and is not affected by the Loop Current, but depends only on the wind variability. The circulation in those areas is also characterized by low levels of eddy kinetic energy, and limited mesoscale variability. On the contrary, the circulation in the central basin is

affected by the Loop Current extension and the Rings, and is overall dominated by mesoscale features.

The dominance of mesoscale variability extends to the whole water column. In most of the basin, mesoscale features are coherent in the top ~ 1000 m of the water column, and below it, but not correlated between the surface and the deep layer. Coherency throughout the whole water column is found only at the south-west corner of the Sigsbee Deep, at the south boundary of the Sigsbee escarpment where the topography constrains the formation and propagation of cyclonic eddies, and under the Loop Current, limited to the eastern Gulf, as shown by Lee and Mellor (2003). The mesoscale variability at depth is never correlated between different runs that differ only for a perturbation in the initial conditions. The Eulerian time scale for the top layer, extending from the surface to approximately 1000 m is 50 days; the Eulerian time scale below 1000 m is shorter, around 30 days, due to the smaller size, and higher speed, relative to the mean currents, of the lower layer eddies.

The chaotic behavior associated with the propagation of the Loop Current eddies and the elevated mesoscale activity restricts the predictability of the system at intra-seasonal scales to the coastal areas. Current data assimilative models have the potential of predicting the circulation in the upper 1000 m. However, the lack of coherency between the mesoscale features in the upper portion of the water column with the ones underneath in most of the basin limits the predictability at depth in the absence of a continuous monitoring system.

CHAPTER 4

MESOSCALE EDDIES, HIGH FREQUENCY WINDS, AND VERTICAL MIXING

The Gulf of Mexico is continually populated by an energetic eddy field as was described and modeled in the previous chapter. The most noticeable mesoscale eddies (~200 km) at the Gulf surface are the ones that form close to the Rio Grande slope when the coastal currents along TAVE and LATEX shelves meet those that have detached from the Loop Current. Loop Current eddies transport water from the Caribbean Sea to the west part of the Gulf and modify temperature and salinity conditions in the upper ocean during their course to the western boundary of the Gulf where they ultimately lose coherence. They also interact with the predominant anticyclonic and cyclonic circulation at the western Gulf and Bay of Campeche respectively. The analysis in this chapter centers on the model representation of mesoscale circulation under low (monthly) and high (6-hourly) frequency forcing (momentum and head fluxes), following the methodology outlined in Cardona and Bracco (2012) for a similar analysis of the South China Sea. Theoretical and idealized model simulations have shown that eddies are responsible for transferring energy from the ocean surface to depth at near and quasi-inertial frequencies. To properly simulate this transfer, however, it is necessary to force a model with atmospheric fluxes in the same temporal frequency band. We evaluate this condition in our domain in order to address the following questions: (1) How does the use of wind and heat flux products at different frequencies modify the representation of ocean

variability? and (2) Are the horizontal and vertical velocity patterns modified by changes in the temporal resolution of atmospheric forcing?

The Gulf of Mexico and the South China Sea (SCS) share similarities given that both are tropical semi-enclosed ocean basins and are, physically and biogeochemically influenced by large river discharge and permanent eddy mesoscale activity. Cardona and Bracco (2012) find that in the SCS the forcing frequency does not significantly modify horizontal circulation. The vertical velocity field, however, displays high sensitivity to the frequency of the wind forcing. If the wind field contains energy at the inertial frequency or higher, then Vortex Rossby waves and near-inertial waves are excited as ageostrophic expression of the vigorous eddy field. Those waves dominate the vertical velocity field in the mixed layer (vortex Rossby waves) and below the first hundred meters (near-inertial waves) and are responsible for the differences in the vertical transport properties under the various forcing fields. Similar behavior has been found in the Gulf of Mexico; however, changes in the horizontal circulation are due to the chaotic behavior of the system described in the previous chapter.

This chapter is divided in five subsections. Subsection 4.1 presents an over view of mesoscale eddies and inertial waves and is followed by a description of the model integrations in Subsection 4.2. The temporal resolution sensitivity analysis of the wind and heat flux forcing is presented in Subsection 4.3, and its impact in the horizontal and vertical dynamics is discussed in Subsections 4.4 and 4.5, respectively.

4.1 Mesoscale eddies and inertial waves

The dynamics of the ocean mesoscale, between about 10 and 500 km, is generally approximated as that of a stably stratified, rapidly rotating flow in the geostrophic, hydrostatic approximation. Horizontal velocities are much larger than the vertical ones, and the motion is approximately two-dimensional and characterized by the presence of coherent vortices or eddies (Provenzale, 1999). Those eddies concentrate energy and vorticity (McWilliams, 1984, 1990), represent dynamical anomalies in variables such as velocity, sea surface height and density (Klein and Lapyre, 2009) and are fundamental to both the horizontal and vertical transport processes and the statistical properties of the turbulence field (Bracco et al., 2000; Bracco and McWilliams, 2010; Capet et al., 2008; Stammer, 1997). They also play a crucial role in the transport of ocean heat and momentum; impact local dynamics with important consequences on tracer dispersion, ocean stirring and mixing processes (Pasquero et al., 2007), and affect the biology of the ocean and nutrient distribution (Abraham, 1998; Bracco et al., 2009; Lévy and Klein, 2004; Martin and Richards, 2001;McGillicuddy et al., 1997; Pasquero et al., 2005). Finally, they contribute substantially to the dissipation of energy introduced by the wind forcing (Munk and Wunch, 1998; Wunsch and Ferrari, 2004) that transfers atmospheric kinetic energy into oceanic kinetic and potential energies (Lueck and Reid, 1984).

Most of the wind energy is trapped at the ocean surface and contributes to the turbulent mixing in the mixed layer (Wunsch and Ferrari, 2004). Part of it, however, can propagate to the ocean interior by mean of internal wave motion and is distributed at different periods and vertical scales (Kundu, 1976; Kunze, 1985; Pollard and Millard, 1970). Vertical shear can then engage wave breaking and enhance mixing (Garret, 2003).

In the ocean eddies contribute to this energy transfer towards the dissipation scale by effectively polarizing quasi- and near-inertial motions.

For quasi-inertial processes here we refer to the development of vortex Rossby waves (VRWs) in eddies, which result from vortex-mean flow interactions. VRW owe their existence to the finite radial gradient of potential vorticity in coherent eddies and are excited by the shear deformation of the mean potential vorticity of eddies by the background flow. Vorticity perturbations in monopolar vortices propagate outward as VRWs, shared away by the angular velocity of the mean axisymmetric vortex. Koszalka et al., (2009) investigated for the first time the formation and structure of VRWs using a regional ocean model in an idealized configuration, and Chavanne et al., (2010) documented their existence in a cyclone observed west of Oahu, Hawaii, using high-frequency radio Doppler current meters and moored acoustic Doppler current profilers (ADCPs).

Near-inertial waves (NIWs) in eddies, on the other hand, have been studied and observed extensively by the oceanographic community. They are trapped within the anticyclonic structures and expelled from the cyclonic ones, as shown by a number of theoretical and idealized numerical studies (Danioux et al., 2008; Koszalka et al., 2009, 2010; Kunze 1985, Lee and Niiler, 1998; to cite a few). The first observational evidence of this behavior was found in the North Pacific and in the Sargasso Sea, where downward propagating near-inertial energy was observed in regions of negative vorticity by Kunze and Sanford (1984; 1986). More recent examples include satellite-tracked drifter observations over the Kuril-Kamchatka Trench (Rabinovich et al., 2002; Rogachev and

Carmack, 2002) and moored current observations in the southwestern East/Japan Sea (Byun et al., 2010). As a consequence, vertical mixing induced by inertial energy is heterogeneous and strongly related to the eddy field properties (Klein et al., 2004; Koszalka et al., 2010).

This heterogeneity makes it difficult to map and measure the overall contribution of quasi- and near- inertial waves trapped in eddies to oceanic vertical mixing and energy dissipation processes. Numerical simulations with state-of-the-art ocean general circulation models may provide a leading order answer (Zhai et al., 2007). Within a modeling framework, however, the frequency of the wind forcing affects the production of NIWs. Indeed, near-inertial motions are effectively excited only by high (with respect to the Coriolis frequency f) frequency (HF) winds as the interaction between winds and NIWs results from a resonance mechanism or 'ringing of the eddy field' (Danioux and Klein, 2008; Klein et al., 2004; Large and Crawford, 1995; Skyllingstadt et al., 2000).

In the Gulf of Mexico, inertial and near-inertial oscillations forced by tropical cyclones (George 2006, Katrina 2005, Opal 1995, Gilbert 1988, Gloria 1985, Josephine 1984, Allen, 1983, Frederic 1979 and more) have been extensively analyzed using in-situ measurements and numerical models (Shay et al., 1997, Brooks 1983, Shay and Elsberry 1987, Prince et al., 1994, Hong et al., 2000). The ocean response to the passage of Hurricane Gilbert in 1988 by Shay et al., (1997) concludes that the observed frequency shifts in the mixed layer currents are in the near-inertial range. Near-inertial currents rotated anticyclonically in the upper ocean providing the enough velocity shear to induce cooling and deepening of the mixed layer in the right-hand side of the hurricane track.

Near-inertial currents in the northern Gulf are also induced by the passage of atmospheric fronts (during 3-10 days) over the DeSoto Canyon region and the LATEX shelf. The near-inertial currents generated by high frequency (near-inertial) variations of the wind stress associated with the fronts have been discussed by Hamilton (2000) and Jarosz et al., (2007). Hamilton (2000) concludes that the presence of large near-inertial currents over locations in the northern Gulf with rough bathymetry could also be related to the trapping of near-inertial energy by negative vorticity generated by energetic mesoscale motion present in the area.

4.2 Description of model integrations

Two interannual time-dependent simulations are analyzed in this chapter. They follow the model description in section 3.1 of the Chapter 3. The model simulations are forced by winds and heat fluxes at monthly (ITD3 or Mon) and 6-hourly frequency (6h) for the period 2005-2007. The wind stress was extracted from NCEP/QUICKSCAT blended winds in the Colorado Research Associates (version 5.0) (Millif et al., 2004; Chin et al., 1998) and NCEP reanalysis surface heat fluxes. The boundary conditions are from Soda 2.1.6 monthly averaged for both simulations. Cardona and Bracco (2012) performed a sensitivity analysis of the wind and heat fluxes temporal resolution using monthly, daily and 6-hourly forcing. By maintaining six hourly wind forcing and using monthly-, daily- or 6-hourly varying heat fluxes, Cardona and Bracco (2012) verify that the main contributor to dynamics variability is the HF wind both wind and heat flux were kept in the same temporal resolution for consistency. However not significant differences will be expected if a lower resolution was used for heat fluxes forcing in the 6h simulation.

The use of wind products containing high (6-hourly) frequency changes allow the evaluation of variations in the modeled fields (temperature, horizontal and vertical velocities), the associated mixing, and the representation of quasi- and near-inertial processes by the model (ROMS). The inertial frequency in the Gulf of Mexico is 0.029 cph, which corresponds to the mean Gulf latitude (21°N). Then, the Coriolis period is 1.39 days and 6 hourly winds contain energy at the frequencies required to ring eddies. As previously mentioned, the presence of near-inertial currents has been measured in the Gulf of Mexico during hurricanes and atmospheric front passages. Therefore, we do not focus in a particular atmospheric event. The Gulf of Mexico, as with the SCS, has particularities in its bathymetry and high mesoscale activity (mainly due to the Loop Current) that allows us to evaluate the relative role of the high frequency (HF) winds-induced and topographically-induced wave fields on the vertical and horizontal mixing.

4.3 From low to high frequency forcing

In this subsection we explain how the modeled circulation in the Gulf of Mexico responds to changes in the atmospheric forcing frequency from monthly to six-hourly timescales focusing on the transport processes. Overall the average circulation measured in terms of eddy kinetic energy, horizontal velocity and vorticity fields does not vary significantly between runs (see for example Figure 36 and Figure 37). However, the integrations are not identical due to the randomness associated with the Loop Current Eddies shedding (LCE), as described in Chapter 3. Nevertheless the overall energy in the system varies in the same range for both simulations. The Gulf of Mexico does not behave exactly like the SCS, where high frequency atmospheric forcing does not have a direct impact on the eddy formation. In this aspect, the Gulf is more similar to other

basins such as the Black Sea (Kara et al., 2005) or the Ligurian Sea (Casella et al., 2011). However, unlike the behavior observed in Black and Ligurian Seas, changes in the strength of the coastal currents in the SCS and Gulf of Mexico are not significant (Cardona and Bracco, 2012).

The temperature, salinity, and density fields depend on the temporal resolution of the atmospheric forcing fields. Figure 33 shows the mean temperature profiles for the two runs, together with the ones derived from SODA and from the ORA-S3 ECMWF (Balmaseda et al., 2008) ocean reanalysis for the boreal winter and summer seasons in the period 2005-2007. Temperature profiles below 1500 m are almost identical and are independent of the season or the forcing temporal resolution. Differences are evident through the water column in the upper 500 m and are particularly strong in the upper 100 m in both seasons. Temperature profiles from the 6h simulation are colder than the ones derived from Mon, Soda, and ECMWF ORA-S3. In the upper 50 m, the modeled profiles are all characterized by colder temperatures than SODA and ORA-S3. The temperature differences are not larger than 0.5°C. On the other hand, the 6h simulation displays a significant temperature decrease, up to 3°C on average over the upper 100 m, compared to Mon (See insert in Figure 33) due to enhanced mixing of surface warm waters within the mixed layer, in agreement with similar studies in the Pacific (Fan et al., 2010, Chen et al., 1999; Lee and Liu, 2005 and Sui et al., 2003), Southern Ocean in austral summer (Kamenkovich, 2005) and South China Sea (Cardona and Bracco, 2012). Immediately below 100 m Soda profiles merge with the ones from the model, and ECMWF-ORA-3 profiles become about 2°C colder than them. All profiles merge around 350m and remain so until the sea floor. Larger differences are exhibited in the upper 150 m, where a

cooling trend for increasing frequency of the atmospheric fluxes is noticeable, which is due to the enhanced mixing of the deeper water column induced by high frequency winds. The Mon run is in closer agreement with SODA and ORA-S3 reanalysis in both seasons in the upper layer. The reanalysis are monthly forced, which may explain why Mon profiles are close to them in this region.

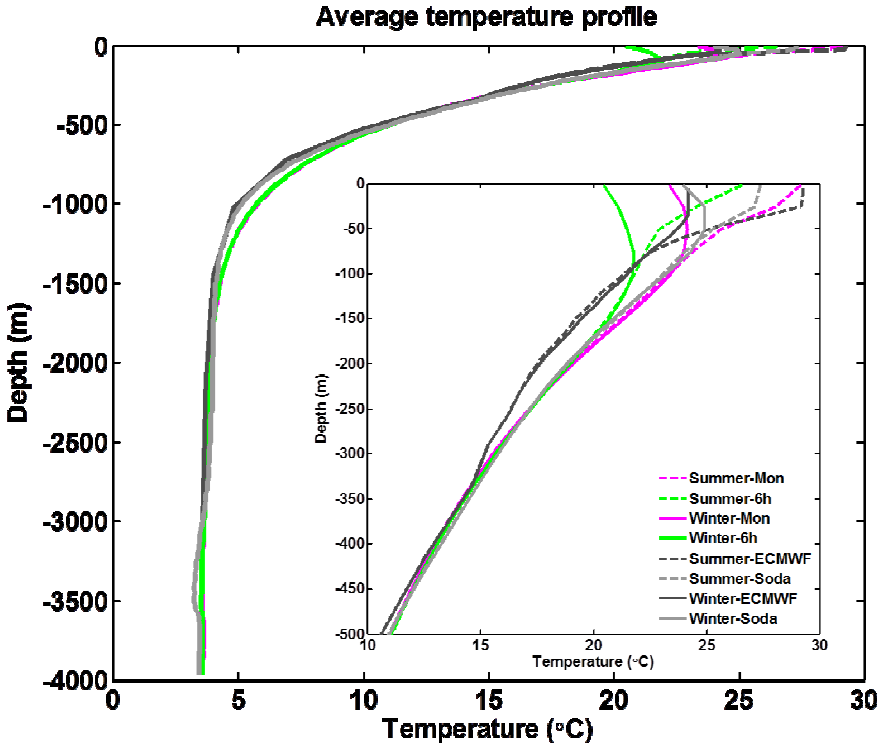

Figure 33. Temperature profile in ºC in boreal winter (DJF, left) and summer (JJA, right). The insets show a zoom over the first 500 m of the water colum.

The general trend between the Mon and 6h integrations described above is enhanced in the temperature differences shown in Figure 34 for a vertical section running across the basin (its location is marked in Figure 35 in white). This section, chosen for the high level of eddy activity and deep waters, displays the mean temperature differences between the

6h and Mon integrations during boreal winter and summer in the whole water column and again suggest that a greater level of mixing occurs whenever HF forcings are used.

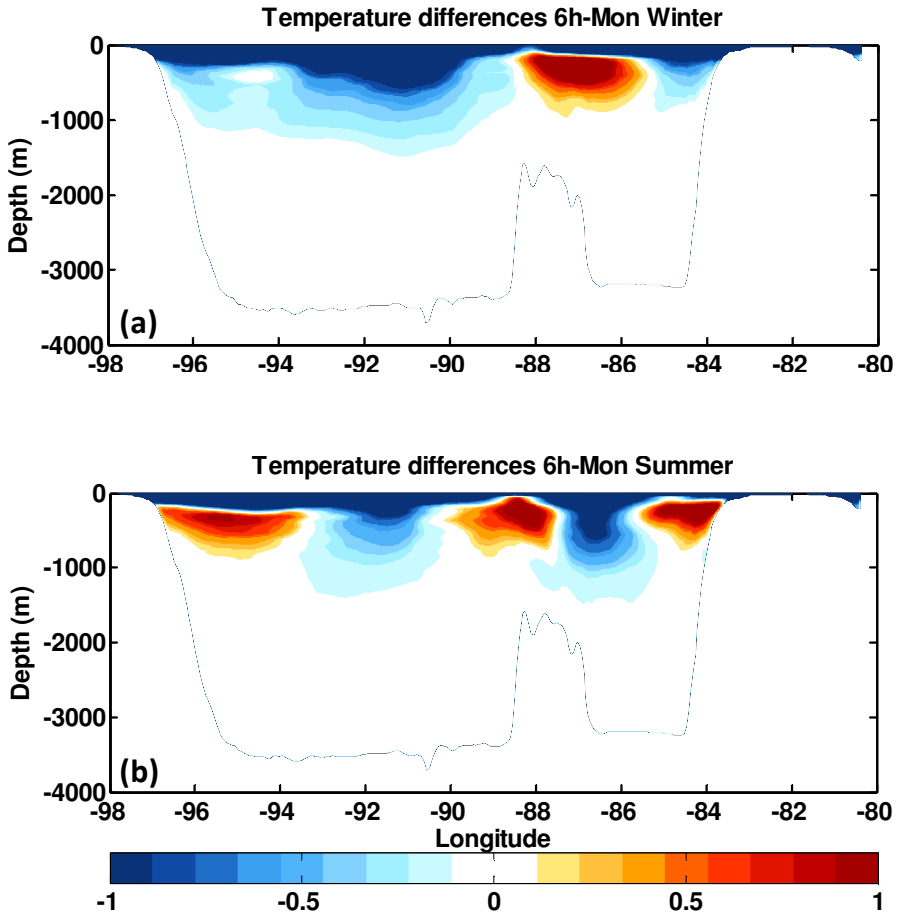

Figure 34. Mean temperature differences in ºC between 6hand Mon of the water column along the section shown in white in Figure 35. (a) boreal winter (DJF) and (b) Summer (JJA).

4.4 High frequency winds and horizontal flow

As described in section 3.2, the horizontal circulation in the upper layer (~1000 m) the Gulf of Mexico is characterized by the Loop Current, large eddies detached from LC, the anticyclonic surface flow in the northwest of the basin and the cyclonic circulation in the Bay of Campeche. Figure 35 shows snapshots of the relative vorticity and horizontal

velocity fields at the surface and at 1000 m depth. Both cyclonic and anticyclonic eddies are present at the surface and in deeper waters. They contribute to the mesoscale field and are surrounded by strong vorticity filaments. As mentioned, the strength of the vorticity field remains in the same range when the forcing goes from monthly to six hourly and large differences are observed in the LC path and LCE location in the western part of the Gulf.

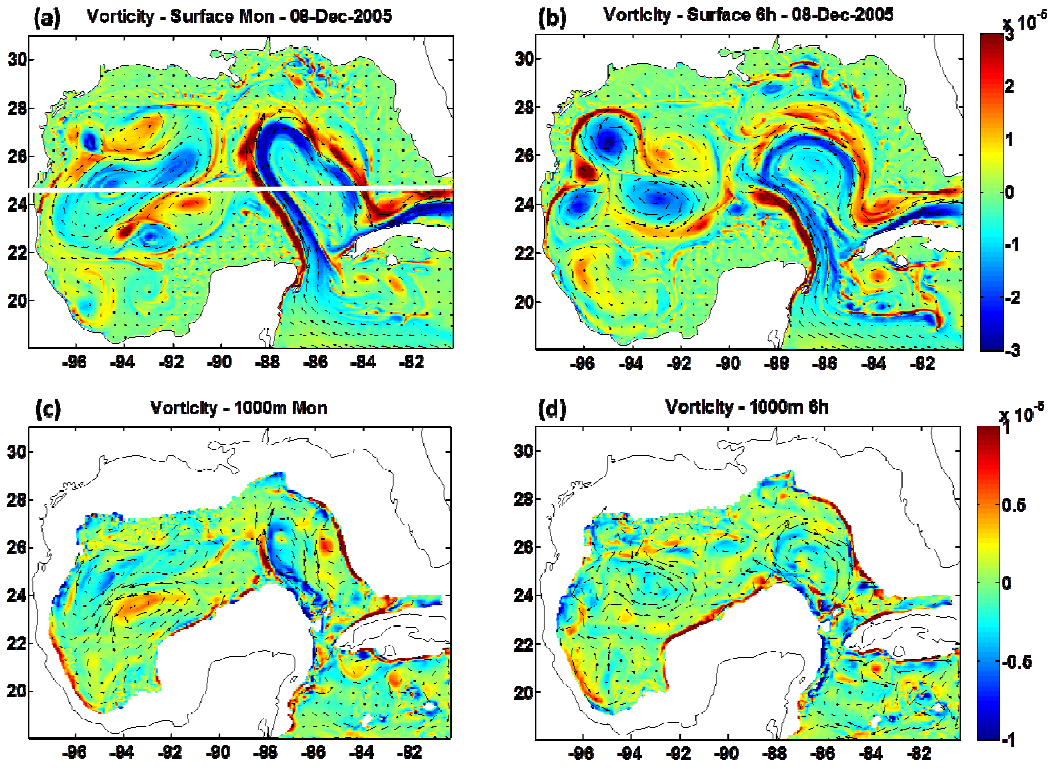

Figure 35. Snapshots of the relative vorticity field (in color) and horizontal velocity (vectors, superimposed). (a) – (b) Surface Mon and 6h and (c) – (d) 1000 m depth. Solid white line illustrates the transversal cross-section paths used in Figure 38.

The averaged vorticity statistics in the surface and 1000 m are also independent of the temporal resolution of the forcing imposed. The level of mesoscale activity (eddy

number and strength) is comparable between the simulations, both at the surface and at depth. Differences are not statistically significant. We quantify the similarities in Figure 36, where we show the probability density functions (PDFs) of relative vorticity calculated by averaging over 1440 snapshots taken every two hours between April and August 2007 at the ocean surface and at 1000 m depth. The PDFs of the ocean surface reveal a heavier anticyclonic vorticity tail, in correspondence of the strongest eddies. Figure 37 shows the time series of the surface eddy kinetic energy (EKE) in the simulations for the 2005-2007 period. Both kept the same mean state whenever monthly or 6-hourly atmospheric forcing is used to force the circulation. Both the seasonal cycle and intraseasonal and interannual variability are similar. Point-by-point differences can be ascribed to variations in LC extension and timing and location of LCE detachment in the west part of the Gulf.

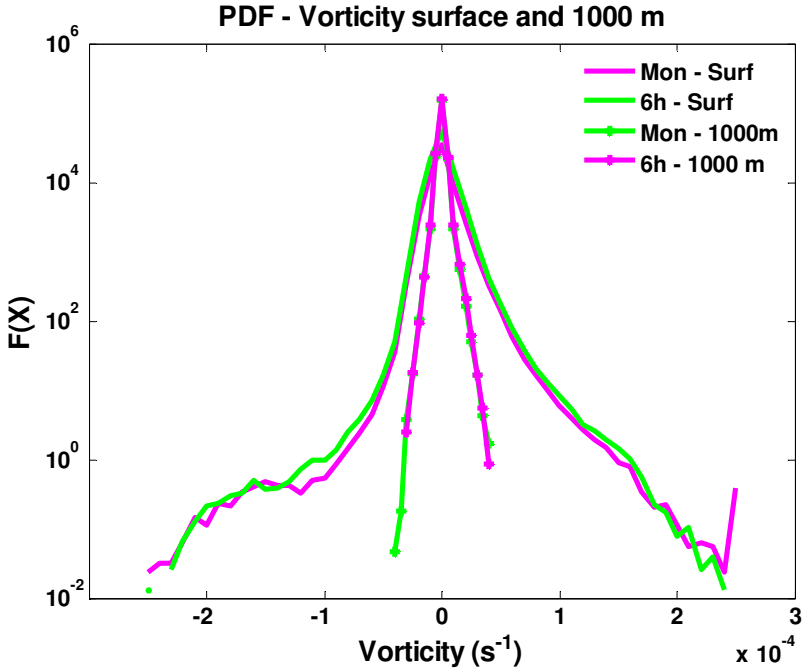

Figure 36. PDF of relative vorticity at the surface and 1000 m.

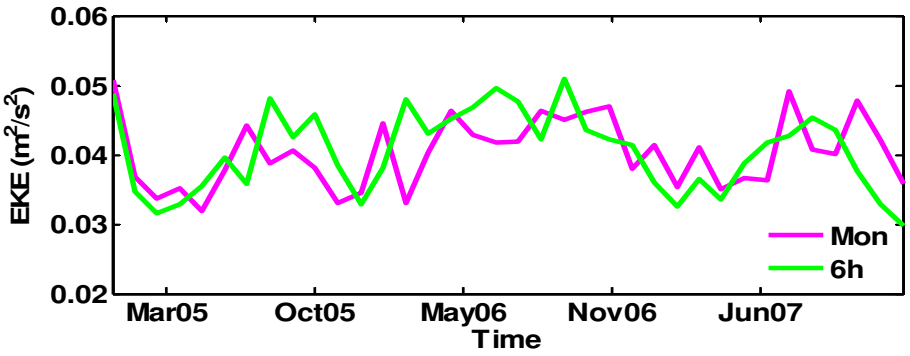

Figure 37. Mean surface eddy kinetic energy time series averaged over whole the domain from 2005 to 2007.

4.5 The vertical circulation

The eddy field contributes to the spatial heterogeneity of the vertical mixing at ocean meso- and submesoscales (Klein et al., 2004; Kunze, 1985; Zhai et al., 2005), and eddies represent localized hotspots of vertical transport (Gill, 1984). Although the level of mesoscale activity (identified as number of eddies and intensity of the vorticity fields and the associated horizontal transport) is comparable between the two simulations, the vertical velocities show major differences.

Figure 38 displays a west to east transversal section of the instantaneous vertical velocity field in the two integrations (see Figure 35 for its location). The frequency of the atmospheric forcing influences the magnitude and spatial distribution of the vertical velocities. When the domain is forced by monthly winds, the vertical velocities are extremely small most of the time; however, in simulations forced by six-hourly winds and heat fluxes, the magnitude of the vertical velocities is several times larger than for monthly winds throughout the water column. The set-up of the numerical experiments suggests that the temporal resolution of the atmospheric forcing field is responsible for

the significant increase in vertical velocities, in agreement with previous studies (Cardona and Bracco, 2012, Danioux et al., 2008; Komori et al., 2008).

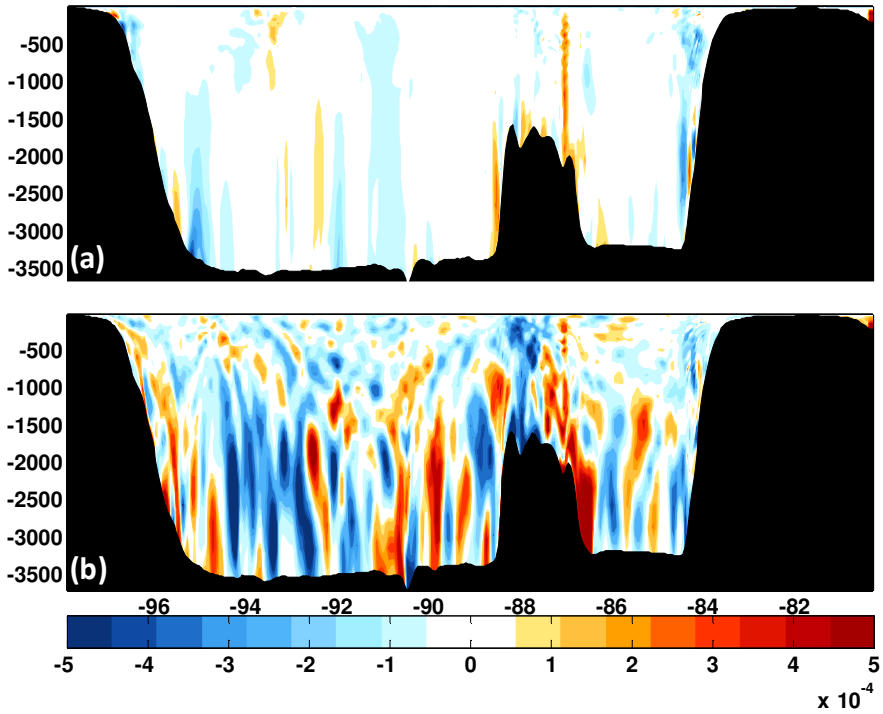

Figure 38. Snapshots of the instantaneous vertical velocity field in m/s over the section indicated in white in Figure 35. (a) Mon and (b) 6h.

In order to quantity the differences in the magnitude in the three simulations, we calculate the root mean square (rms) of the horizontally-averaged vertical velocities (Figure 39) over the Sigsbee Deep where the interaction of the mean flow and the bathymetry to the vertical velocity field is negligible. The magnitude of the rms increases by a factor of ten between the Mon and 6h integrations. In the monthly profile, the rms below the mixed layer remains constant throughout the water column, with an average value of 3.9×10^{-5} m/s. In contrast, the 6h profile shows a continuous increase until about 2500 m, settling at 3.4×10^{-4} m/s.

The analysis of the time evolution of the vertical velocity fluctuations points to near-inertial waves associated to the mesoscale field as mainly responsible for the large amplitudes seen in the 6h case. Evidence of this is provided in Figure 40, which shows the frequency spectra for the vertical velocity field at various depths averaged over the Sigsbee Deep, where motion induced by changes in the bathymetry can be neglected and the presence of vortices is permanent. There is a noticeable difference between the frequency spectra for the monthly and 6-hourly runs with respect to the amplitude of a peak centered at 0.03 cph, which is enhanced for increasing wind frequency. The peak is more prominent as depth increases and its position is very close to the inertial frequency of 0.029 cph for the region, in agreement with the theoretical studies by Danoiux and Klein (2008) and Danoiux et al., (2008), the idealized numerical investigation by Koszalka et al., (2009, 2010), and the analysis of a coupled general circulation model run at very high resolution by Komori et al., (2008).

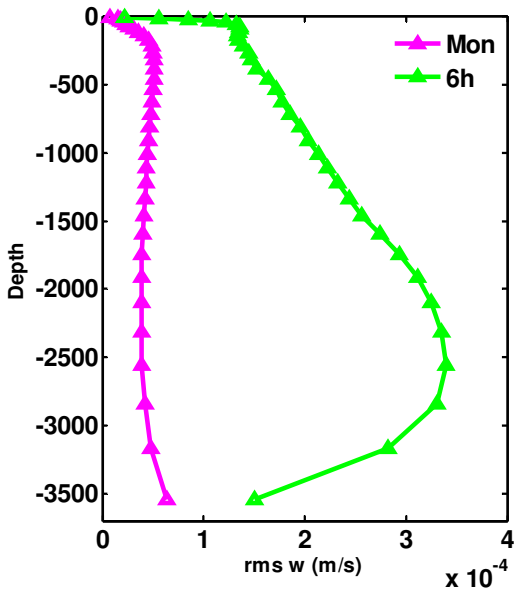

Figure 39. Vertical profile of the rms fluctuations of the vertical velocity averaged over the Sisgbee Deep.

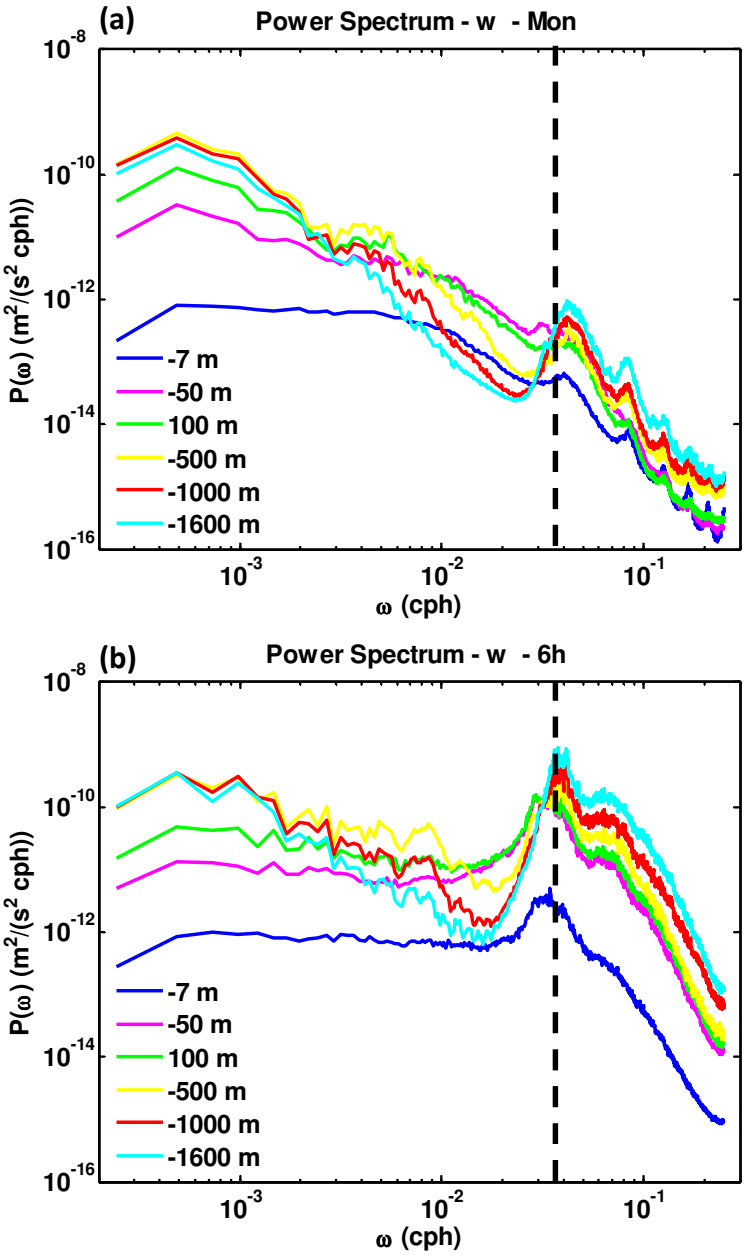

Figure 40. Power spectra of the vertical velocities at 7 m, 50 m, 100 m, 500 m, 1000 m, and 1600 m depth. (a) Mon and (b) 6h. The dash line indicates the inertial frequency.

The difference in the spatial distribution of the vertical velocity field between monthly and 6-hourly simulations also points to the eddy field as responsible for trapping quasi- and near-inertial energy and transporting it through the water column. This can be

seen in the vertical velocity field associated with a mesoscale dipole shown for the two simulations in Figure 41. Dipoles formed over the Sigsbee Deep as a result of the interaction of the TAVE coastal current and the LCE. At the surface, positive and negative vorticity defines the mesoscale field (Figure 41 (a), (d)). The associated vertical velocity patterns close to the surface (6 m depth; middle panels) illustrate how the mesoscale eddies confine and transport the energy from the atmospheric forcing fields to the ocean, affecting the magnitude and spatial distribution of the vertical velocity field. In the 6h run, vertical velocities in the first meters exhibit a spiraling pattern, barely noticeable in the Mon run and particularly marked in correspondence of the anticyclonic eddy. Those bands have been described in previous works as outward-propagating vortex Rossby-waves (Graves et al., 2006; Koszalka et al., 2009, 2010; McWilliams et al., 2003; Montgomery and Kallenbach, 1997).

Using a weakly-nonlinear shallow-water model, Graves et al., (2006) demonstrated that in the vortex relaxation process VRWs lead to a weakening of cyclones and a strengthening and reaxisymmetrization of perturbed anticyclones. In other words, cyclonic vortices, formed at the surface by the interaction of the main currents with the bathymetry at a rate analogous to anticyclones, are more prone to weakening by VRWs. The overall spiraling shape of the vertical velocity field within and around the vortices is determined by the tilting term in the diagnostic equation for the vertical velocity (see Koszalka et al., 2009, 2010 for its mathematical expression). Below the first fifty meters, the tilting term becomes negligible compared to the ageostrophic term in the diagnostic equation for the vertical velocity, and near-inertial waves dominate the vertical velocity field, as seen also in the frequency spectra, again in agreement with the analysis by

Koszalka et al., (2009) for an idealized eddy field and Cardona and Bracco (2012) in the SCS. Differences between the Mon and 6h runs occur below the first few hundred meters of the water column, with the energy injected by the winds into the eddies vanishing at such depth in the simulation forced by monthly fields, but reaching the bottom for the 6-hourly runs.

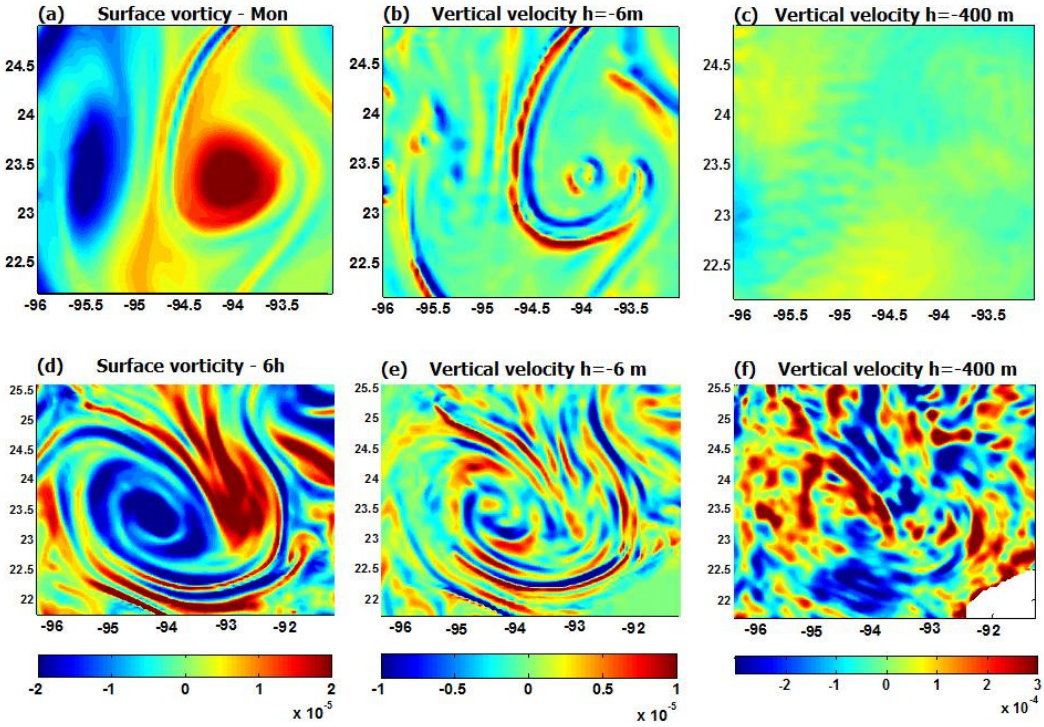

Figure 41. Snapshots of a mesoscale dipole in the-Mon (top), and 6h (bottom) simulations. Left to righ: Surface vorticiy (m/s^2), vertical velocity (m/s) at 6 m depth and vertical velocity at 400 m depth.

4.6 Conclusions

In this chapter we investigated the impact of high frequency atmospheric forcing on simulated mesoscale transport in the Gulf of Mexico. The Gulf is characterized by an intense eddy field generated primarily by eddies detached from the Loop Current. We

confirm that variations in the temporal scale of the wind forcing (i.e. monthly to 6-hourly) impact the timing of horizontal dynamics but not the strength. Variables, such as sea surface height, horizontal velocities, relative vorticity and eddy kinetic energy at all levels, do not exhibit significant differences. Monthly and 6-hourly heat fluxes were also implemented. However, they do not modify substantially the modeling of the transport, horizontal, and vertical dynamics as was presented by Cardona and Bracco (2012).

HF winds impact the representation of the vertical transport that gets stronger as the temporal resolution increases. The magnitude of the vertical velocities associated with the mesoscale eddy field is strongly modified by the wind frequency. Vertical velocity in the simulation forced by 6-hourly winds is ten times greater than the one obtained from monthly averaged wind forcing. The energy injected by the winds into the ocean is transported in the water column by mesoscale eddies and near-inertial oscillations, whenever the wind forcing contains energy at frequencies in the inertial bands (1.4 days in the Gulf). If the forcing used by the models is in a temporal resolution larger than the inertial band, they underestimate the vertical transport processes which are particularly important for the biological activity in the ocean upper layers since they contribute to the input of nutrients into the euphotic zone.

CHAPTER 5

SUMMARY AND CONCLUSIONS

In this thesis the main objective was to investigate the variability of the mesoscale circulation in the Gulf of Mexico system from interannual to daily time scales, and its dynamical interaction with biological productivity. In this work mesoscale circulation identifies processes at scales between 10 and 500 km.

Satellite images of the color of the ocean's surface show a correspondence between physical and biological activity at the mesoscales. Patches and swirls of chlorophyll pigments are related to the structures of eddies (Bakum 2006). At the same time the mesoscale variability limits the predictability of the system and our ability to simulate its evolution.

To accomplished our goal, we analyzed an ensemble of simulations performed with ROMS over the Gulf of Mexico covering the period 2000-2008, hydrographic and nutrient concentration measurements collected during 2010, 2011, and 2012 summer seasons in the northern Gulf, and chlorophyll-a concentration derived from MODIS satellite data.

First, we explored the relationship between the Mississippi-Atchafalaya River discharge, nutrient loads, and biological activity in the northern Gulf using our field data. We collected data from 784 locations at the sea surface. At 121stations we also included

a water column analysis. The distribution of the stations allowed us to sample along a large salinity gradient ranging from 10 to 37 psu. The measurement campaigns took place under very different conditions of Mississippi river discharge, including the late phase of the 2011 runoff that represents the highest peak discharge since 1927. The river discharge registered normal levels in 2010. However, the sampling happened under rare conditions caused by the Deepwater horizon oil spill. The field campaign took place one month after the rig was capped on July 15 2010.

A negative correlation between nutrient concentration and salinity, seen in previous campaigns and common to most basin subjected to strong river outflows (e.g. east equatorial Atlantic due to the Amazon plume, or South China Sea due to the Mekong outflow) was confirmed at the surface and in the upper 60m of the water column for nitrite, nitrate, phosphate and silicate. No major changes in the nutrient concentrations were found between our data, collected in the period 2010 – 2012, and previous measurements from twenty years ago. Current concentrations lie in the same range as twenty years ago; also they have maintained similar relationships to salinity despite changes in the land and fertilizer uses in the basin (Alexander et al., 2008). Chlorophyll-a along the salinity gradient behaves similarly to all macronutrients analyzed, except that high values concentrate at intermediate salinities instead of low salinities. The biological activity in the stations sampled is nitrogen limited in 79% of them and phosphorus limited in 8% according with Dorch and Whitledge (1992) and Chen et al., (2000) criteria.

Besides the direct input of nutrients from river discharges, the distribution of nutrients in intermediate and high salinity waters in the euphotic layer is influenced by dynamical processes at the ocean mesoscales such as eddies, internal waves, coastal upwelling events and Loop current intrusion. Using an ensemble of four integrations we investigate how mesoscale motions dominate the variability of the Gulf of Mexico circulation both at the surface and in deep waters on intraseasonal time scales. We particularly focus on its predictability by exploring the impact of small variations in the initial conditions and the role of the boundary conditions in the evolution of the Gulf of Mexico circulation. All integrations are performed on a 5 km horizontal resolution grid that covers the entire Gulf with 35 terrain-following vertical layers. The model domain has open boundaries to the east and the south and all simulations are initialized from a run forced by momentum and heat fluxes monthly averaged over the period 1958-2008 plus a small random perturbation. Three simulations that retain interannual variability in the forcing and boundary conditions are performed over the period January 2000-December 2008. In two of them we implemented a nested grid covering the Mississippi-Atchafalaya river shelf and a large portion of the northern Gulf where the horizontal resolution reaches 1.6 km. The last case keeps the variability in the surface forcing but includes climatology boundaries conditions. In all runs, the model provides a good representation of the mean circulation features, the Yucatan transport, and the horizontal and vertical extension of the Loop Current eddies. The shedding of the Loop Eddies differs in each run considered, and our analysis shows that the detachment of the Rings from the Loop Current is essentially a chaotic process. By comparing the simulation that includes climatology conditions at the boundaries with the ones that retain the interannual

variability on them, we show that the interannual variability at the model boundaries affects the representation of the Loop Current strength and of the Yucatan Channel transport. On the other hand, the circulation in the LATEX Shelf, TAVE Shelf, and Bay of Campeche is insensitive to the details of the model boundaries, and is not affected by the Loop Current, but depends only on the wind variability. On the contrary, the circulation in the central basin is affected by the Loop Current extension and by the Rings, and overall dominated by mesoscale features. In most of the basin, mesoscale features are coherent in the top ~ 1000 m of the water column, and below it, but not correlated between the surface and the deep layer. Coherency throughout the whole water column is attributed to particular topographic features such as the south-west corner of the Sigsbee Deep and the south boundary of the Sigsbee escarpment.

The chaotic behavior associated with the propagation of the Loop Current eddies and the elevated mesoscale activity restricts the predictability of the system at intra-seasonal scales to the coastal areas. Current data assimilative models have the potential of predicting the circulation in the upper 1000 m. However, the lack of coherency between the mesoscale features in the upper portion of the water column with the ones underneath in most of the basin limits the predictability at depth. It was evidenced during the Deepwaster Horizon spill in 2010, when data assimilative models diverged in both their predictions of surface oil trajectories and general currents behavior.

Since mesoscale activity is the key factor to fully understand the horizontal and vertical dynamics that take place in the Gulf, we further analyzed the model representation of mesoscale circulation under low (monthly) and high (6 hourly)

frequency forcing. Hence a fifth simulation is included in the ensemble. It uses high frequency wind and heat fluxes to force the regional ocean model. Our results confirm that the temporal scale variation from monthly to 6-hourly in the wind forcing impact the timing of horizontal dynamics but not the strength. Variables, such as sea surface height, horizontal velocities, relative vorticity and eddy kinetic energy at all levels, do not exhibit significant differences. However, the chaotic behavior in the system restricts their comparisons over time. High frequency winds impact the representation of the vertical transport that gets stronger as the temporal resolution of the atmospheric forcing fields increases. Vertical velocity in the simulation forced by 6-hourly winds is ten times greater than the one obtained from monthly averaged wind forcing. The energy injected by the winds into the ocean is transported in the water column by mesoscale eddies and near-inertial oscillations, whenever the wind forcing contains energy at frequencies in the inertial bands (1.4 days in the Gulf). If the forcing used by the models is in a temporal resolution larger than the inertial band, they underestimate the vertical transport processes which are particularly important for the biological activity in the ocean upper layers since they contribute to the input of nutrients into the euphotic zone.

REFERENCES

Abraham, E. R. (1998), The generation of plankton patchiness by turbulent stirring, Nature, 391(6667), 577-580.

Adcroft, A., R. Hallberg, J. P. Dunne, B. L. Samuels, J. A. Galt, C. H. Barker, and D. Payton (2010), Simulations of underwater plumes of dissolved oil in the Gulf of Mexico, Geophysical Research Letters, 37(18), doi:10.1029/2010gl044689.

Alexander, R. B., R. A. Smith, G. E. Schwarz, E. W. Boyer, J. V. Nolan, and J. W. Brakebill (2008), Differences in Phosphorus and Nitrogen Delivery to The Gulf of Mexico from the Mississippi River Basin, Environmental Science & Technology, 42(3), 822-830, doi:10.1021/es0716103.

Balmaseda, M. A., A. Vidard, and D. L. T. Anderson (2008), The ECMWF Ocean Analysis System: ORA-S3, Monthly Weather Review, 136(8), 3018-3034, doi:10.1175/2008MWR2433.1.

Bombar, D., P. H. Moisander, J. W. Dippner, R. A. Foster, M. Voss, B. Karfeld, and J. P. Zehr (2011), Distribution of diazotrophic microorganisms and nifH gene expression in the Mekong River plume during intermonsoon, Marine Ecology Progress Series, 424, 39-52, doi:10.3354/meps08976.

Bracco, A., S. Clayton, and C. Pasquero (2009), Horizontal advection, diffusion, and plankton spectra at the sea surface, Journal of Geophysical Research: Oceans, 114(C2), C02001, doi:10.1029/2007jc004671.

Bracco, A., J. LaCasce, C. Pasquero, and A. Provenzale (2000), The velocity distribution of barotropic turbulence, Physics of Fluids, 12(10), 2478.

Bracco, A., and J. C. McWilliams (2010), Reynolds-number dependency in homogeneous, stationary two-dimensional turbulence, Journal of Fluid Mechanics, 646, 517-526, doi:10.1017/S0022112009993661.

Bracco, A., J. Pedlosky, and R. S. Pickart (2008), Eddy Formation near the West Coast of Greenland, Journal of Physical Oceanography, 38(9), 1992-2002, doi:10.1175/2008jpo3669.1.

Brooks, D. A. (1983), The Wake of Hurricane Allen in the Western Gulf of Mexico, Journal of Physical Oceanography, 13(1), 117-129, doi:10.1175/1520-0485

Bunge, L., J. Ochoa, A. Badan, J. Candela, and J. Sheinbaum (2002), Deep flows in the Yucatan Channel and their relation to changes in the Loop Current extension, Journal of Geophysical Research: Oceans, 107(C12), 26-21-26-27, doi:10.1029/2001jc001256.

Byun, S.-S., J. J. Park, K.-I. Chang, and R. W. Schmitt (2010), Observation of near-inertial wave reflections within the thermostat layer of an anticyclonic mesoscale eddy, Geophys. Res. Lett., 37(1), L01606.

Camilli, R., C. M. Reddy, D. R. Yoerger, B. A. S. Van Mooy, M. V. Jakuba, J. C. Kinsey, C. P. McIntyre, S. P. Sylva, and J. V. Maloney (2010), Tracking Hydrocarbon Plume Transport and Biodegradation at Deepwater Horizon, Science, 330(6001), 201-204, doi:10.1126/science.1195223.

Candela, J., J. Sheinbaum, J. Ochoa, A. Badan, and R. Leben (2002), The potential vorticity flux through the Yucatan Channel and the Loop Current in the Gulf of Mexico, Geophysical Research Letters, 29(22), 16-11-16-14, doi:10.1029/2002gl015587.

Capet, X., J. C. McWilliams, M. J. Molemaker, and A. F. Shchepetkin (2008), Mesoscale to Submesoscale Transition in the California Current System. Part I: Flow Structure, Eddy Flux, and Observational Tests, Journal of Physical Oceanography, 38(1), 29-43.

Carton, J. A., and B. S. Giese (2008), A Reanalysis of Ocean Climate Using Simple Ocean Data Assimilation (SODA), Monthly Weather Review, 136(8), 2999-3017, doi:10.1175/2007mwr1978.1.

Casella, E., A. Molcard, and A. Provenzale (2011), Mesoscale vortices in the Ligurian Sea and their effect on coastal upwelling processes, Journal of Marine Systems, 88(1), 12-19, doi:http://dx.doi.org/10.1016/j.jmarsys.2011.02.019.

Chang, Y. L., and L. Y. Oey (2010), Eddy and Wind-Forced Heat Transports in the Gulf of Mexico, Journal of Physical Oceanography, 40(12), 2728-2742, doi:10.1175/2010jpo4474.1.

Chang, Y. L., and L. Y. Oey (2010), Loop Current Cycle: Coupled Response of the Loop Current with Deep Flows, Journal of Physical Oceanography, 41(3), 458-471, doi:10.1175/2010jpo4479.1.

Chang, Y. L., and L. Y. Oey (2010), Why Can Wind Delay the Shedding of Loop Current Eddies?, Journal of Physical Oceanography, 40(11), 2481-2495, doi:10.1175/2010jpo4460.1.

Chang, Y. L., and L. Y. Oey (2012), Why does the Loop Current tend to shed more eddies in summer and winter?, Geophysical Research Letters, 39(5), doi:10.1029/2011gl050773.

Chang, Y.-L., L. Oey, F.-H. Xu, H.-F. Lu, and A. Fujisaki (2011), 2010 oil spill: trajectory projections based on ensemble drifter analyses, Ocean Dynamics, 61(6), 829-839, doi:10.1007/s10236-011-0397-4.

Chassignet, E. P., H. E. Hurlburt, O. M. Smedstad, G. R. Halliwell, P. J. Hogan, A. J. Wallcraft, R. Baraille, and R. Bleck (2007), The HYCOM (HYbrid Coordinate Ocean Model) data assimilative system, Journal of Marine Systems, 65(1–4), 60-83, doi:http://dx.doi.org/10.1016/j.jmarsys.2005.09.016.

Chavanne, C. P., P. Flament, D. S. Luther, and K.-W. Gurgel (2010), Observations of Vortex Rossby Waves Associated with a Mesoscale Cyclone*, Journal of Physical Oceanography, 40(10), 2333-2340, doi:10.1175/2010jpo4495.1.

Chen, D., W. T. Liu, S. E. Zebiak, M. A. Cane, Y. Kushnir, and D. Witter (1999), Sensitivity of the tropical Pacific Ocean simulation to the temporal and spatial resolution of wind forcing, J. Geophys. Res., 104(C5), 11261-11271.

Chen, X., S. E. Lohrenz, and D. A. Wiesenburg (2000), Distribution and controlling mechanisms of primary production on the Louisiana–Texas continental shelf, Journal of Marine Systems, 25(2), 179-207, doi:http://dx.doi.org/10.1016/S0924-7963(00)00014-2.

Chin, T. M., R. F. Milliff, and W. G. Large (1998), Basin-Scale, High-Wavenumber Sea Surface Wind Fields from a Multiresolution Analysis of Scatterometer Data, Journal of Atmospheric and Oceanic Technology, 15(3), 741-763, doi:10.1175/1520-0426.

Chiswell, S. M., and G. J. Rickard (2008), Eulerian and Lagrangian statistics in the Bluelink numerical model and AVISO altimetry: Validation of model eddy kinetics, Journal of Geophysical Research: Oceans, 113(C10), n/a-n/a, doi:10.1029/2007jc004673.

Cho, K., R. O. Reid, and W. D. Nowlin (1998), Objectively mapped stream function fields on the Texas-Louisiana shelf based on 32 months of moored current meter data, Journal of Geophysical Research: Oceans, 103(C5), 10377-10390, doi:10.1029/98jc00099.

Cochrane, J. D., and F. J. Kelly (1986), Low-frequency circulation on the Texas-Louisiana continental shelf, Journal of Geophysical Research: Oceans, 91(C9), 10645-10659, doi:10.1029/JC091iC09p10645.

Counillon, F., and L. Bertino (2009), Ensemble Optimal Interpolation: multivariate properties in the Gulf of Mexico, Tellus: Series A, 61(2), 296-308, doi:10.1111/j.1600-0870.2008.00383.x.

Danioux, E., and P. Klein (2008), A Resonance Mechanism Leading to Wind-Forced Motions with a 2f Frequency, Journal of Physical Oceanography, 38(10), 2322-2329, doi:10.1175/2008JPO3822.1.

Danioux, E., P. Klein, and P. Riviere (2008), Propagation of Wind Energy into the Deep Ocean through a Fully Turbulent Mesoscale Eddy Field, Journal of Physical Oceanography, 38(10), 2224-2241, doi:10.1175/2008JPO3821.1.

Debreu, L., P. Marchesiello, P. Penven, and G. Cambon (2012), Two-way nesting in split-explicit ocean models: Algorithms, implementation and validation, Ocean Modelling, 49–50(0), 1-21, doi:http://dx.doi.org/10.1016/j.ocemod.2012.03.003.

DeHaan, C. J., and W. Sturges (2005), Deep Cyclonic Circulation in the Gulf of Mexico, Journal of Physical Oceanography, 35(10), 1801-1812, doi:10.1175/jpo2790.1.

DiMarco, S. F., M. K. Howard, and R. O. Reid (2000), Seasonal variation of wind-driven diurnal current cycling on the Texas-Louisiana Continental Shelf, Geophysical Research Letters, 27(7), 1017-1020, doi:10.1029/1999gl010491.

DiMarco, S. F., W. D. Nowlin, Jr., and R. O. Reid (2005), A statistical description of the velocity fields from upper ocean drifters in the Gulf of Mexico, in Circulation in the Gulf of Mexico: Observations and Models, edited, pp. 101-110, AGU, Washington, DC, doi:10.1029/161gm08.

Dortch, Q., and T. E. Whitledge (1992), Does nitrogen or silicon limit phytoplankton production in the Mississippi River plume and nearby regions?, Continental Shelf Research, 12(11), 1293-1309, doi:10.1016/0278-4343(92)90065-R.

Dukhovskoy, D. S., S. L. Morey, P. J. Martin, J. J. O'Brien, and C. Cooper (2009), Application of a vanishing, quasi-sigma, vertical coordinate for simulation of high-speed, deep currents over the Sigsbee Escarpment in the Gulf of Mexico, Ocean Modelling, 28(4), 250-265, doi: 10.1016/j.ocemod.2009.02.009.

Dunn, D. D. (1996), Trends in nutrient inflows to the Gulf of Mexico from streams draining the conterminous United States, 1972-93Rep., 68 pp, U.S. Environmental Protection Agency, Austin, Texas.

Elliott, B. A. (1982), Anticyclonic Rings in the Gulf of Mexico, Journal of Physical Oceanography, 12(11), 1292-1309, doi:10.1175/1520-0485.

Ezer, T., L.-Y. Oey, H.-C. Lee, and W. Sturges (2003), The variability of currents in the Yucatan Channel: Analysis of results from a numerical ocean model, Journal of Geophysical Research: Oceans, 108(C1), doi:10.1029/2002jc001509.

Fan, C., J. Wang, and J. Song (2010), Factors influencing the climatological mixed layer depth in the South China Sea: numerical simulations, Chinese Journal of Oceanology and Limnology, 28(5), 1112-1118.

Garrett, C. (2003), Internal Tides and Ocean Mixing, Science, 301(5641), 1858-1859, doi:10.1126/science.1090002.

Gill, A. E. (1984), On the Behavior of Internal Waves in the Wakes of Storms, Journal of Physical Oceanography, 14(7), 1129-1151, doi:doi:10.1175/1520-0485.

Goldman, J. C., J. J. McCarthy, and D. G. Peavey (1979), Growth rate influence on the chemical composition of phytoplankton in oceanic waters, Nature, 279(5710), 210-215.

Graves, L. P., J. C. McWilliams, and M. T. Montgomery (2006), Vortex evolution due to straining: a mechanism for dominance of strong, interior anticyclones, Geophysical & Astrophysical Fluid Dynamics, 100(3), 151-183.

Green, R. E., G. A. Breed, M. J. Dagg, and S. E. Lohrenz (2008), Modeling the response of primary production and sedimentation to variable nitrate loading in the Mississippi River plume, Continental Shelf Research, 28(12), 1451-1465, doi:10.1016/j.csr.2007.02.008.

Håkanson, L., and J. M. Eklund (2010), Relationships Between Chlorophyll, Salinity, Phosphorus, and Nitrogen in Lakes and Marine Areas, Journal of Coastal Research, 263, 412-423, doi:10.2112/08-1121.1.

Hamilton, P. (1990), Deep Currents in the Gulf of Mexico, Journal of Physical Oceanography, 20(7), 1087-1104, doi:10.1175/1520-0485.

Hamilton, P. (2009), Topographic Rossby waves in the Gulf of Mexico, Progress in Oceanography, 82(1), 1-31, doi:10.1016/j.pocean.2009.04.019.

Hamilton, P., T. J. Berger, J. J. Singer, E. Waddell, J. H. Churchill, R. Leben, T. N. Lee, and W. Sturges (2000), DeSoto Canyon Eddy Intrusion Study. Final ReportRep., 275 pp, U.S. Department of the Interior, New Orleans, LA.

Hamilton, P., and A. Lugo-Fernandez (2001), Observations of high speed deep currents in the northern Gulf of Mexico, Geophysical Research Letters, 28(14), 2867-2870, doi:10.1029/2001gl013039.

He, R., and R. H. Weisberg (2003), A Loop Current Intrusion Case Study on the West Florida Shelf, Journal of Physical Oceanography, 33(2), 465-477, doi:10.1175/1520-0485.

Hitchcock, G. L., W. J. Wiseman Jr, W. C. Boicourt, A. J. Mariano, N. Walker, T. A. Nelsen, and E. Ryan (1997), Property fields in an effluent plume of the Mississippi river, Journal of Marine Systems, 12(1–4), 109-126, doi:10.1016/S0924-7963(96)00092-9.

Hong, X., S. W. Chang, S. Raman, L. K. Shay, and R. Hodur (2000), The Interaction between Hurricane Opal (1995) and a Warm Core Ring in the Gulf of Mexico, Monthly Weather Review, 128(5), 1347-1365, doi:10.1175/1520-0493.

Jarosz, E., Z. R. Hallock, and W. J. Teague (2007), Near-inertial currents in the DeSoto Canyon region, Continental Shelf Research, 27(19), 2407-2426, doi:10.1016/j.csr.2007.06.014.

Johnson, M. W., K. L. Heck Jr, and J. W. Fourqurean (2006), Nutrient content of seagrasses and epiphytes in the northern Gulf of Mexico: Evidence of phosphorus and nitrogen limitation, Aquatic Botany, 85(2), 103-111, doi: 10.1016/j.aquabot.2006.02.003.

Josey, S. A. (2001), A Comparison of ECMWF, NCEP–NCAR, and SOC Surface Heat Fluxes with Moored Buoy Measurements in the Subduction Region of the Northeast Atlantic, Journal of Climate, 14(8), 1780-1789, doi:10.1175/1520-0442.

Joye, S. B., et al. (2011), Comment on "A Persistent Oxygen Anomaly Reveals the Fate of Spilled Methane in the Deep Gulf of Mexico", Science, 332(6033), 1033, doi:10.1126/science.1203307.

Justić, D., N. N. Rabalais, and R. E. Turner (1995), Stoichiometric nutrient balance and origin of coastal eutrophication, Marine Pollution Bulletin, 30(1), 41-46, doi:10.1016/0025-326X(94)00105-I.

Kamenkovich, I. V. (2005), Role of daily surface forcing in setting the temperature and mixed layer structure of the Southern Ocean, J. Geophys. Res., 110(C7), C07006.

Kara, A. B., H. E. Hurlburt, A. J. Wallcraft, and M. A. Bourassa (2005), Black Sea Mixed Layer Sensitivity to Various Wind and Thermal Forcing Products on Climatological Time Scales, Journal of Climate, 18(24), 5266-5293, doi:doi:10.1175/JCLI3573R2.1.

Kistler, R., et al. (2001), The NCEP–NCAR 50–Year Reanalysis: Monthly Means CD–ROM and Documentation, Bulletin of the American Meteorological Society, 82(2), 247-267, doi:10.1175/1520-0477.

Klein, P., and G. Lapeyre (2009), The Oceanic Vertical Pump Induced by Mesoscale and Submesoscale Turbulence, Annual Review of Marine Science, 1(1), 351-375, doi:10.1146/annurev.marine.010908.163704.

Klein, P., G. Lapeyre, and W. G. Large (2004), Wind ringing of the ocean in presence of mesoscale eddies, Geophys. Res. Lett., 31(15), L15306.

Klemas, V. (2010), Tracking Oil Slicks and Predicting their Trajectories Using Remote Sensors and Models: Case Studies of the Sea Princess and Deepwater Horizon Oil Spills, Journal of Coastal Research, 789-797, doi:10.2112/10a-00012.1.

Knapke, E. M. (2012), Influence of the Mississippi River plume on diazotroph distributions in the northern Gulf of Mexico during summer 2011, University of Texas at Austin.

Kolodziejczyk, N., J. Ochoa, J. Candela, and J. Sheinbaum (2012), Observations of intermittent deep currents and eddies in the Gulf of Mexico, Journal of Geophysical Research: Oceans, 117(C9), doi:10.1029/2012jc007890.

Komori, N., W. Ohfuchi, B. Taguchi, H. Sasaki, and P. Klein (2008), Deep ocean inertia-gravity waves simulated in a high-resolution global coupled atmosphere GCM, Geophys. Res. Lett., 35(4), L04610.

Koszalka, I., A. Bracco, J. C. McWilliams, and A. Provenzale (2009), Dynamics of wind-forced coherent anticyclones in the open ocean, J. Geophys. Res., 114(C8), C08011.

Koszalka, I., L. Ceballos, and A. Bracco (2010), Vertical mixing and coherent anticyclones in the ocean: the role of stratification, Nonlin. Processes Geophys., 17(1), 37-47.

Kundu, P. K., and R. E. Thomson (1985), Inertial Oscillations due to a Moving Front, Journal of Physical Oceanography, 15(8), 1076-1084, doi:doi:10.1175/1520-0485.

Kunze, E., and T. B. Sanford (1984), Observations of Near-Inertial Waves in a Front, Journal of Physical Oceanography, 14(3), 566-581, doi:doi:10.1175/1520-0485.

Kunze, E., and T. B. Sanford (1986), Near-Inertial Wave Interactions with Mean Flow and Bottom Topography near Caryn Seamount, Journal of Physical Oceanography, 16(1), 109-120, doi:doi:10.1175/1520-0485.

Large, W. G., and G. B. Crawford (1995), Observations and Simulations of Upper-Ocean Response to Wind Events during the Ocean Storms Experiment, Journal of Physical Oceanography, 25(11), 2831-2852, doi:10.1175/1520-0485.

Le Hénaff, M., V. H. Kourafalou, C. B. Paris, J. Helgers, Z. M. Aman, P. J. Hogan, and A. Srinivasan (2012), Surface Evolution of the Deepwater Horizon Oil Spill Patch:

Combined Effects of Circulation and Wind-Induced Drift, Environmental Science & Technology, 46(13), 7267-7273, doi:10.1021/es301570w.

Leben, R. R. (2005), Altimeter-derived loop current metrics, in Circulation in the Gulf of Mexico: Observations and Models, edited, pp. 181-201, AGU, Washington, DC, doi:10.1029/161gm15.

Leben, R. R., and G. H. Born (1993), Tracking Loop Current eddies with satellite altimetry, Advances in Space Research, 13(11), 325-333, doi: 10.1016/0273-1177(93)90235-4.

Lee, D.-K., and P. P. Niiler (1998), The inertial chimney: The near-inertial energy drainage from the ocean surface to the deep layer, J. Geophys. Res., 103(C4), 7579-7591.

Lee, H.-C., and G. Mellor (2003), Numerical Simulation of the Gulf Stream and the Deep Circulation, Journal of Oceanography, 59(3), 343-357, doi:10.1023/a:1025520027948.

Lee, T., and W. T. Liu (2005), Effects of high-frequency wind sampling on simulated mixed layer depth and upper ocean temperature, J. Geophys. Res., 110(C5), C05002.

Lee, Z., A. Weidemann, J. Kindle, R. Arnone, K. L. Carder, and C. Davis (2007), Euphotic zone depth: Its derivation and implication to ocean-color remote sensing, Journal of Geophysical Research: Oceans, 112(C3), C03009, doi:10.1029/2006JC003802.

Levy, M., and P. Klein (2004), Does the low frequency variability of mesoscale dynamics explain a part of the phytoplankton and zooplankton spectral variability?, Proceedings of the Royal Society of London. Series A: Mathematical, Physical and Engineering Sciences, 460(2046), 1673-1687, doi:10.1098/rspa.2003.1219.

Liu, Y., R. H. Weisberg, C. Hu, C. Kovach, and R. Riethmuller (2011), Evolution of the Loop Current System During the Deepwater Horizon Oil Spill Event as Observed With Drifters and Satellites, in Monitoring and Modeling the Deepwater Horizon Oil

Spill: A Record-Breaking Enterprise, edited, pp. 91-101, AGU, Washington, DC, doi:10.1029/2011gm001127.

Lohrenz, S. E., M. J. Dagg, and T. E. Whitledge (1990), Enhanced primary production at the plume/oceanic interface of the Mississippi River, Continental Shelf Research, 10(7), 639-664, doi: 10.1016/0278-4343(90)90043-L.

Lohrenz, S. E., G.L. Fahnenstiel, D.G. Redalje, G. A. Lang, X. Chen, and M. J. Dagg (1997), Variations in primary production of northern Gulf of Mexico continental shelf waters linked to nutrient inputs from the Mississippi River, Marine Ecology Progress Series, 155, 45-54, doi:10.3354/meps155045.

Lohrenz, S. E., G. L. Fahnenstiel, D. G. Redalje, G. A. Lang, M. J. Dagg, T. E. Whitledge, and Q. Dortch (1999), Nutrients, irradiance, and mixing as factors regulating primary production in coastal waters impacted by the Mississippi River plume, Continental Shelf Research, 19(9), 1113-1141, doi: 10.1016/S0278-4343(99)00012-6.

Lohrenz, S. E., D. G. Redalje, W.-J. Cai, J. Acker, and M. Dagg (2008), A retrospective analysis of nutrients and phytoplankton productivity in the Mississippi River plume, Continental Shelf Research, 28(12), 1466-1475, doi:10.1016/j.csr.2007.06.019.

Lueck, R., and R. Reid (1984), On the Production and Dissipation of Mechanical Energy in the Ocean, J. Geophys. Res., 89(C3), 3439-3445.

Lugo-Fernández, A. (2007), Is the Loop Current a Chaotic Oscillator?, Journal of Physical Oceanography, 37(6), 1455-1469, doi:10.1175/jpo3066.1.

Marchesiello, P., J. C. McWilliams, and A. Shchepetkin (2003), Equilibrium Structure and Dynamics of the California Current System, Journal of Physical Oceanography, 33(4), 753-783, doi:10.1175/1520-0485.

Martin, A. P., and K. J. Richards (2001), Mechanisms for vertical nutrient transport within a North Atlantic mesoscale eddy, Deep Sea Research Part II: Topical Studies in Oceanography, 48(4-5), 757-773.

McGillicuddy, D. J., and A. R. Robinson (1997), Eddy-induced nutrient supply and new production in the Sargasso Sea, Deep Sea Research Part I: Oceanographic Research Papers, 44(8), 1427-1450.

McWilliams, J. C. (1984), The emergence of isolated coherent vortices in turbulent flow, Journal of Fluid Mechanics, 146, 21-43, doi:10.1017/S0022112084001750.

McWilliams, J. C. (1990), The vortices of two-dimensional turbulence, Journal of Fluid Mechanics, 219, 361-385, doi:10.1017/S0022112090002981.

McWilliams, J. C., L. P. Graves, and M. T. Montogomery (2003), A Formal Theory for Vortex Rossby Waves and Vortex Evolution, Geophysical & Astrophysical Fluid Dynamics, 97(4), 275.

Milliff, R. F., J. Morzel, D. B. Chelton, and M. H. Freilich (2004), Wind Stress Curl and Wind Stress Divergence Biases from Rain Effects on QSCAT Surface Wind Retrievals, Journal of Atmospheric and Oceanic Technology, 21(8), 1216-1231, doi:10.1175/1520-0426.

Montgomery, M. T., and R. J. Kallenbach (1997), A theory for vortex rossby-waves and its application to spiral bands and intensity changes in hurricanes, Quarterly Journal of the Royal Meteorological Society, 123(538), 435-465.

Munk, W., and C. Wunsch (1998), Abyssal recipes II: energetics of tidal and wind mixing, Deep Sea Research Part I: Oceanographic Research Papers, 45(12), 1977-2010.

Nakamura, M., and T. Kagimoto (2006), Potential vorticity and eddy potential enstrophy in the North Atlantic Ocean simulated by a global eddy-resolving model, Dynamics of Atmospheres and Oceans, 41(1), 28-59, doi: 10.1016/j.dynatmoce.2005.10.002.

Nowlin, W. D., Jr., A. E. Jochens, S. F. DiMarco, and R. O. Reid (2000), Physical oceanography. Deepwater Gulf of Mexico environmental and socioeconomic data search and synthesis, Narrative Report, OCS Study MMS 2000-049,Gulf of Mexico

OCS Regional Office, Minerals Management Service, U.S. Department of the Interior 1, 60.

Oey, L.-Y. (1996), Simulation of Mesoscale Variability in the Gulf of Mexico: Sensitivity Studies, Comparison with Observations, and Trapped Wave Propagation, Journal of Physical Oceanography, 26(2), 145-175, doi:10.1175/1520-0485.

Oey, L.-Y. (2004), Vorticity flux through the Yucatan Channel and Loop Current variability in the Gulf of Mexico, Journal of Geophysical Research: Oceans, 109(C10), doi:10.1029/2004jc002400.

Oey, L. Y., and H. C. Lee (2002), Deep Eddy Energy and Topographic Rossby Waves in the Gulf of Mexico, Journal of Physical Oceanography, 32(12), 3499-3527, doi:10.1175/1520-0485.

Oey, L. Y., H. C. Lee, and W. J. Schmitz (2003), Effects of winds and Caribbean eddies on the frequency of Loop Current eddy shedding: A numerical model study, Journal of Geophysical Research: Oceans, 108(C10), doi:10.1029/2002jc001698.

Ohlmann, J. C., and P. P. Niiler (2005), Circulation over the continental shelf in the northern Gulf of Mexico, Progress in Oceanography, 64(1), 45-81, doi:10.1016/j.pocean.2005.02.001.

Paris, C. B., M. L. Hénaff, Z. M. Aman, A. Subramaniam, J. Helgers, D.-P. Wang, V. H. Kourafalou, and A. Srinivasan (2012), Evolution of the Macondo Well Blowout: Simulating the Effects of the Circulation and Synthetic Dispersants on the Subsea Oil Transport, Environmental Science & Technology, 46(24), 13293-13302, doi:10.1021/es303197h.

Pasquero, C., A. Bracco, Provenzale, and J. B. Weiss (2007), Particle motion in the sea of eddies, in Lagrangian Analysis and Prediction of Coastal and Ocean Dynamics, edited, pp. 89-118, Cambridge University Press.

Pasquero, C., A. Bracco, and A. Provenzale (2005), Impact of the spatiotemporal variability of the nutrient flux on primary productivity in the ocean, J. Geophys. Res., 110(C7), C07005.

Penven, P., P. Marchesiello, L. Debreu, and J. Lefèvre (2008), Software tools for pre- and post-processing of oceanic regional simulations, Environmental Modelling & Software, 23(5), 660-662, doi:10.1016/j.envsoft.2007.07.004.

Pérez-Brunius, P., P. García-Carrillo, J. Dubranna, J. Sheinbaum, and J. Candela (2012), Direct observations of the upper layer circulation in the southern Gulf of Mexico, Deep Sea Research Part II: Topical Studies in Oceanography(0), doi:10.1016/j.dsr2.2012.07.020.

Pollard, R. T., and R. C. Millard Jr (1970), Comparison between observed and simulated wind-generated inertial oscillations, Deep Sea Research and Oceanographic Abstracts, 17(4), 813-816, IN815, 817-821.

Price, J. F., T. B. Sanford, and G. Z. Forristall (1994), Forced Stage Response to a Moving Hurricane, Journal of Physical Oceanography, 24(2), 233-260, doi:10.1175/1520-0485.

Provenzale, A. (1999), Transport by coherent barotropic vortices, Annual Review of Fluid Mechanics, 31(1), 55.

Qian, Y., A. E. Jochens, M. C. Kennicutt Ii, and D. C. Biggs (2003), Spatial and temporal variability of phytoplankton biomass and community structure over the continental margin of the northeast Gulf of Mexico based on pigment analysis, Continental Shelf Research, 23(1), 1-17, doi:10.1016/S0278-4343(02)00173-5.

Rabalais, N. N., R. E. Turner, D. Justic, Q. Dortch, W. J. Wiseman, and B. K. SenGupta (1996), Nutrient changes in the Mississippi River and system responses on the adjacent continental shelf, Estuaries, 19(2B), 386-407, doi:10.2307/1352458.

Rabinovich, A., R. Thomson, and S. Bograd (2002), Drifter Observations of Anticyclonic Eddies near Bussol' Strait, the Kuril Islands, Journal of Oceanography, 58(5), 661-671.

Redfield, A. C. (1934), On the proportions of organic derivatives in sea water and their relation to the composition of plankton, James Johnstone Memorial Volume . R. J. Daniel, 177.

Rhines, P. (1970), Edge , bottom , and Rossby waves in a rotating stratified fluid, Geophysical Fluid Dynamics, 1(3-4), 273-302, doi:10.1080/03091927009365776.

Rogachev, K., and E. Carmack (2002), Evidence for the Trapping and Amplification of Near-Inertial Motions in a Large Anticyclonic Ring in the Oyashio, Journal of Oceanography, 58(5), 673-682.

Salas-Perez, J. J., and A. Granados-Barba (2008), Oceanographic characterization of the Veracruz reefs system, Atmósfera, 21, 281-301.

Scavia, D., and K. A. Donnelly (2007), Reassessing Hypoxia Forecasts for the Gulf of Mexico, Environmental Science & Technology, 41(23), 8111-8117, doi:10.1021/es0714235.

SE, L., F. GL, R. DG, L. GA, C. X, and D. MJ (1997), Variations in primary production of northern Gulf of Mexico continental shelf waters linked to nutrient inputs from the Mississippi River, Marine Ecology Progress Series, 155, 45-54, doi:10.3354/meps155045.

Shay, L. K., and R. L. Elsberry (1987), Near-Inertial Ocean Current Response to Hurricane Frederic, Journal of Physical Oceanography, 17(8), 1249-1269, doi:10.1175/1520-0485(1987)017<1249:niocrt>2.0.co;2.

Shay, L. K., A. J. Mariano, S. D. Jacob, and E. H. Ryan (1998), Mean and Near-Inertial Ocean Current Response to Hurricane Gilbert, Journal of Physical Oceanography, 28(5), 858-889, doi:10.1175/1520-0485.

Sheinbaum, J., J. Candela, A. Badan, and J. Ochoa (2002), Flow structure and transport in the Yucatan Channel, Geophysical Research Letters, 29(3), 10-11-10-14, doi:10.1029/2001gl013990.

Skyllingstad, E. D., W. D. Smyth, and G. B. Crawford (2000), Resonant Wind-Driven Mixing in the Ocean Boundary Layer, Journal of Physical Oceanography, 30(8), 1866-1890, doi: 10.1175/1520-0485.

Smith, S., and G. Hitchcock (1994), Nutrient enrichments and phytoplankton growth in the surface waters of the Louisiana Bight, Estuaries, 17(4), 740-753, doi:10.2307/1352744.

Smith, T. M., and R. W. Reynolds (2004), Improved Extended Reconstruction of SST (1854–1997), Journal of Climate, 17(12), 2466-2477, doi:10.1175/1520-0442.

Stammer, D. (1997), Global Characteristics of Ocean Variability Estimated from Regional TOPEX/POSEIDON Altimeter Measurements, Journal of Physical Oceanography, 27(8), 1743-1769, doi:doi:10.1175/1520-0485.

Sturges, W., J. C. Evans, S. Welsh, and W. Holland (1993), Separation of Warm-Core Rings in the Gulf of Mexico, Journal of Physical Oceanography, 23(2), 250-268, doi:10.1175/1520-0485.

Sturges, W., N. G. Hoffmann, and R. R. Leben (2009), A Trigger Mechanism for Loop Current Ring Separations, Journal of Physical Oceanography, 40(5), 900-913, doi:10.1175/2009jpo4245.1.

Sturges, W., and R. Leben (2000), Frequency of Ring Separations from the Loop Current in the Gulf of Mexico: A Revised Estimate, Journal of Physical Oceanography, 30(7), 1814-1819, doi:10.1175/1520-0485.

Sui, C.-H., X. Li, M. M. Rienecker, K.-M. Lau, I. Laszlo, and R. T. Pinker (2003), The Role of Daily Surface Forcing in the Upper Ocean over the Tropical Pacific: A Numerical Study, Journal of Climate, 16(4), 756-766, doi:doi:10.1175/1520-0442.

Sylvan, J. B., Q. Dortch, D. M. Nelson, A. F. Maier Brown, W. Morrison, and J. W. Ammerman (2006), Phosphorus Limits Phytoplankton Growth on the Louisiana Shelf During the Period of Hypoxia Formation, Environmental Science & Technology, 40(24), 7548-7553, doi:10.1021/es061417t.

Toner, M., A. D. Kirwan, A. C. Poje, L. H. Kantha, F. E. Müller-Karger, and C. K. R. T. Jones (2003), Chlorophyll dispersal by eddy-eddy interactions in the Gulf of Mexico, Journal of Geophysical Research: Oceans, 108(C4), 3105, doi:10.1029/2002JC001499.

Turner, R. E., and N. N. Rabalais (2013), Nitrogen and phosphorus phytoplankton growth limitation in the northern Gulf of Mexico, Aquatic Microbial Ecology, 68(2), 159-169, doi:10.3354/ame01607.

Turner, R. E., N. N. Rabalais, R. B. Alexander, G. McIsaac, and R. W. Howarth (2007), Characterization of nutrient, organic carbon, and sediment loads and concentrations from the Mississippi River into the northern Gulf of Mexico, Estuaries and Coasts: J ERF, 30(5), 773-790, doi:10.1007/bf02841333.

Vazquez de la Cerda, A. M., R. O. Reid, S. F. DiMarco, and A. E. Jochens (2005), Bay of Campeche circulation: An update, in Circulation in the Gulf of Mexico: Observations and Models, edited, pp. 279-293, AGU, Washington, DC, doi:10.1029/161gm20.

Vidal, V. M. V., F. V. Vidal, and J. M. Pérez-Molero (1992), Collision of a loop current anticyclonic ring against the continental shelf slope of the western Gulf of Mexico, Journal of Geophysical Research: Oceans, 97(C2), 2155-2172, doi:10.1029/91jc00486.

Vukovich, F. M. (2007), Climatology of Ocean Features in the Gulf of Mexico Using Satellite Remote Sensing Data, Journal of Physical Oceanography, 37(3), 689-707, doi:10.1175/jpo2989.1.

Vukovich, F. M. (2012), Changes in the Loop Current's Eddy Shedding in the Period 2001–2010, International Journal of Oceanography, 2012, 18, doi:10.1155/2012/439042.

Vukovich, F. M., and B. W. Crissman (1986), Aspects of warm rings in the Gulf of Mexico, Journal of Geophysical Research: Oceans, 91(C2), 2645-2660, doi:10.1029/JC091iC02p02645.

Walker, N. D., W. J. Wiseman, L. J. Rouse, and A. Babin (2005), Effects of River Discharge, Wind Stress, and Slope Eddies on Circulation and the Satellite-Observed Structure of the Mississippi River Plume, Journal of Coastal Research, 1228-1244, doi:10.2112/04-0347.1.

Weisberg, R. H., B. D. Black, and Z. Li (2000), An upwelling case study on Florida's west coast, Journal of Geophysical Research: Oceans, 105(C5), 11459-11469, doi:10.1029/2000jc900006.

Welsh, S. E., and M. Inoue (2000), Loop Current rings and the deep circulation in the Gulf of Mexico, Journal of Geophysical Research: Oceans, 105(C7), 16951-16959, doi:10.1029/2000jc900054.

Wunsch, C., and R. Ferrari (2004), Vertical mixing, energy, and the general circulation of the oceans, Annual Review of Fluid Mechanics, 36(1), 281-314, doi:doi:10.1146/annurev.fluid.36.050802.122121.

Wysocki, L. A., T. S. Bianchi, R. T. Powell, and N. Reuss (2006), Spatial variability in the coupling of organic carbon, nutrients, and phytoplankton pigments in surface waters and sediments of the Mississippi River plume, Estuarine, Coastal and Shelf Science, 69(1-2), 47-63, doi:10.1016/j.ecss.2006.03.022.

Zavala-Hidalgo, J., S. L. Morey, J. J. O'Brien, and L. Zambudio (2006), On the Loop Current eddy shedding variability, Atmósfera, 19(001), 8.

Zavala-Hidalgo, J., S. L. Morey, and J. J. O'Brien (2003), Seasonal circulation on the western shelf of the Gulf of Mexico using a high-resolution numerical model, Journal of Geophysical Research: Oceans, 108(C12), n/a-n/a, doi:10.1029/2003jc001879.

Zehr, J. P., and B. B. Ward (2002), Nitrogen Cycling in the Ocean: New Perspectives on Processes and Paradigms, Applied and Environmental Microbiology, 68(3), 1015-1024, doi:10.1128/aem.68.3.1015-1024.2002.

Zhai, X., R. J. Greatbatch, and C. Eden (2007), Spreading of near-inertial energy in a 1/12° model of the North Atlantic Ocean, Geophys. Res. Lett., 34(10), L10609.

Zhai, X., R. J. Greatbatch, and J. Zhao (2005), Enhanced vertical propagation of storm-induced near-inertial energy in an eddying ocean channel model, Geophys. Res. Lett., 32(18), L18602.